Case Study of Seasonal Variation in the Subgrade and Subbase Layers of Highway US 20

PGA

PARTNERSHIP FOR GEOTECHNICAL ADVANCEMENT

Final Report
May 2008

Sponsored by
the Iowa Highway Research Board
(IHRB Project TR-516)

ctre
Center for Transportation Research and Education

IOWA STATE UNIVERSITY

About the PGA

The mission of the Partnership for Geotechnical Advancement is to increase highway performance in a cost-effective manner by developing and implementing methods, materials, and technologies to solve highway construction problems in a continuing and sustainable manner.

Technical Report Documentation Page

1. Report No.	**2. Government Accession No.**	**3. Recipient's Catalog No.**
CTRE Project 04-172 IHRB Project TR-516		

4. Title and Subtitle Case Study of Seasonal Variation in the Subgrade and Subbase Layers of Highway US 20	**5. Report Date** May 2008 **6. Performing Organization Code**
7. Author(s) Thang Huu Phan, Matthew Cushman, David J. White, Chuck Jahren, Vern Schaefer, Radhey Sharma	**8. Performing Organization Report No.**
9. Performing Organization Name and Address Center for Transportation Research and Education Iowa State University 2711 South Loop Drive, Suite 4700 Ames, IA 50010-8664	**10. Work Unit No. (TRAIS)** **11. Contract or Grant No.**
12. Sponsoring Organization Name and Address Iowa Highway Research Board Iowa Department of Transportation 800 Lincoln Way Ames, IA 50010	**13. Type of Report and Period Covered** **14. Sponsoring Agency Code**

15. Supplementary Notes

Visit www.ctre.iastate.edu for color PDF files of this and other research reports.

16. Abstract

Seasonal variations in ground temperature and moisture content influence the load carrying capacity of pavement subgrade layers. To improve pavement performance, pavement design guidelines require knowledge of environmental factors and subgrade stiffness relationships. As part of this study, in-ground instrumentation was installed in the pavement foundation layers of a newly constructed section along US Highway 20 near Fort Dodge, Iowa, to monitor the seasonal variations in temperature, frost depth, groundwater levels, and moisture regime. Dynamic cone penetrometer (DCP), nuclear gauge, and Clegg hammer tests were performed at 64 test points in a 6-ft x 6-ft grid pattern to characterize the subgrade stiffness properties (i.e., resilient modulus) prior to paving. The purpose of this paper is to present the field instrumentation results and the observed changes in soil properties due to seasonal environmental effects.

17. Key Words	**18. Distribution Statement**
load carrying capacity—pavement distress—resilient modulus—seasonal variation— subbase layer—subgrade—US Highway 20	No restrictions.

19. Security Classification (of this report)	**20. Security Classification (of this page)**	**21. No. of Pages**	**22. Price**
Unclassified.	Unclassified.	90	NA

Form DOT F 1700.7 (8-72) **Reproduction of completed page authorized**

Case Study of Seasonal Variation in the Subgrade and Subbase Layers of Highway US20

Final Report
May 2008

Principal Investigators
David J. White, Associate Professor of Civil Engineering
Vern Schaefer, Professor of Civil Engineering
Radhey Sharma, Assistant Professor of Civil Engineering (formerly)

Research Assistants
Thang Huu Phan
Matthew Cushman

Authors
Thang Huu Phan, Matthew Cushman, David J. White, Chuck Jahren, Vernon Schaefer and Radhey Sharma

Sponsored by
the Iowa Highway Research Board
(IHRB Project TR-516)

Preparation of this report was financed in part
through funds provided by the Iowa Department of Transportation
through its research management agreement with the
Center for Transportation Research and Education,
CTRE Project 04-172.

A report from
Center for Transportation Research and Education
Iowa State University
2711 South Loop Drive, Suite 4700
Ames, IA 50010-8664
Phone: 515-294-8103
Fax: 515-294-0467
www.ctre.iastate.edu

TABLE OF CONTENTS

LIST OF FIGURES

LIST OF TABLES

ACKNOWLEDGMENTS

The authors would like to thank Iowa Department of Transportation (DOT) and Iowa State University for sponsoring this research. Acknowledgement is also paid to Iowa Environmental Mesonet, and the Iowa State University Department of Agronomy, from whom the data of weather in the Fort Dodge station was downloaded for this research. Chris Brakke, Mark Dunn, Todd Hanson, and Kevin Merryman participated on the Iowa DOT technical advisory committee. Isaac Drew, Clinton Halverson, Mohamed Mekkawy, and Muhammad Suleiman from Iowa State University assisted with field measurements. The opinions, findings, and conclusions expressed in this report are those of the authors and not necessarily those of the sponsoring agencies.

EXECUTIVE SUMMARY

Results from in-situ testing of newly constructed pavement foundation layers to determine spatial variability, and in-ground instrumentation to monitor changes in pavement foundation layer properties are presented in this report. The project was conducted on a new section of US 20 near Fort Dodge, Iowa. In-situ testing prior to paving with PCC provided measurements of moisture content, density, Clegg hammer impact values, and dynamic cone penetration index. Tests were performed on a six-by-six-foot test grid at the surface of the subgrade and subbase layers. The data from these tests provided results for spatial variation analysis. The subgrade was generally characterized as being very stiff, well compacted, and relatively uniform.

The average value of Clegg Impact Value was 14. CBR value and M_r – CBR Clegg were 21 and 222 MPa, respectively. The average DPI (mm/blow) for three sub-layers 0-1 ft, 1-2 ft, and 2-3 ft of the subgrade layer were 18, 20, and 18, respectively. CBR values estimated from these DPI values were 12, 11, and 12, respectively. The resilient moduli, M_r – CBR DPI (MPa), for three sub-layers 0-1 ft, 1-2 ft, and 2-3 ft of the subgrade layer were 120, 109, and 128, respectively. The average dry density and moisture content obtained from in-situ testing were 116.5 pcf and 10.2%, respectively. Relative compaction averaged 100% based on standard Proctor compaction energy. The ground water table under the pavement surface fluctuated from 9 to 13 feet.

Spatial kriging plots showed the variations of soil moisture content, wet density, Clegg Hammer, and DPI of the test section. The Clegg impact values showed that the northern lane had a higher stiffness, possibly resulting from more roller passes. The coefficient of variations of the Clegg impact values, moisture content, and dry density were 38%, 9%, and 2%, respectively.

The average values of resilient modulus in the subgrade layer estimated from the DCP 2 years after construction at depths 0-1 ft and 1-2 ft were 121 MPa and 159 MPa, respectively. The average value of resilient modulus obtained from laboratory test was 47 MPa.

Long-term instrumentation was installed after in-situ testing and prior to paving to provide rainfall, moisture content, air temperature, ground water table, and frost depth information during the period of May 2005 to April 2008. Temperature in the subbase and subgrade layers could not be collected for the entire monitoring period because several sensors failed. Moisture content in the subbase layer remained relatively constant throughout the year except during freezing periods. The subgrade moisture content was lower in the winter season compared to summer. Moisture contents of the subgrade layer increased deeper into the layer and were affected by seasonal variations.

In the subgrade layer, freezing penetrated downward, but thawing occurred in both downward and upward directions. The PCC pavement experienced greater temperature extremes and it changed at a higher rate than the subbase and subgrade layers. The temperature gradient within one hour at PCC surface was up to 18^{o}F.

INTRODUCTION

Seasonal temperature and moisture content variations within pavement subgrade and subbase layers influence pavement load carrying capacity. Loss of support conditions (i.e., a reduction in stiffness) in these layers can occur during thawing periods and/or saturated conditions and is one of the contributors to pavement distress. A better understanding of the influence of seasonal variation of pavement foundation layer properties in Iowa could potentially benefit pavement design, material selection, and construction specifications. As a part of this study, in-situ testing was conducted and field instrumentation were installed to monitor the seasonal variations in temperature, moisture content, frost depth, and groundwater levels.

This research was conducted on a newly constructed PCC pavement on US 20 near Fort Dodge, Iowa (near mile marker 199.90 and state 930+00). In-situ field tests included a dynamic cone penetrometer (DCP), nuclear density gauge, and Clegg hammer impact tests. Tests were performed at 64 test locations on the surface of compacted subgrade prior to placement of the aggregate subbase layer. Results provided a statistically significant dataset for spatial variability analysis. Approximately two years after construction, the subgrade soil was sampled for laboratory resilient modulus testing. In addition, DCP tests were also performed during two seasons of freeze-thaw cycles to observe the changes in subgrade stiffness.

The major objectives of the project were the following:

- Conduct field tests on a newly compacted subgrade to document spatial variation in stiffness parameters.
- Monitor changes in subgrade stiffness due to seasonal variation in moisture and temperature.
- Conduct field tests on the subgrade layer during freezing and thawing conditions.

The quality of a pavement subgrade layer depends on many factors, including spatial variation, initial compaction density, mineralogy, and impact from environmental factors. The benefit of this study was to document the measurements of changes in engineering properties of subgrade materials in Iowa due to spatial and seasonal effects.

This report is divided into several sections. In the background section, a brief description of the project and its location is included. Findings from the literature are reviewed and summarized. The methods section describes how in-ground instrumentation, in-situ tests, and lab tests were conducted. The materials section analyzes the test results and instrumentation. A discussion of the results documents the evaluation of results and their significance. The conclusion and recommendations sections are the final sections included in the report.

BACKGROUND

Resilient Modulus

Resilient modulus is a key input parameter to mechanistic pavement design. The effects of water content and compaction density on the resilient modulus have been studied by a number of researchers. A study of the seasonal variations in these parameters is related to highway pavement response are necessary for pavement design.

Resilient modulus, M_r, which was first proposed by Seed et al. (1962), is the ratio between repeated deviator stress σ_d and recoverable strain ε_r in the direction of major principle stress (Li et al. 1994). Resilient stresses, strains, and deflections of the pavement layers can be calculated based on this modulus. Resilient modulus is dependent on many factors, including soil properties, water content, and compaction. Many studies have shown that seasonal variation of moisture content in the subgrade layer after the construction strongly influence the resilient modulus. A small increment of moisture content may result in a significant reduction in resilient modulus.

The subgrade layer, which is an important component of a highway support system, is subject to repeated traffic loading. The material of this layer is characterized by the resilient modulus. Resilient modulus M_r is usually determined by repeated load triaxial tests and is a ratio between repeated deviator stress and recoverable (resilient) strain. In these tests, confining pressure σ_3 is kept constant and deviator stress σ_d is cycled between the hydrostatic state and some positive deviator stress ($\sigma_1 - \sigma_3$).

$$M_r = \frac{\sigma_d}{\varepsilon_r} \tag{1}$$

In practice, resilient modulus can be estimated from empirical correlations to California bearing ratio (CBR), R-value, and soil index test results. The American Association of State Highway and Transportation Officials (AASHTO) Guide for Design of Pavement Structures (1986) gives this correlation to CBR:

$$M_r(psi) = 1500 \times CBR \tag{2}$$

The M_r data from which this correlation was developed ranged from 750 to 3,000 times CBR. This relation has been widely used and is considered reasonable for fine-grained soil with soaked CBRs of 10 or less. The Asphalt Institute has also developed similar relationships that relate R-value to resilient modulus. For fine-grained soils, the correlation is:

$$M_r = 1000 + 555 \times (R - value) \tag{3}$$

Resilient modulus in fine-grained soils is not a constant stiffness property but is dependent upon many factors (Li et al. 1994). The authors have grouped the factors into three categories: (1) Loading conditions or stress states that include the magnitude of deviator and confining stresses, the number of repetitive loadings and their sequences; (2) soil type and its structure, which depends on compaction method and compaction effort for a new subgrade layer; (3) soil physical state, including moisture content and dry density that are subject to the change of environment.

Confining pressure and repeated deviator stress strongly affect resilient modulus. Relevant studies show that resilient modulus increases with increasing confining stress. However, confining pressure has a less significant effect compared to deviator stress, which is the most important factor affecting resilient modulus for fine-grained subgrade soils (Li et al. 1994). Resilient modulus decreases with increasing deviator stress. The number of stress applications also influences M_r, but if the deviator stress is below a certain level with regard to failure, M_r tends to be constant regardless of the number of stress applications.

Effects of Moisture Variation on Subgrade Resilient Modulus

The soil physical states presented by Li et al. (1994) consist of moisture content and dry density. These two quantities are related by the soil-compaction curve for a given compaction method. Thus, the author established the influence of soil physical state on resilient modulus by means of the compaction curves. Soil physical state can be changed by the effect of environment and the effect of compaction caused by traffic. In practice, moisture content in the subgrade layer significantly changes with seasons and ground water condition. Thawing time in the spring is a period when groundwater is high and the subgrade layer saturated.

For the case of constant dry density, correlation between resilient modulus and changes in moisture has been developed in relevant studies. Li et al. (1994) presented 27 repeated load triaxial test results on 11 fine-grained soils. The best fit polynomial equation for these data was:

$$R_{m1} = 0.98 - 0.28(w - w_{opt}) + 0.029(w - w_{opt})^2 \quad (4)$$

where $R_{m1} = M_r/M_{r\,(\mathrm{opt})}$ for the case of constant dry density; M_r is resilient modulus at moisture content w (%) and the same dry density as $M_{r\,(\mathrm{opt})}$; $M_{r\,(\mathrm{opt})}$ is resilient modulus at maximum dry density and optimum moisture content w_{opt} (%) for any compaction effort. The relation coefficient, r^2, is equal to 0.76.

The relation between resilient modulus with moisture content with the same compaction efforts was also developed. Twenty-six repeated load triaxial tests results of 10 fine-grained soils from literature were collected. The best fit polynomial equation for these data was:

$$R_{m2} = 0.96 - 0.18(w - w_{opt}) + 0.0067(w - w_{opt})^2 \quad (5)$$

where $R_{m2} = M_r/M_{r\,(opt)}$ for the case of constant compaction effort; M_r is resilient modulus at moisture content w (%) and the same compaction effort as $M_{r\,(opt)}$; The regression coefficient, r^2, is equal to 0.83.

According to these relationships, a small change of moisture content can result in significant changes in the resilient modulus. Given a constant dry density, M_r can be three times higher than $M_{r(opt)}$ if w is 5% lower than w_{opt}. M_r is equal to half of $M_{r(opt)}$ when w is 2% higher than w_{opt}. In case of constant compaction energy, M_r is approximately two times higher than $M_{r(opt)}$ if w is 5% lower than w_{opt}, and M_r is equal to half of $M_{r(opt)}$ when w is 3% higher than w_{opt}.

Drumm et al. (1997) studied the saturation effects on the subgrade resilient modulus, M_r, for use in the mechanistic design methods for flexible pavement. A series of resilient modulus tests were conducted to investigate the variation in M_r due to the increases of water content after compaction. The test results indicated that an increase of water content resulted in a decrease of the resilient modulus, though the magnitude of the decrease in M_r depended on the soil type. The AASHTO A-7-5 and A-7-6 soils had the largest M_r at optimum, but also had greater reduction in M_r with post-compaction water content than A-4 and A-6 soils.

PREVIOUS STUDIES

The Federal Highway Administration (FHWA) set guidelines for seasonal monitoring programs, outlining the instrumentation, installation methods and data collection (FHWA 1994). Several test sites across the United States have been instrumented to monitor long-term pavement performance (LTPP) and collect seasonal information. A seasonal monitoring site, as outlined by the FHWA, has not been located in Iowa prior to this investigation. A brief summary of previous test sites is given as follows.

Tennessee

Instruments were installed at four sites across Tennessee to monitor seasonal variations for factors affecting flexible pavement response. The four test sections were newly constructed roadways (Rainwater et al. 1999).

A weather station was installed at each of the test sites. Air temperature, precipitation, relative humidity, wind speed, and solar radiation were measured. During construction, thermistors and TDR probes were installed to collect temperature and water content data at different depths in the pavement system. Thermistors were installed at the same depth as the TDR probes. The TDR probes and temperature sensors were installed horizontally beneath the outer wheel path of the roadway from a trench constructed in the shoulder. Two pan lysimeters were installed in the stone subbase layer. Diverting the collected water from the lysimeters to a tipping bucket rain gauge made a direct measurement of infiltration. In addition to the automated instrumentation, the pavement response was monitored each month by FWD tests. The FWD tests permitted direct observation of seasonal effects on pavement response (Rainwater et at. 1999)

Bulk soil samples and undisturbed tube samples were collected to determine soil properties, including bulk density, in-situ water content, resilient modulus, and soil water characteristic curves. The subgrade materials classified as A-7-5(20), A-4(1), A-7-6(9) and A-7-6(20) according to the AASHTO classification system.

The Tennessee sites showed that subgrade volumetric water contents varied very little, except for brief periods after heavy rainfall events. Rainwater et al. (1999) speculated that because all four pavement sections were newly constructed, subgrade changes were small. In addition, they anticipated that as weathering and additional loading cycles occurred, the seasonal moisture changes would increase.

Ohio

US Highway 23 in Delaware County, Ohio, was equipped in 18 locations to monitor climatic effects on pavement performance constructed of asphalt concrete and portland cement concrete. The pavement instrumentations measured variations in temperature, moisture, and frost penetration to a depth of about six and one-half feet below the pavement surface. The groundwater table was also monitored. The instrument data was collected 14 times per calendar year (Heydinger 2003).

Ten TDRs for moisture content, one MRC thermistor probe for temperature, and one CRREL (Cold Region Research and Engineering Laboratory) resistivity probe to measure frost depth were installed at the test site. The instrument installation and monitoring followed the LTPP Seasonal Monitoring Program (SMP) manual. In addition, three tensiometers were installed under the roadway at depths approximately 0, 12, and 24 inches below the subbase layer.

The aggregate subbase material classified as A-1-a and the subgrade materials classified as A-6 and A-7-6 under the AASHTO classification system. The liquid limit ranged between 29 and 40 and the plasticity index between 12 and 20.

Heydinger (2003) found that sinusoidal equations could be used to develop expressions for the seasonal variations of temperature and moisture as a function of time (based on five years of data). Heydinger suggested additional research to verify these findings and to develop expressions for the seasonal variations of soil temperature and moisture.

Montana

Several seasonal monitoring sites were located in Montana. Zhou et al. (1994) reported on a test section located along US Highway 12, approximately 60 miles northwest of Billings, Montana. This test section consisted of three inches of asphalt concrete over approximately 19 inches of crushed gravel aggregate subbase on subgrade composed predominately of sandy clay with silty sand. Zhou et al. (1994) followed the LTPP guide and installed a thermistor probe, 10 TDR sensors, and a CRREL resistivity probe in one 14-inch square hole located in the outside wheel path. In addition, an observation well was installed about 100 feet from the instrumentation hole along the edge of the pavement shoulder. Deflection measurements were performed with a FWD following LTPP protocols. The deflection data was analyzed using two back calculation programs, MODULUS and BOUSDEF. The pavement structure was modeled as a three-layer system.

Janoo et al. (2000) studied 10 flexible pavement sites across Montana to monitor seasonal variations with a focus on spring thawing. These test sites were selected based on the classification of the subgrade soils. The base courses classified mainly as A-1, and the subgrade soils classified as A-1, A-4, A-6, and A-2-4 under the AASHTO classification system. Each site was instrumented with seven to eight VITEL Hydra soil probes. The VITEL Hydra probe determines the soil temperature and moisture content. The pavement response was evaluated using a FWD on a monthly basis, except during the spring thaw, when it was evaluated biweekly.

Zhou et al. (1994) found that when frozen, the subbase and subgrade moduli increased. In addition, the authors found that most temperature variations were in the upper 20 inches of the pavement, but temperature changes (about 30 °F) were also found about seven-feet deep in the subgrade. The FWD deflections were higher in warmer months (September, October, and

November) than colder months (December and February). Janoo et al. (2000) found that the length of thaw weakening varied from four days to three weeks. In addition, it was found that during the spring thaw, the moisture content in the base and subgrade increased rapidly when the ground temperature was around -2°C.

SITE DESRIPTIONS AND MATERIALS

Geomorphic Description Soil Classification

Soils expected to be encountered for the pavement of the new US 20 from County Road D20 East to US Highway 169

Soils within the project area are part of the Webster-Clarion-Nicollet association. Table 1 summarizes the soil types identified within the project area. A sketch of typical relief and positions of soils within the Webster-Clarion-Nicollet association are shown in Figure 1. The topography of the site was mainly level with maximum slopes of 5% and most was within the range of zero to 3%. Exact bedrock elevations were not determined. However, bedrock elevations were at a depth greater than 60 inches. The groundwater table in the project area reportedly ranges from the ground surface to 6 feet below.

Table 1. Soils expected to be encountered (modified from USDA, 1975)

Symbol	Soil type	Slope, %	Depth to WT	Depth to bedrock
6	Okoboji silty clay loam	0 to 1	+1' to -1'	>60"
55	Nicollet loam	1 to 3	1.0 to 3.5 feet	>60"
95	Harps clay loam	0 to 2	0 to 1 foot	>60"
107	Webster silty clay loam	0 to 2	1 to 3 feet	>60"
138	Clarion loam	2 to 5	4 to 6 feet	>60"
507	Canisteo clay loam	0 to 2	0 to 1 foot	>60"

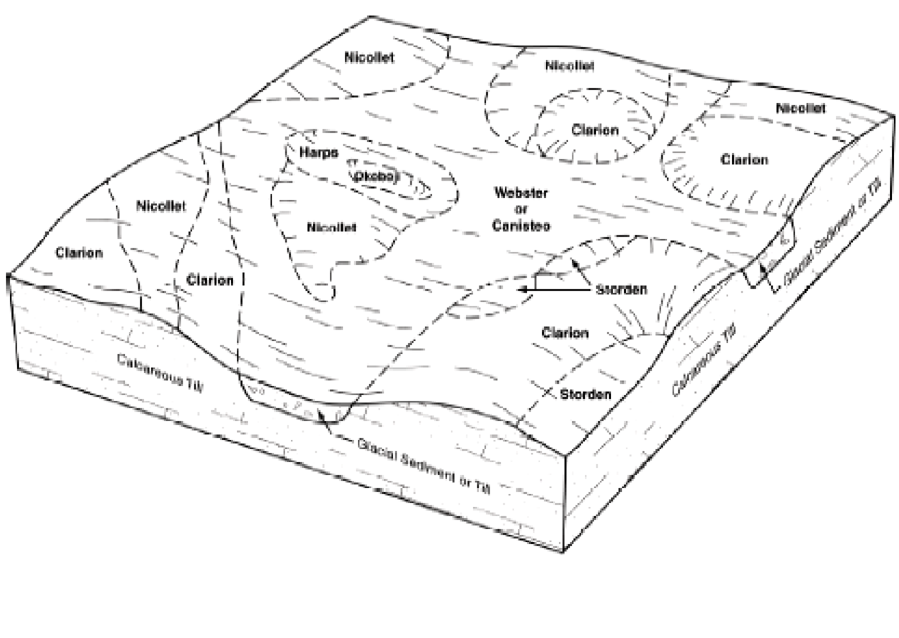

Figure 1. Typical pattern of soils and parent materials in the Webster-Clarion-Nicollet association (USDA, 1975)

Engineering Classification

The soil located in the project area ranged from very poorly drained to moderately well drained. The soil varied from silty clay, silty clay loam, clay loam, and sandy loam. Following the Unified Soil Classification System, the soil is classified as clay with low plasticity, clay with high plasticity, silt with low plasticity, silt with high plasticity, clayey sand, and clayey silt. Following the AASHTO system, the soil is classified under groups A-4, A-6, and A-7. Table 2 summarizes each soil type and the respective classification.

Table 2. Soil classifications (modified from USDA, 1975 and Natural Resources Conservation Service)

Soil type	USDA texture	Unified classification	AASHTO
Okoboji silty clay loam	silty clay loam, silty clay	CL, CH	A-7
Nicollet loam	clay loam, loam, silty clay loam	ML, CL	A-6, A-7
Harps clay loam	loam, clay loam, sandy loam	CL, CH, CL-ML, SC-SM, SC	A-4, A-6, A-7
Webster silty clay loam	silty clay loam, clay loam, loam	CL, CH	A-6, A-7-5, A-7-6
Clarion loam	loam, clay loam, sandy loam, silt loam	CL, CL-ML, SC, SC-SM	A-4, A-6
Canisteo clay loam	clay loam, loam, silty clay loam	CL, CL-ML, SC, SC-SM	A-6, A-7

Potential Construction Problems

The combination of a high water table and high clay content makes the project site problematic. The severe shrink-swell of the soil has the potential to damage roadways (Table 3, Table 4). Flooding of the site is possible with an intense rain event coupled with a high water table. Excavations may require dewatering devices to mitigate ponding. Low soil strengths may hamper construction equipment from maneuvering the project site. Uncoated steel has a high risk of corrosion (Table 5). The potential for frost action is high. Limited engineering laboratory test results are available for some of the soils expected to be encountered (Table 6).

Table 3. Construction issues (modified from USDA, 1975)

Soil type	Roads and streets	Shallow excavations
Okoboji silty clay loam	Severe: shrink-swell, low strength, ponding	Severe: ponding
Nicollet loam	Severe: low strength, frost action	Moderate: wetness
Harps clay loam	Severe: low strength, frost action	Severe: wetness
Webster silty clay loam	-	
Clarion loam	Moderate: frost action	Slight
Canisteo clay loam	Severe: low strength, frost action	Severe: wetness

Table 4. Physical properties (modified from USDA, 1975)

Soil type	Clay content (%)	Shrink-swell potential
Okoboji silty clay loam	35-42, 20-30(36-60")	high, moderate(36-60")
Nicollet loam	22-35	moderate, low(40-60")
Harps clay loam	18-30	moderate
Webster silty clay loam	-	moderate
Clarion loam	12-30	low
Canisteo clay loam	20-35	moderate, low(42-60")

Table 5. Chemical properties (modified from USDA, 1975)

Soil type	pH	Potential frost action	Risk of corrosion	
			Uncoated steel	Concrete
Okoboji silty clay loam	6.6-8.4	high	high	low
Nicollet loam	5.6-8.4	high	high	low
Harps clay loam	-	high	high	low
Webster silty clay loam	6.6-8.4	-	-	-
Clarion loam	5.6-8.4	moderate	low	low
Canisteo clay loam	7.4-8.4	high	high	low

Table 6. Standard Proctor properties (modified from USDA, 1975)

Soil type	Moisture density	Liquid limit	Plasticity index
Okoboji silty clay loam	82/25, 85/27, 84/25	63, 65, 66	33, 37, 39
Nicollet loam	91/24, 99/20, 104/21	46, 43, 35	20, 23, 16
Harps clay loam	-	-	-
Webster silty clay loam	-	-	-
Clarion loam	102/18, 104/18, 115/14	36, 36, 27	15, 17, 11
Canisteo clay loam	-	-	-

Subgrade Material Classification

Glacial till material from a local borrow area was used to build the subgrade layer. Soil samples were taken to determine grain size distribution and classification in the lab, as shown in Figure 3.

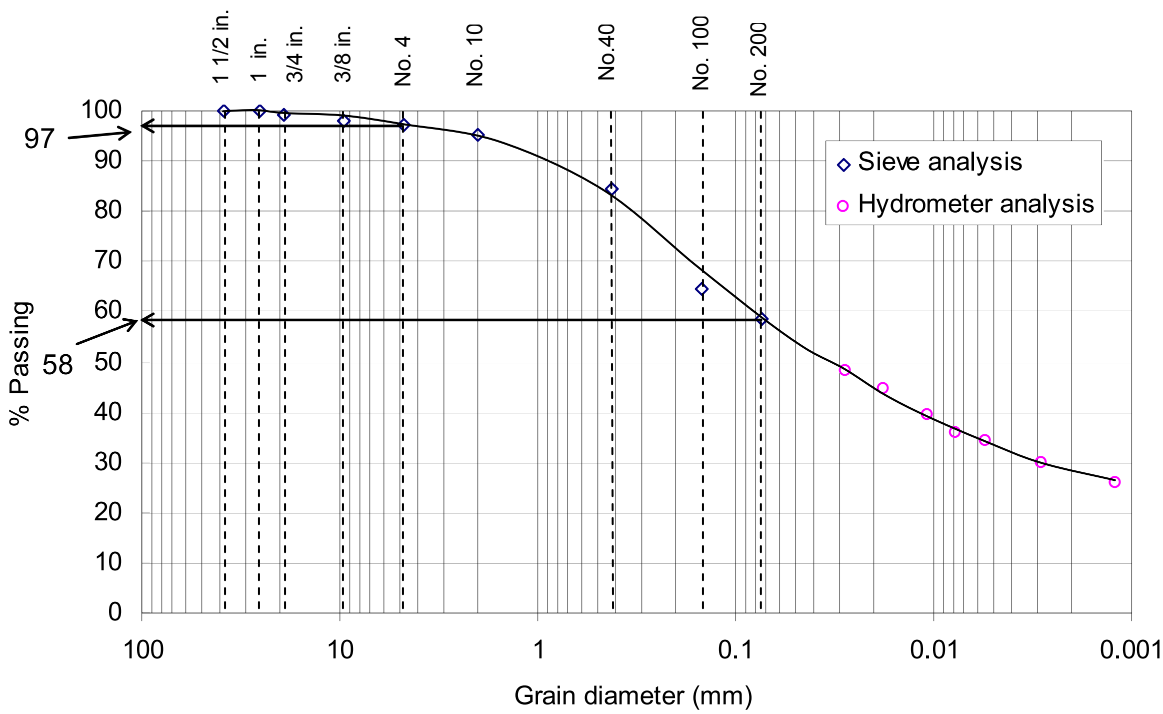

Figure 2. Grain size distribution curve of the subgrade material during construction period

A bulk sample of material excavated from the in-ground installation trench was returned to the laboratory for testing. After air drying the bulk sample, modified and standard Proctor compaction tests were completed on material passing the #4 sieve. In addition, grain size distribution (including hydrometer analysis) and Atterberg limits tests were completed on the bulk sample. The following graphs show the results of the laboratory testing.

Table 7. Atterberg limits results

Sample ID	Liquid Limit (LL)	Plastic Limit (PL)	Plasticity Index (PI)
Bulk sample	28	16	12

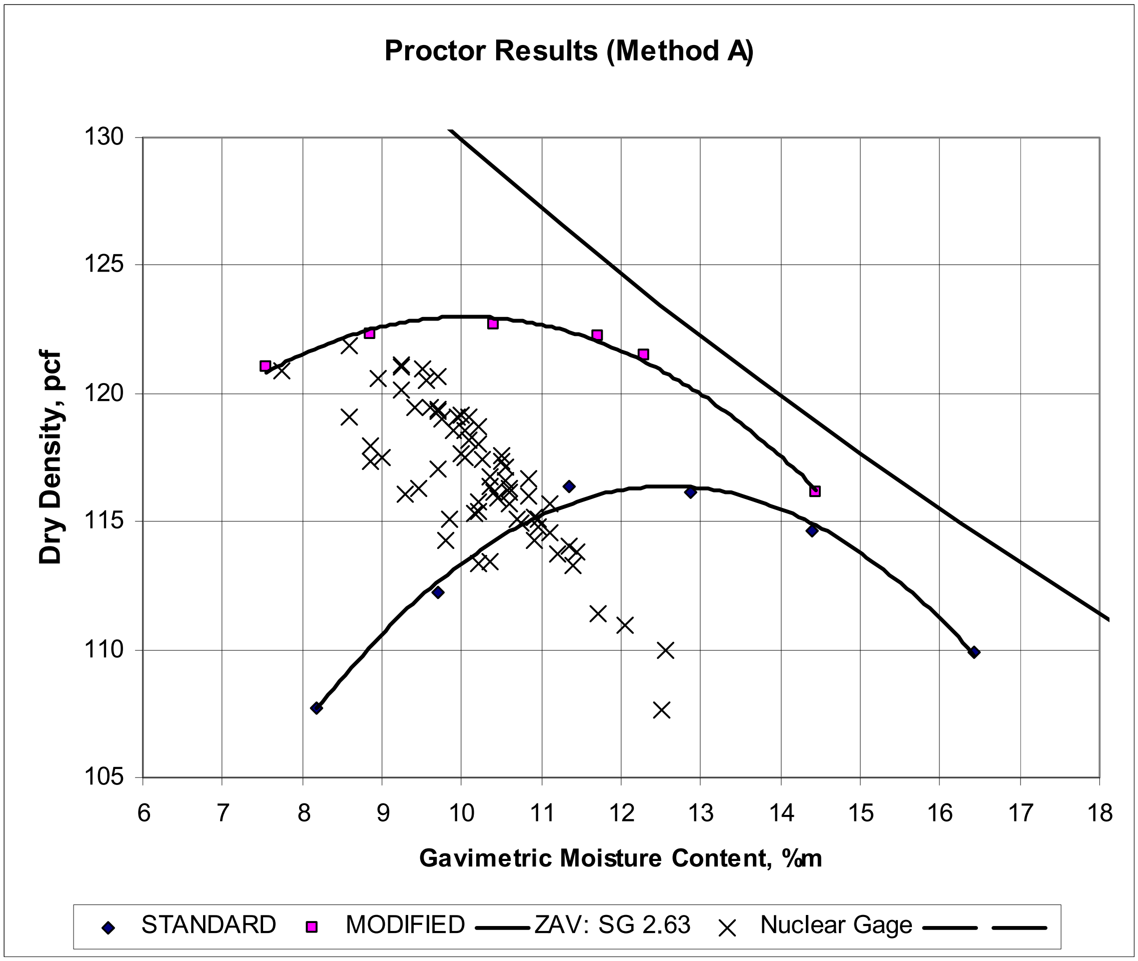

Figure 3. Standard and modified Proctor results

Table 8. Proctor results

Compaction Energy	Maximum Dry Density	Optimum Moisture Content
Standard Proctor	116.5 pcf	12.5%
Modified Proctor	123.0 pcf	10.0%

Based on the results of the laboratory testing, subgrade materials at the test site classify as A-6(4) according to the AASHTO classification system. In the USCS system, the soil is classified as silty clay (CL).

FIELD INSTRUMENTATION

Site Description

The project site for this study was located along US 20 (mile marker 119.90) about one-half mile west of Kansas Avenue in Fort Dodge, Iowa. A test section was selected to determine the spatial and seasonal variations of pavement foundation properties (i.e., density, moisture content, temperature, etc.). Similar studies have been conducted across the United States through the SMP and LTPP programs, although none have been previously completed in Iowa.

Field tests were conducted on the newly compacted subgrade to document spatial variation in stiffness parameters. Field instrumentation was also installed to monitor seasonal variation in moisture content, temperature, freeze/thaw depth in subgrade and subbase layers. Air temperature, ground water table and rainfall have also been collected. The data logger was installed at station 930+00 (M).

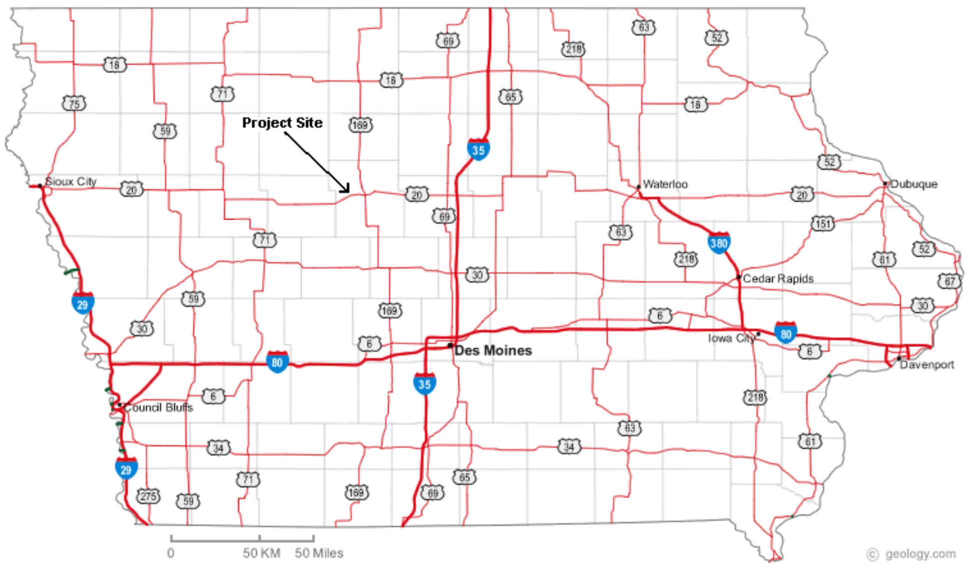

Figure 4. Plan view of the US 20 project in Webster County

Before the test section was paved, the spatial variation of density, moisture content, and strength in the subgrade was determined using a nuclear moisture/density gage, DCP and Clegg hammer. The layout of instruments installed in the test section closely followed the SMP guidelines. The instruments monitored and recorded site conditions, which include the depth to the groundwater table, the depth of frost penetration, the volumetric moisture content of the subbase and subgrade layers, the temperature profile of the pavement, subbase, and subgrade layers, and a limited weather station measuring air temperature and rainfall events. A large bulk sample was collected during installation and several thin-walled Shelby tubes were pushed after paving was complete for laboratory testing.

Figure 5. Aerial photo of project site

Field Instrumentation

Ten TDR probes, 10 temperature sensors, one resistivity probe, and two piezometers were installed at station 930+00. Table 9 summarizes the instrumentation and respective positions/elevations.

The project site was instrumented with several sensors closely following the LTPP guidelines to monitor the in situ conditions over an extended period of time. The installation of the instruments in the pavement subgrade was completed using a vertical trench excavated near the pavement shoulder, and the sensors placed into the trench wall (see Figure 6). This method was used to reduce disturbance to the in-situ materials. Figure 7 through 13 show the plan, profile and cross-section views of the instrumentation installation.

Table 9. US 20 instrument elevations

Sensor I.D.	Depth below roadway surface (ft)
Temperature iButton 1	0.17
Temperature iButton 2	0.75
Temperature iButton 3 & TDR 1	1.10
Temperature iButton 4 & TDR 2	1.28
Resistivity Probe (top)	1.32
Temperature iButton 5 & TDR 3	1.74
Temperature iButton 6 & TDR 4	2.21
Temperature iButton 7 & TDR 5	2.82
Temperature iButton 8 & TDR 6	3.31
TDR 7	3.75
Temperature iButton 9 & TDR 8	4.25
TDR 9	4.73
Temperature iButton 10 & TDR 10	5.21
VW Piezometer 1	13.86
VW Piezometer 2	13.82

Figure 6. Vertical trench for sensor installation

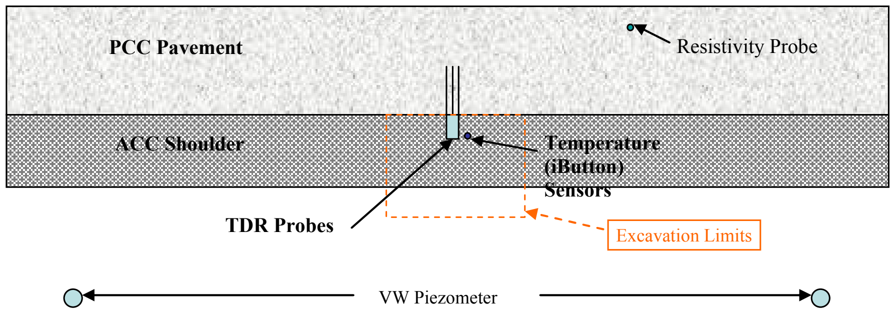

Figure 7. Plan view of instrumented data logger

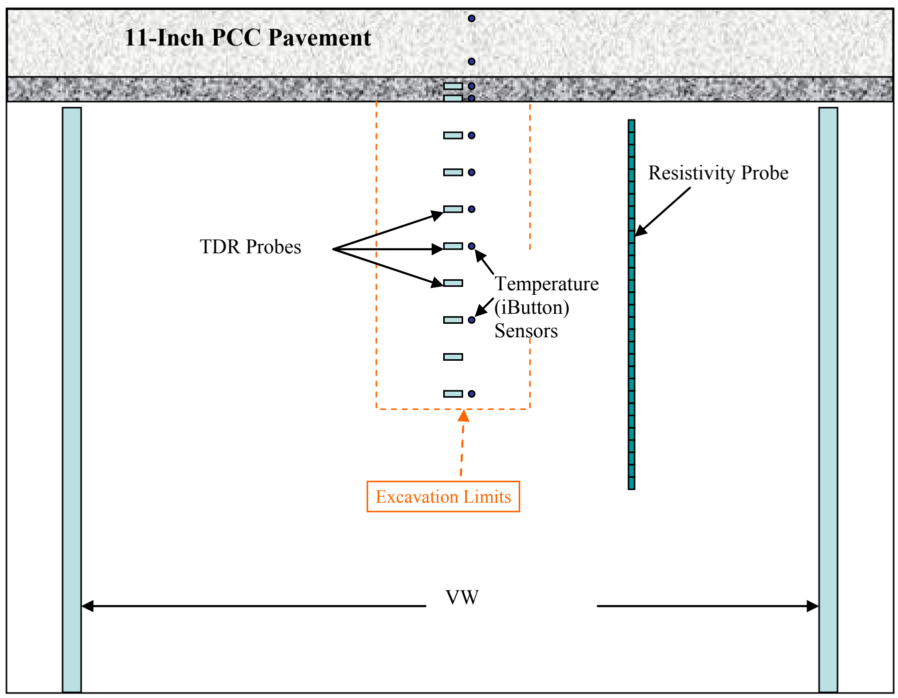

Figure 8. Profile view of instrumentation

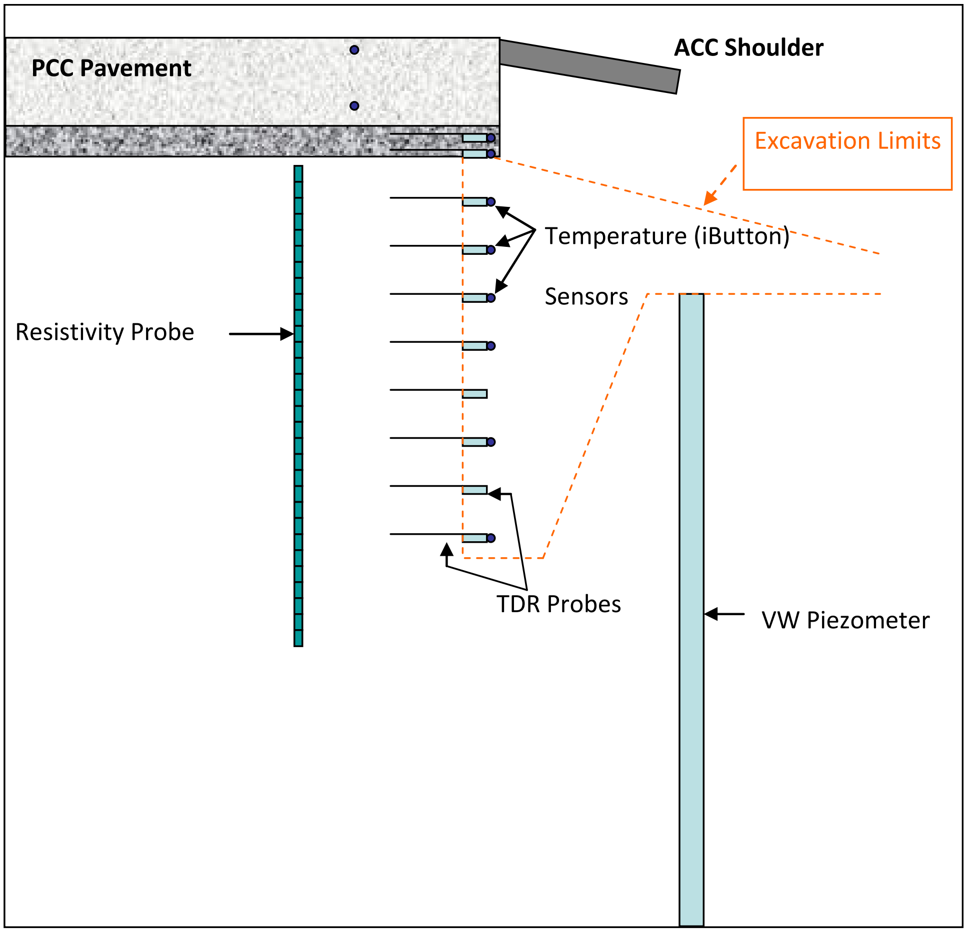

Figure 9. Cross-section view of installation

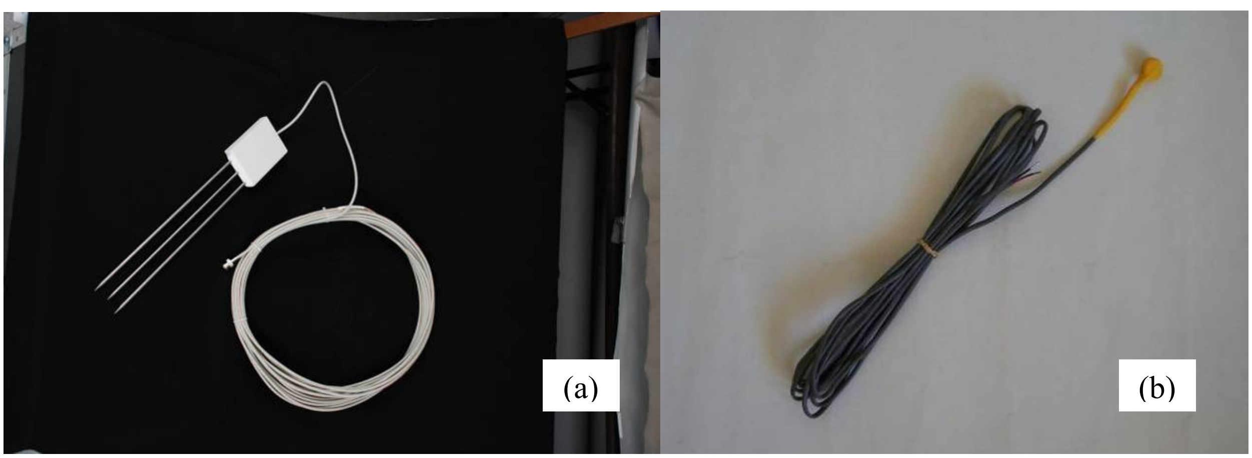

Figure 10. Installation sensors: a) TDR probes; b) Temperature iButton sensor

Figure 11. Resistivity probe

Figure 12. Instrumentation installation at station 930+00

Figure 13. Data logger at station 930+00 during installation process

SPATIAL VARIABILITY

Field Measurements

The study section was tested to determine spatial variability of the subgrade soils approximately one week prior to placement of the aggregate subbase layer. The Clegg impact hammer, DCP, and nuclear moisture density gauge were used to quantify variability. A test grid was developed that extended beyond the planned sensor installation location by approximately 50 feet to the east and west. The test locations were spaced six feet apart in the east-west and north-south directions. The test grid consisted of four rows spanning the two lanes of westbound traffic, and 16 columns for a total of 64 test locations. Figures 14–18 show testing of the subgrade prior to paving.

Figure 14. Eastern half of the US 20 test grid

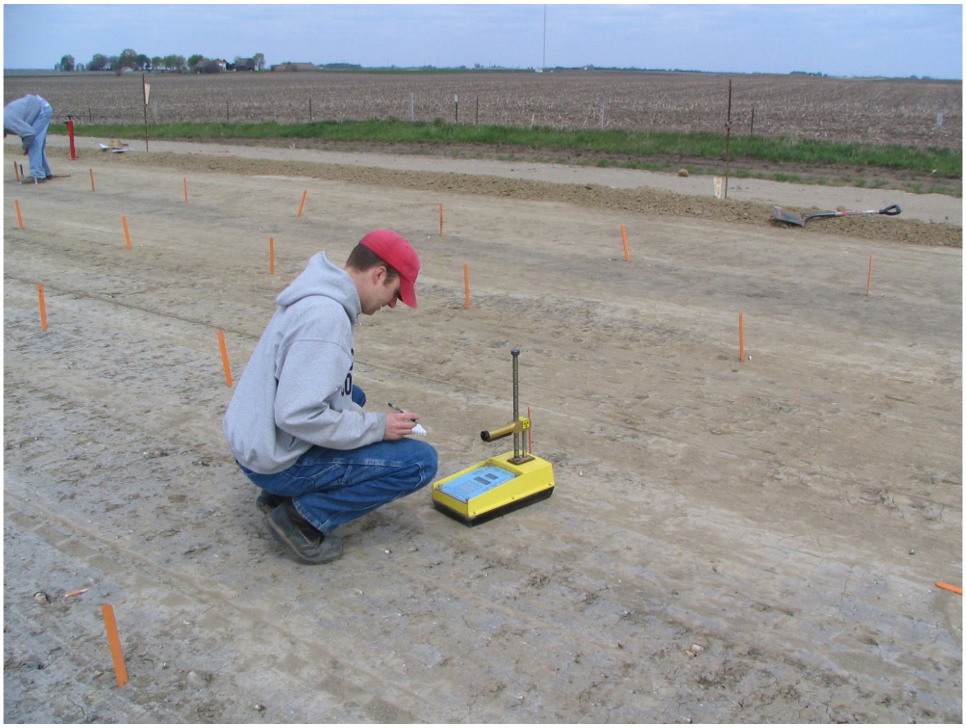

Figure 15. Nuclear moisture density gage testing

Figure 16. Clegg Impact Hammer testing

Figure 17. Cobbles included as part of subgrade

Figure 18. Cobbles removed during final grading

A description of the equipment used to obtain the field measurements is provided below.

Clegg Impact Hammer

The Clegg Hammer consists of a 4.5-kg drop weight inside a guide housing. The hammer is raised to a height of 450 millimeters and then released. When the hammer weight is dropped, the deceleration is recorded as the hammer strikes the ground surface. The maximum deceleration is then converted into a Clegg impact value (NCHRP 1999). Clegg impact values were converted to CBR values using the following equation:

$$CBR = [0.24(CIV) + 1]^2 \qquad (6)$$

Dynamic Cone Penetrometer (DCP)

The DCP consists of driving a cone tip using a 17.6 pound drop hammer, with a fall height of 22.6 inch. For each hammer blow, the penetration depth is recorded. The penetration per hammer blow is the DCP penetration index (DPI). DPI was converted to CBR value following ASTM D6951-03 and the equation:

$$CBR = 292 / DPI^{1.12} \qquad (7)$$

Nuclear Moisture Density Gage

The nuclear gage contains two radioactive elements: Cesium 137 and Americium-Beryllium. The Cesium releases gamma energy that is detected by a Geiger counter to determine the density of the measured material. The Americium-Beryllium releases free neutrons that react with the hydrogen in the surrounding material and are measured by a neutron detector to estimate the moisture content. The nuclear test results are provided in Figure 5 and show that the in-situ densities were generally between standard and modified Proctor density and the moisture contents were dry of standard optimum moisture content.

Data Analysis (Kriging)

The results of field tests were analyzed using a statistical technique known as kriging. Kriging is a linear least squares estimation algorithm. This technique is used to interpolate some variable over an area where known values were recorded. In this study, the field test results (i.e., DCP CBR value, density, moisture, etc.) along the test grid are used to develop a topographic style graph. The kriging results are shown in the following figures.

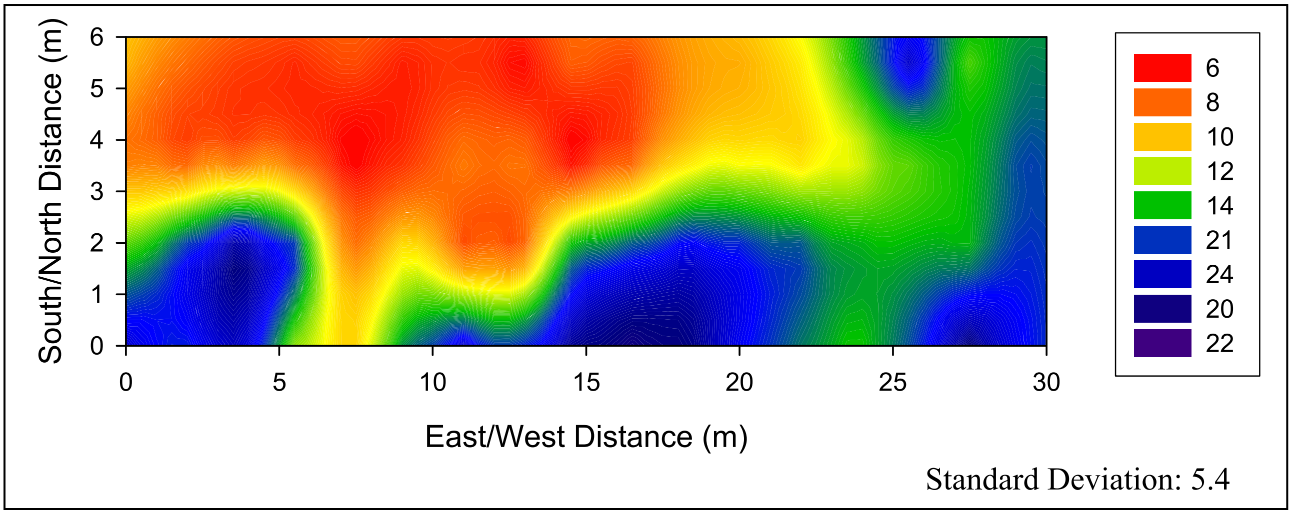

Figure 19. Kriging output - Clegg Impact Hammer

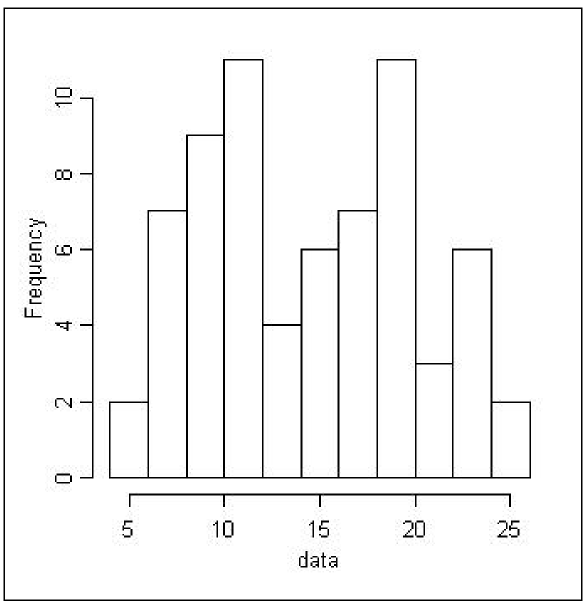

Figure 20. Histogram - Clegg Hammer

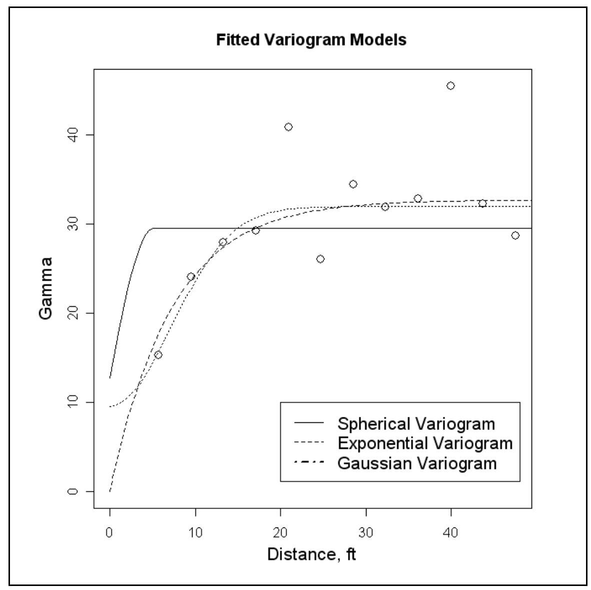

Figure 21. Variogram - Clegg Hammer

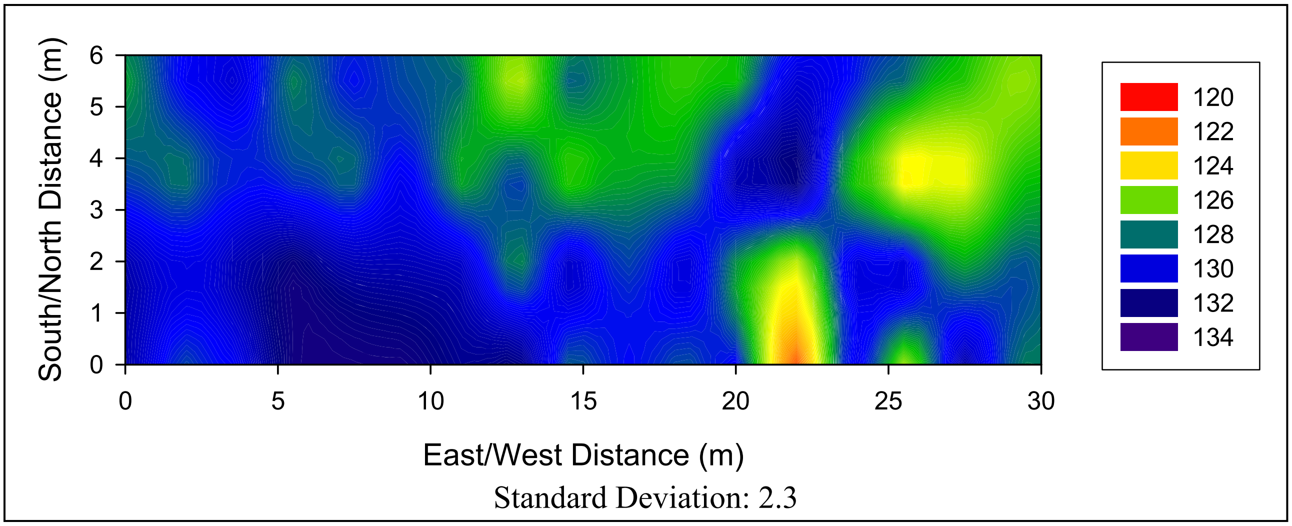

Figure 22. Kriging output - nuclear densities

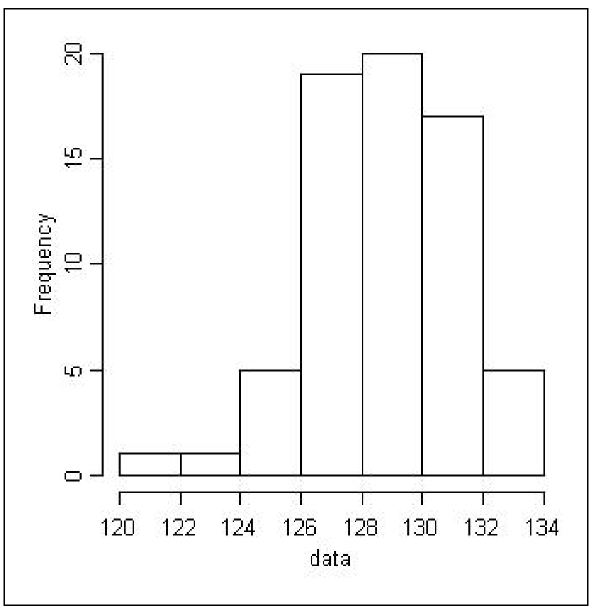

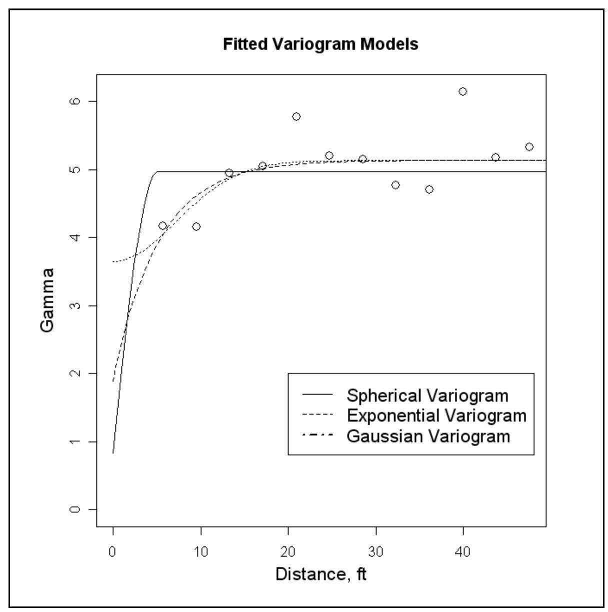

Figure 23. Histogram - nuclear density

Figure 24. Variogram - nuclear density

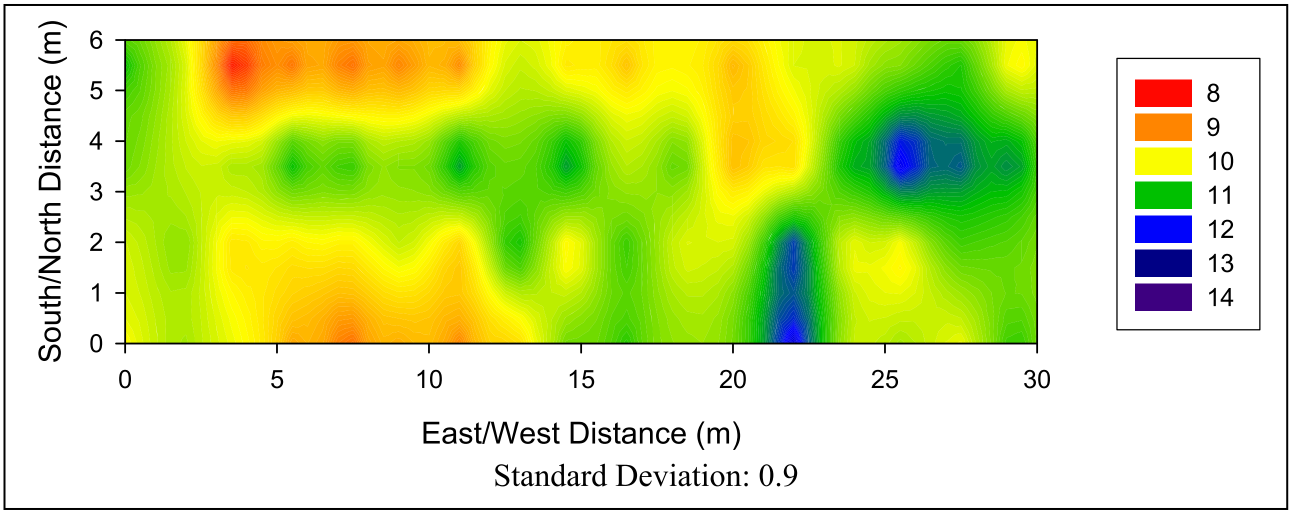

Figure 25. Kriging output - nuclear moistures

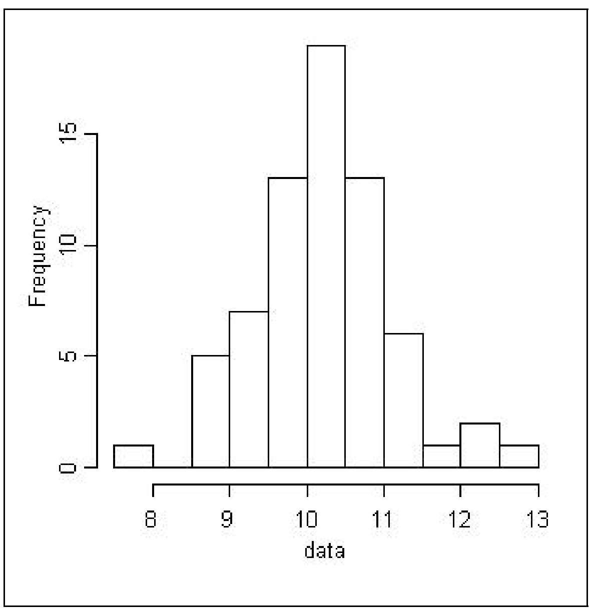

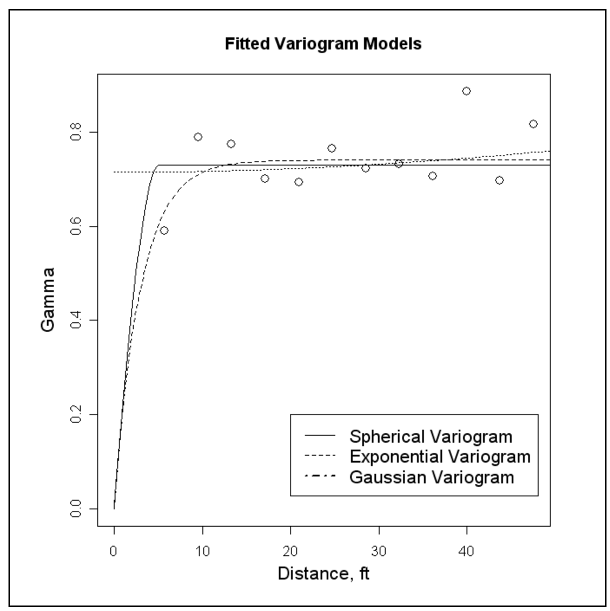

Figure 26. Histogram - nuclear moisture

Figure 27. Variogram - nuclear moisture

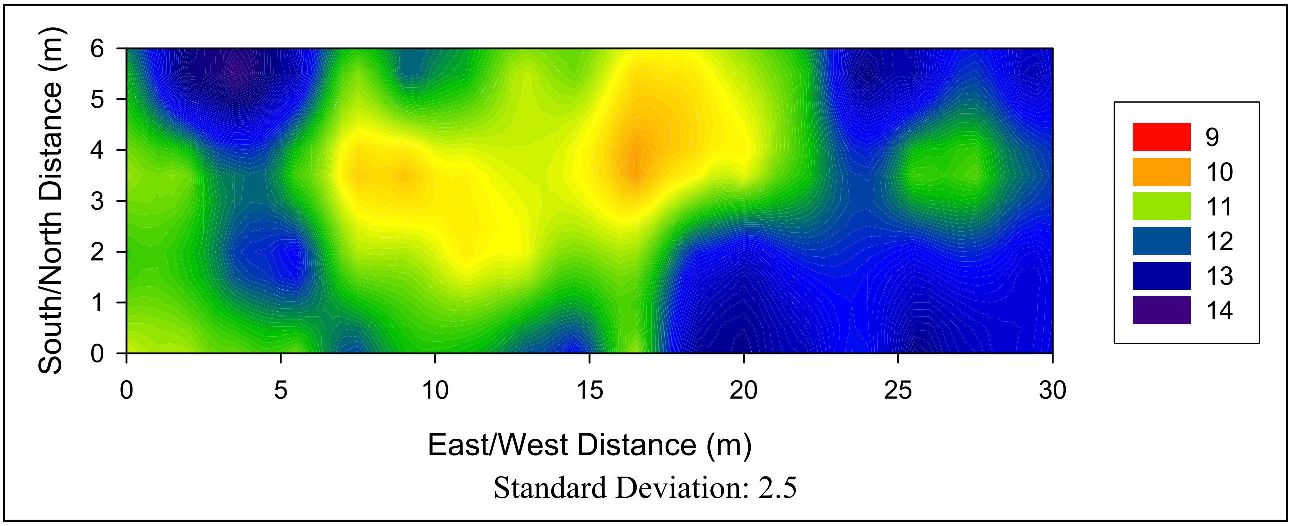

Figure 28. Kriging output - DCP CBR values (0 to 1 foot)

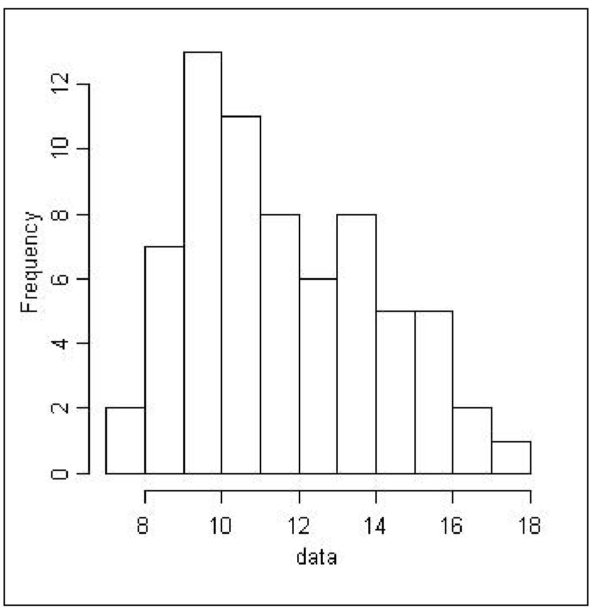

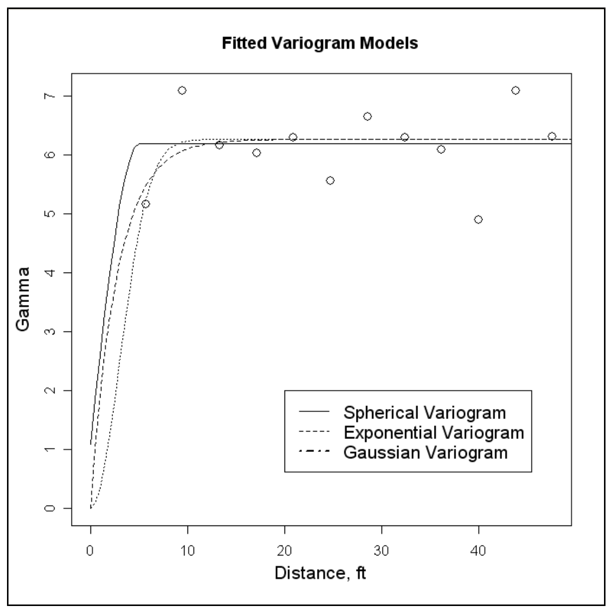

Figure 29. Histogram - CBR (0 to 1 foot)

Figure 30. Variogram - CBR (0 to 1 foot)

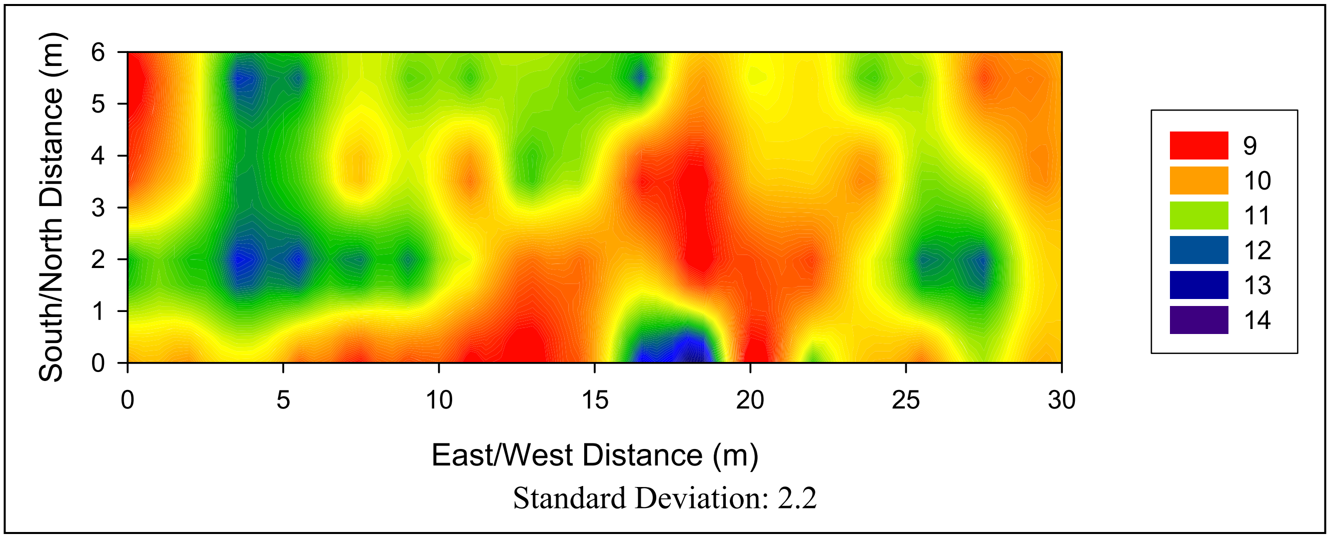

Figure 31. Kriging output – DCP CBR values (1 to 2 feet)

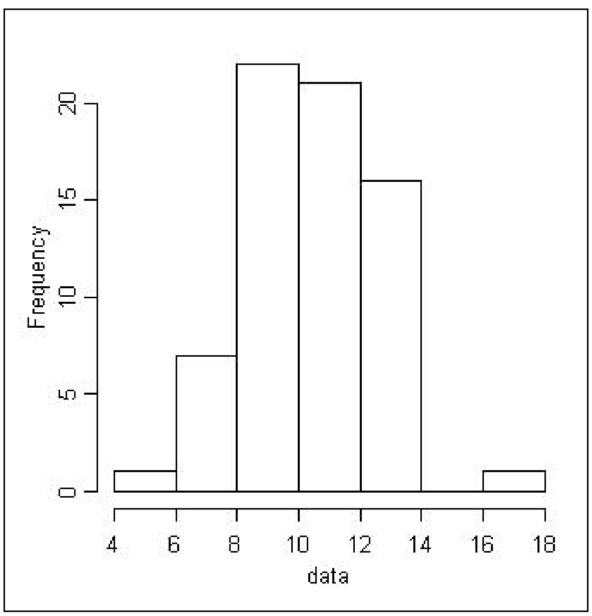

Figure 32. Histogram - CBR (1 to 2 feet)

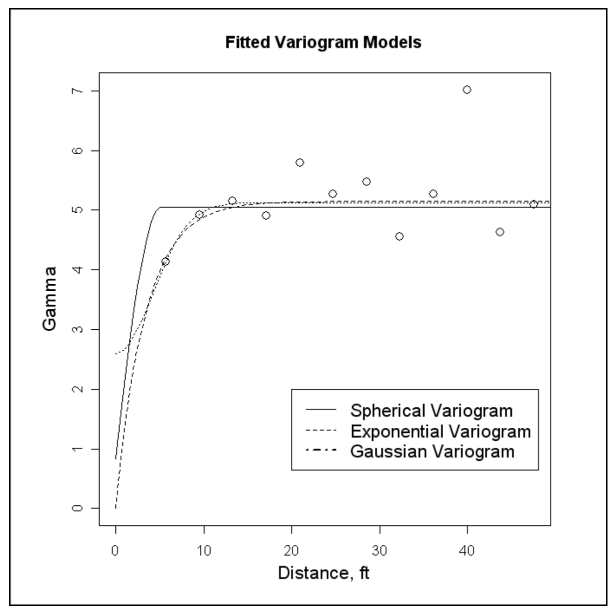

Figure 33. Variogram - CBR (1 to 2 feet)

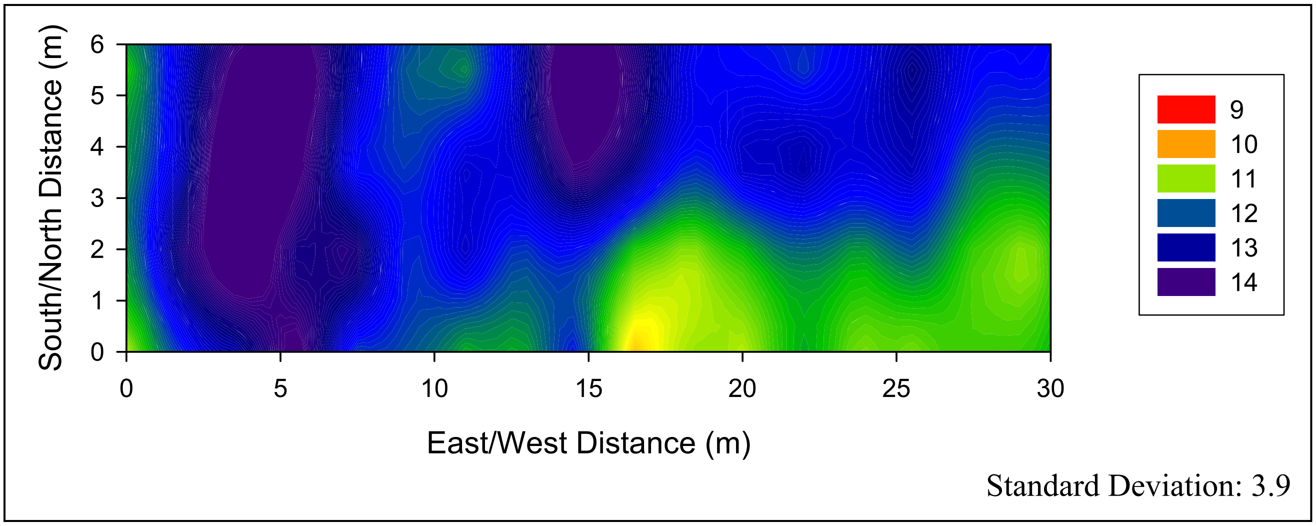

Figure 34. Kriging output – DCP CBR values (2 to 3 feet)

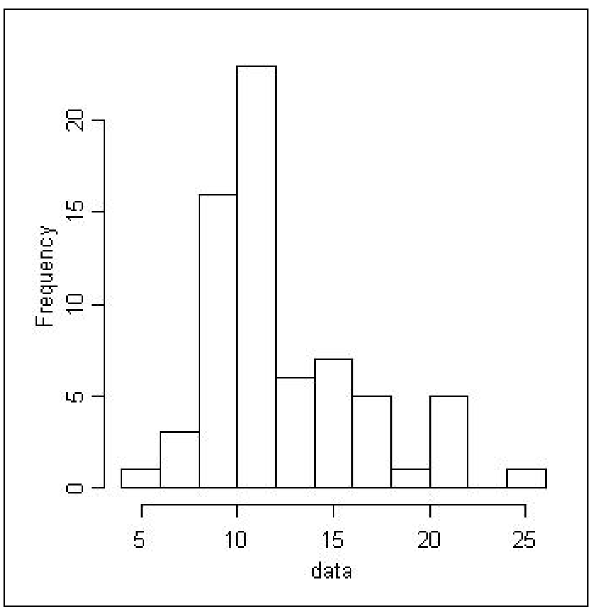

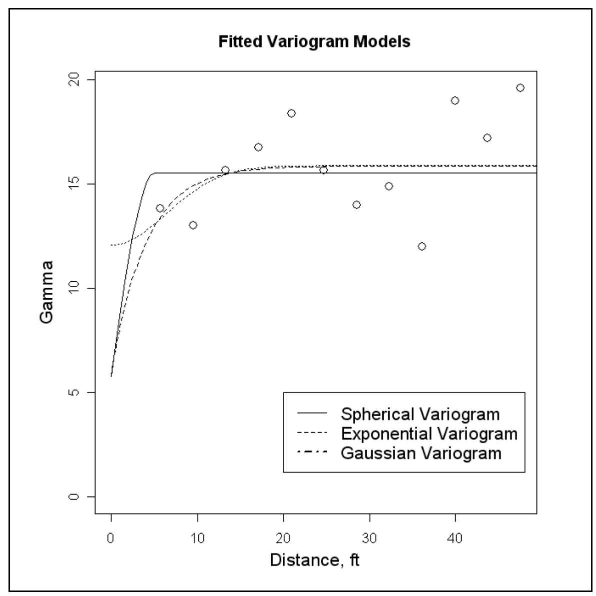

Figure 35. Histogram - CBR (2 to 3 feet)

Figure 36. Variogram - CBR (2 to 3 feet)

Table 10. Summary of kriging correlation distances

Data set	Correlation distance, feet		
	Spherical variogram	Exponential variogram	Gaussian variogram
Clegg impact hammer	3.7	14.2	9.0
Nuclear density	2.3	14.2	7.7
Nuclear moisture content	3.3	---	5.0
Weighted DCP CBR (0 to 1 foot)	3.3	6.5	3.8
Weighted DCP CBR (1 to 2 feet)	3.0	8.5	4.7
Weighted DCP CBR (2 to 3 feet)	3.2	12.8	4.7

The grid spacing of the US 20 test section was six feet in the north-south and east-west direction. A correlation distance that was smaller than the test data spacing indicates that the data points were independent of each other. Given the data set for this project, predictions could not be made using a spherical variogram model for any of the field tests. A Gaussian variogram model could not be used to predict moisture contents or CBR values. In addition, the Gaussian variogram model predictions of density and the Clegg Impact value were limited; i.e., the correlation distances were 7.7 feet and 9 feet, respectively.

The exponential variogram model appeared to fit the data best. The correlation distance for the field testing (excluding moisture content) ranged from 6.5 feet to 14.2 feet. The exponential model for the nuclear moisture content did not have an initial tangent, resulting in a correlation distance of zero. The kriging plot of Clegg hammer impact values showed a definite east-west correlation, which may reflect the construction sequence typically used for highway fill. In general, a truck unloads fill materials, which are then spread in the direction of the road alignment and then compacted in the same direction. Such a system should result in a strong correlation in a direction parallel to the roadway alignment. The nuclear density data less clearly shows a trend. It was expected that the moisture content would also show a strong correlation along the alignment of the roadway, but all three variogram models resulted in a correlation distance less than the grid spacing.

Table 11 summarizes the average values of in-situ measurements during construction. In this table, the Clegg Impact value is the average the CIV values measured on the surface of the subgrade layer. CBR values and resilient modulus were estimated using Clegg hammer measurements. The DPI indices with different depths were calculated by averaging the normalized DPI values for each layer. CBR-DPI values and resilient modulus, M_r – CBR DPI, were estimated based on the DPI values. The average moisture content of 10.2% was within the range of optimum moisture contents for Standard and Modified Proctor tests 10%-12.5%. The average dry density measured by nuclear gauge was 116.5 pcf, which was equal to the maximum dry density obtained from the Standard Proctor tests.

Table 11. Summary of average In-situ Measurements Values

Measurements	Average	Coefficient of Variation (%)
Clegg Impact Value	14.4	38
CBR - Clegg	21.5	56
M_r – CBR Clegg (MPa)	222	56
DPI (mm/blow)		
0 -1 ft	18.4	190
1-2 ft	20.3	20
2-3 ft	18.2	28
CBR - DPI (mm/blow)		
0 -1 ft	11.6	21
1-2 ft	10.5	21
2-3 ft	12.4	32
M_r – CBR DPI (MPa)		
0 -1 ft	120	21
1-2 ft	108	21
2-3 ft	128	32
Moisture Content (%)	10.2	8.8
Dry Density (pcf)	116.5	1.8
% Compaction (based on standard Proctor compaction energy	100.0%	-
% Compaction (based on modified Proctor compaction energy	94.7%	-

SEASONAL VARIATION MEASUREMENT

The seasonal variation study was established for long-term monitoring. A weather station was installed at the data logger location to measure air temperature and precipitation. The pavement instrumentation measured variations in moisture content, temperature, groundwater table, and frost depth in the subgrade and subbase layer. The data were collected during the period from May 2005 to April 2008 were analyzed.

Air Temperature, Rainfall, and Ground Water Table

A thermistor, protected by a radiation shield, and a tipping bucket rain gage were used to record seasonal variations in air temperature and rain events, respectively. The air temperature probe was placed in a radiation shield to limit the effects of direct sunlight on the sensor readings. The air temperature was recorded every five minutes with an average value being stored once per hour.

Air temperature was collected automatically every hour beginning May 7, 2005. Figure 37 shows the air temperature from May 7, 2005 to March 9, 2007. Due to some unknown reason, some data are missing in two periods—from June 2, 2005 to June 30, 2005 and from September 9, 2005 to November 7, 2005. The Iowa Environmental Mesonet (IEM) and the Iowa State University Department of Agronomy also collect air temperature near Fort Dodge (Figure 38). Data from these two sources provided similar air temperature variations during the same period of time.

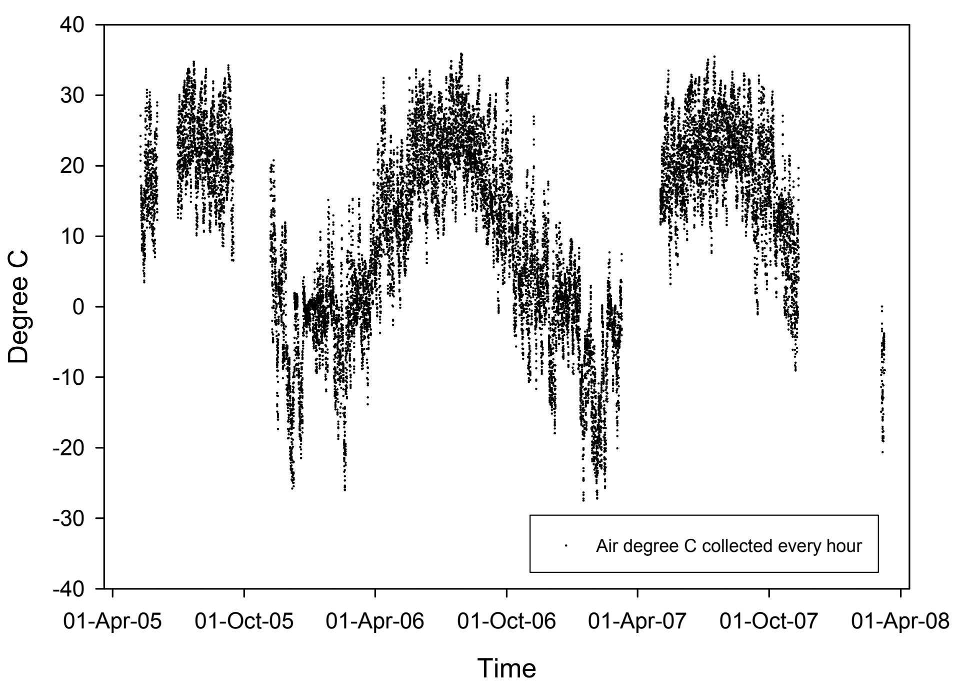

Figure 37. Air temperature from May 2005 to April 2008

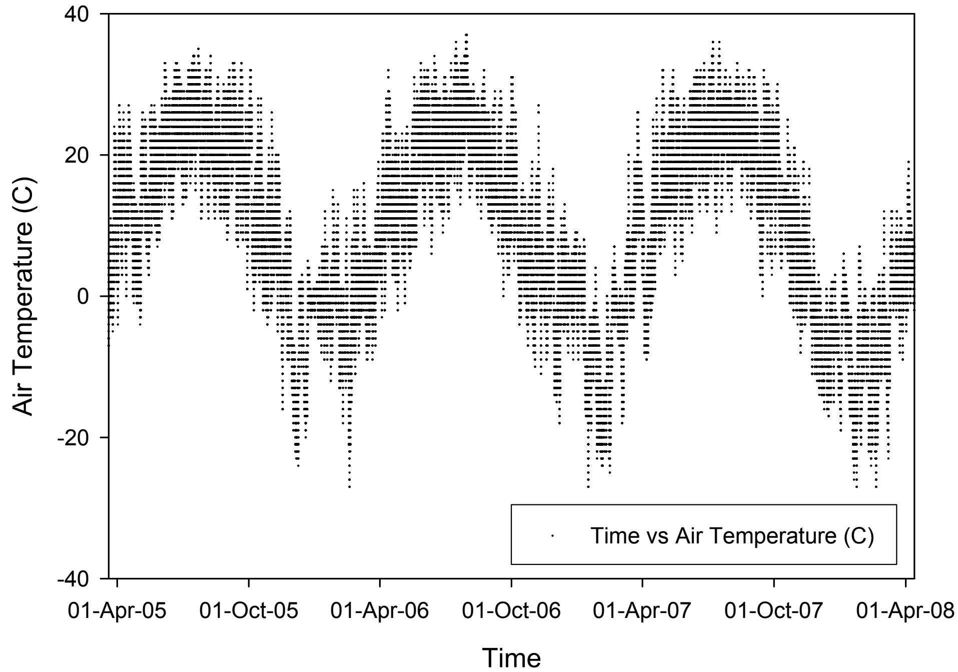

Figure 38. Air temperature from May 2005 to April 2008 (Source: IEM)

The rain gage used during the study collected precipitation that was funneled into a calibrated bucket mechanism. The rain gage then recorded the number of times a "bucket" tipped. Once a certain volume of water was collected, the water weight caused the bucket mechanism to tip over, resetting the process. The rain gage was calibrated so that each tip was equivalent to 0.01 inches of rainfall. The number of bucket tips was stored once per hour.

Figure 39 shows the rainfall in inch per hour collected from the weather station of the project from May 7, 2005 to March 9, 2007. Rainfall fluctuated with high values in the early stage of measurement, from May 2005 to August 2005, but the hourly precipitation was low from August 2005 to March 2007. During the same period of time from May 2006 to August 2006, the collected data seemed to provide a low value of rainfall. The precipitation in inch per hour in the same period obtained from IEM for the Fort Dodge station is shown in Figure 40. In a year, the rainy season goes from April to September. The figure clearly shows the variations of precipitation with time. This data was used to check the precipitation data obtained from the project weather station. It suggests that the data collected from the field station was not reliable during some periods.

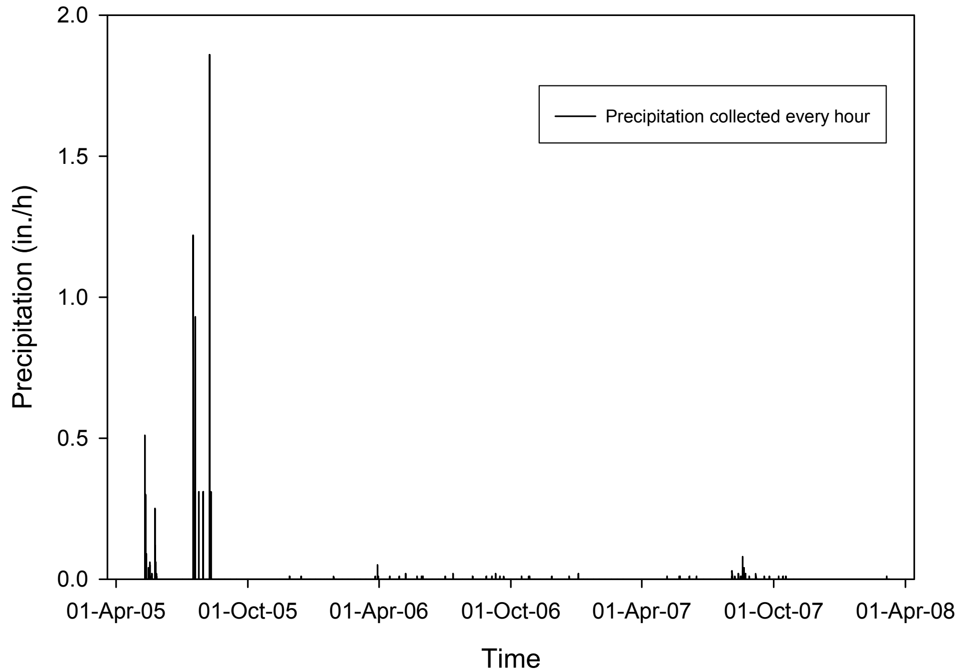

Figure 39. Hourly collected rainfall from May 2005 to April 2008

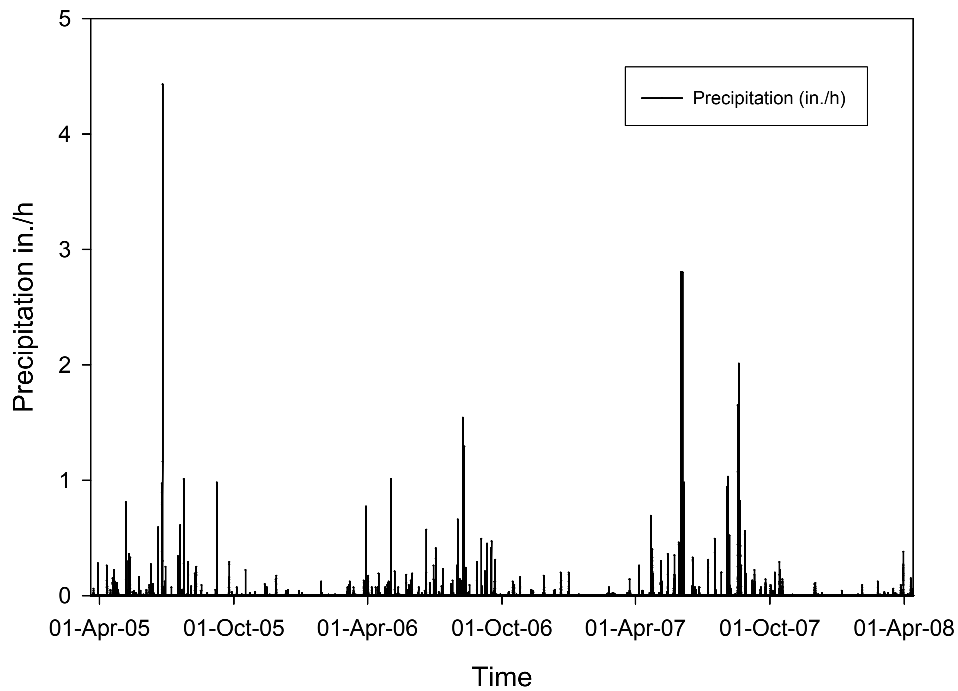

Figure 40. Hourly collected rainfall from May 2005 to April 2008 (Source: IEM)

Vibrating wire (VW) piezometers were installed at two offset locations a distance of approximately 10 feet on both sides (east and west) of the instrumentation trench. A borehole was completed at each location and a perforated PVC pipe was placed in the borehole. Concrete sand was placed around the annulus of the PVC pipes. The VW piezometers were lowered into the PVC pipes and the sensor elevations were recorded. The top of the PVC pipes were located about 1.5 feet below the existing ground surface. The embankment fill over the piezometers limited the influence of changing barometric pressures, due to weather conditions, on sensor readings.

The VW piezometer contained a tensioned steel wire that, when excited, produced a frequency signal in hertz. The frequency signal was then converted into a pressure value (i.e., feet of pressure head) using factory supplied calibration equations. Combining the elevations of the sensors with the measured pressure head, the depth of the groundwater table to the pavement surface was determined. Groundwater level measurements were recorded once every three hours.

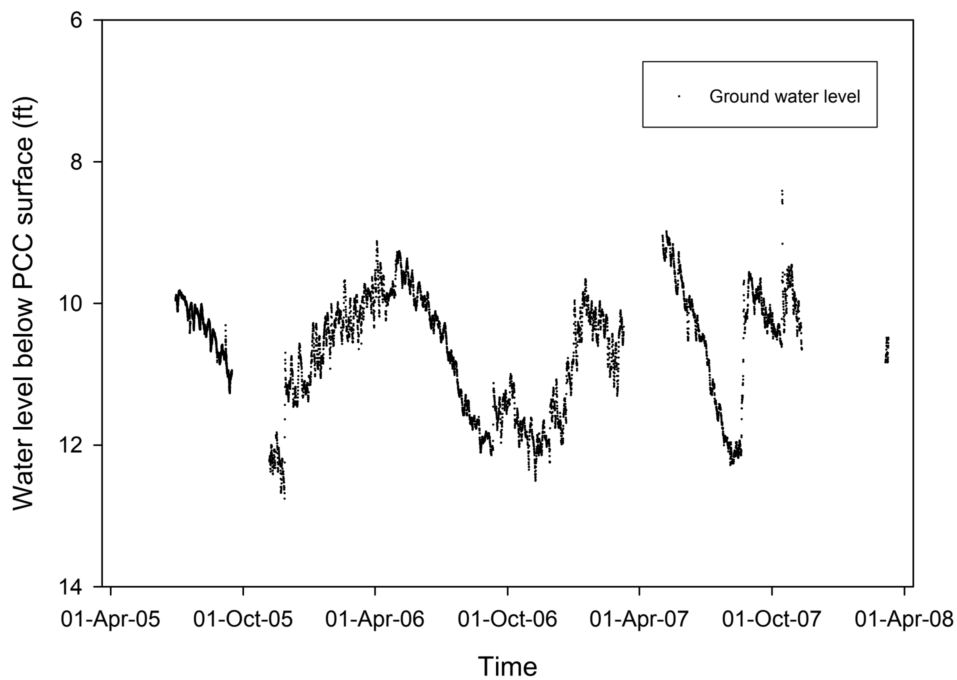

Figure 41. Groundwater table collected by two piezometers relative to pavement surface

Figure 41 shows a relatively constant groundwater level below the US 20 project site over a two-year span. Since instrument installation, the groundwater reached its highest level of approximately nine feet below the pavement surface during the first week of April 2006. The groundwater reached its lowest level of approximately 13 feet below the pavement surface during the last week of November 2005. The general trend shows that during late winter and springtime the groundwater levels rose and that during the summer and fall months the groundwater level lowered. High water table occurred from March to June, which coincides with the thawing period and rainy season.

Subbase and Subgrade Moisture Contents

Volumetric moisture content (VMC) in the subbase and subgrade was determined from analyzing the waveform data from the TDR probes. The principle of TDR is based on measuring the one-way travel time of an electromagnetic wave from a source to an electrical discontinuity (Diefenderfer et al., 2000). The reflectometer produces an electromagnetic pulse, which is sent to a TDR probe, and then records the resulting reflection waveform. The TDR probes utilized in this study consisted of three evenly spaced stainless steel rods. The impedance along the length of the rods varied with the dielectric constant of the surrounding soils. Based on the assumption that the dielectric constant of a soil is dependent on the moisture content, the volumetric water content of the soil surrounding the TDR probe rods could be estimated from its reflected waveform.

Ten TDR probes were installed for this project. One probe was placed in the center of the aggregate subbase layer. One was placed at the subbase/subgrade interface. The remaining eight probes were placed at six-inch intervals below the subbase/subgrade interface. The following graphs show typical waveforms collected from the granular subbase layer and subgrade soils.

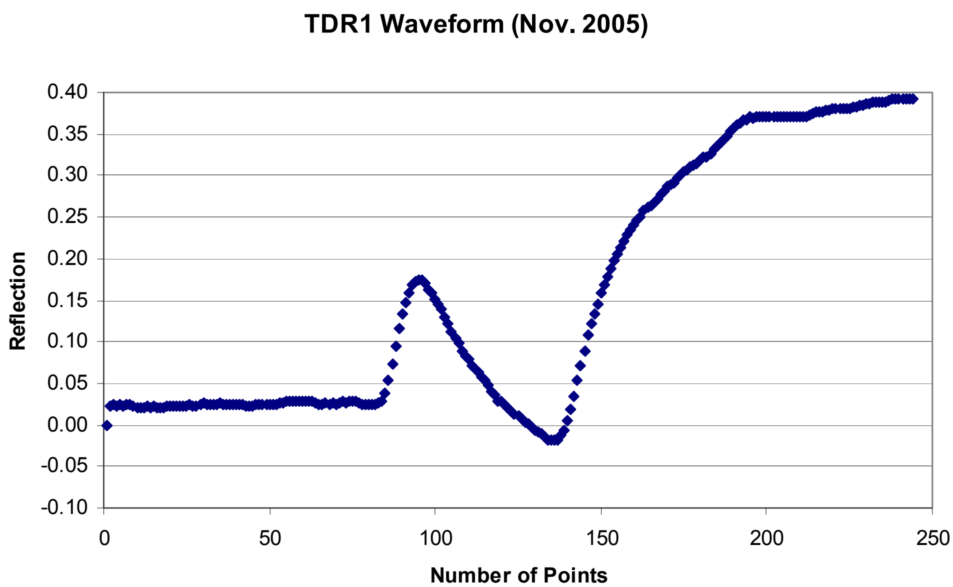

Figure 42. Typical subbase layer waveform

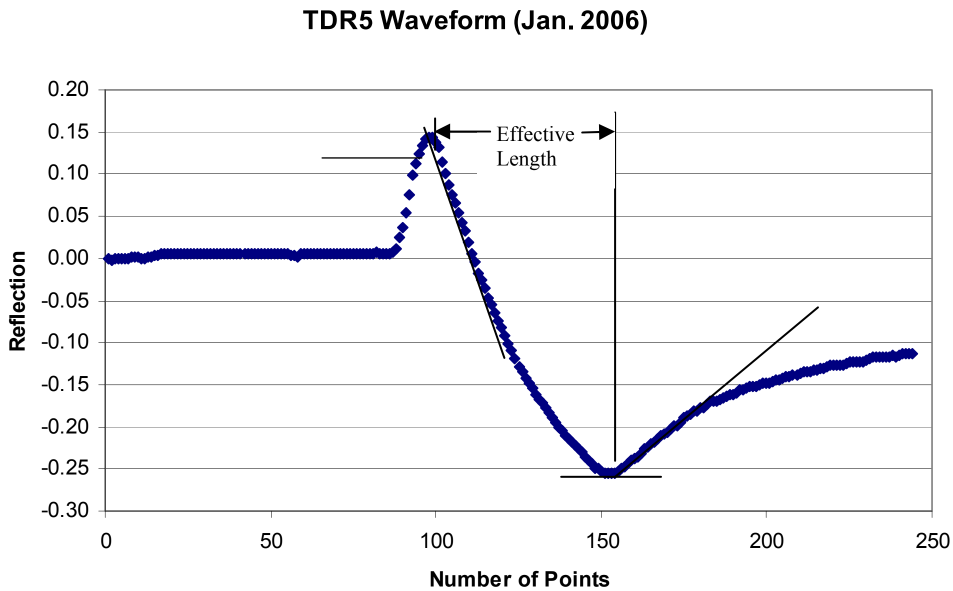

Figure 43. Typical subgrade layer waveform

The TDR probes were installed horizontally into the sidewall of the installation trench near the outer wheel path into relatively undisturbed soil. The probes were installed using a guide tool. The guide held the TDR probe rods parallel during insertion into the subgrade.

Several empirical relationships between the dielectric constant and soil volumetric water content have been developed. The most commonly used equation (and the one used in this study) was presented by Topp et al. (1980) and is given as follows.

$$\theta_v = -5.3*10^{-2} + 2.92*10^{-2}K_a - 5.5*10^{-4}K_a^2 + 4.3*10^{-6}K_a^3$$

where θ_v is the volumetric water content and K_a is the dielectric constant.

Results from the TDR probes are shown in Figures 44 to 48 for the VMC in subbase and subgrade layers. During the freezing periods, the apparent dielectric constant of the soil reduced the computed water contents. Freezing periods in the subbase layer and on top of subgrade layer were from early November 2005 to early February 2006 and from the middle of November 2006 to nearly the end of February 2007. Freezing lasted longer at deeper levels. At approximately five feet below the PCC surface, the freezing periods were from the middle of November 2005 to early March 2006 (Figure 48). Volumetric moisture contents in the subgrade layer increased after the freezing periods to their peaks in the middle of July, which was at the tail end of the rainy season. It appears that there was a relationship between VMC and precipitation for the probes in subbase and subgrade soil layers.

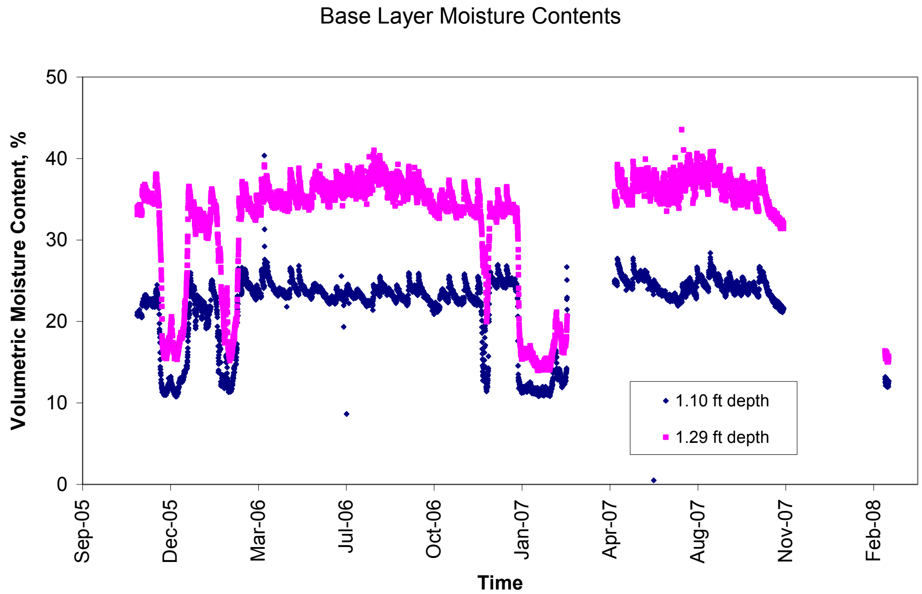

Figure 44. Subbase moisture content (1.1 and 1.3 ft below the pavement surface)

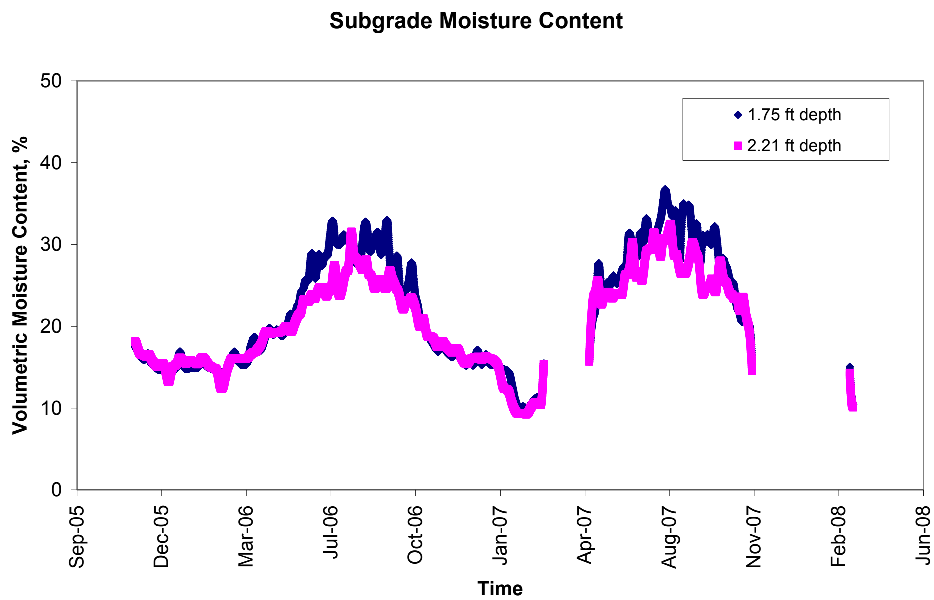

Figure 45. Subgrade moisture content (1.7 and 2.2 ft below the pavement surface)

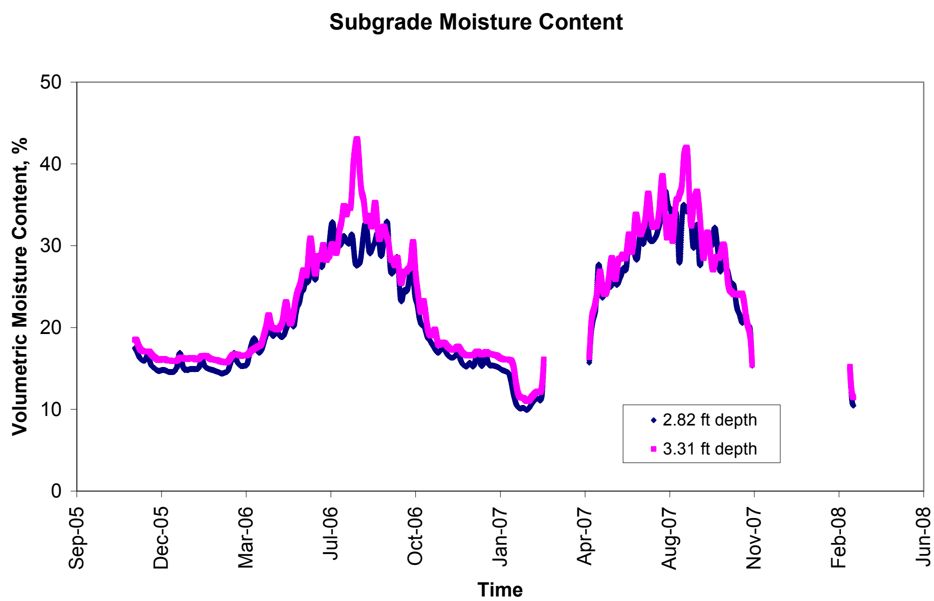

Figure 46. Subgrade moisture content (2.8 and 3.3 ft below the pavement surface)

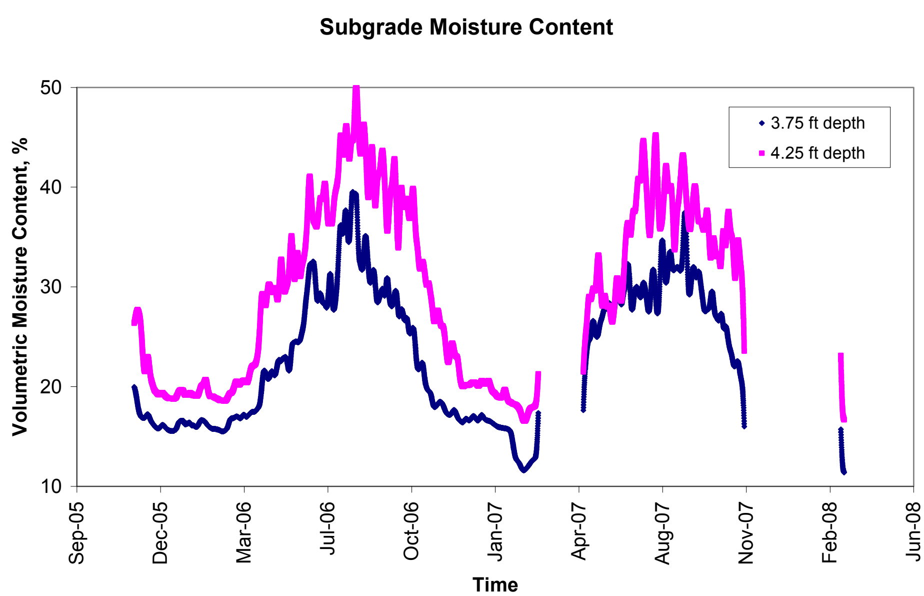

Figure 47. Subgrade moisture content (3.8 and 4.3 ft below the pavement surface)

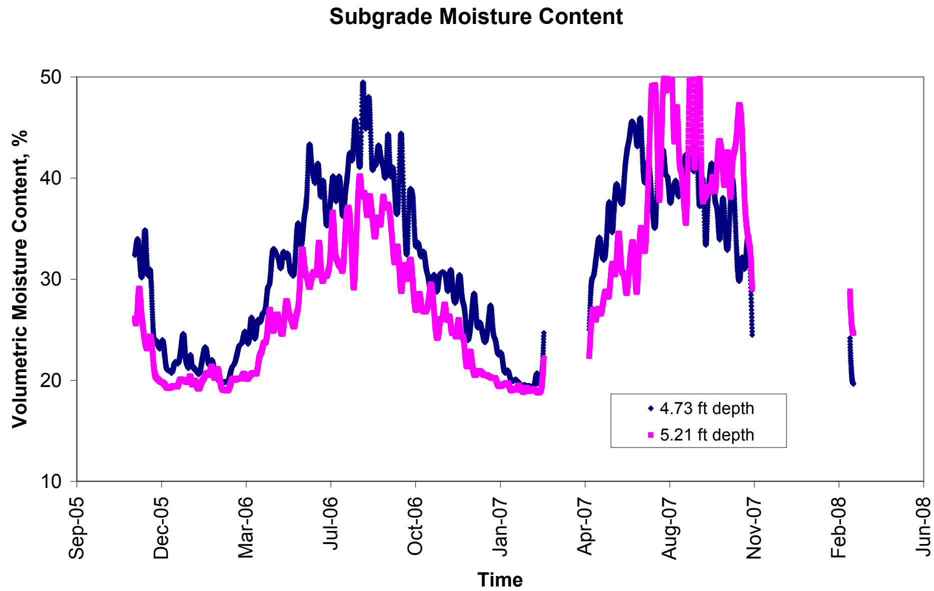

Figure 48. Subgrade moisture content (4.7 and 5.2 ft below the pavement surface)

In general, the subbase layer moisture content remained relatively constant. The moisture content in this layer sharply decreased during periods between the winter and the spring when the temperature was below the freezing point. Moisture content in the subgrade layer increased during the spring, was relatively constant during the summer, and then decreased during the fall.

Of note were the sharp decreases in the apparent moisture contents of the TDR probes during December and February of 2006 and during February of 2007. The dielectric constant of these soils changed when the base layer and subgrade soils froze. This principal was utilized by the resistivity probe to determine the depth of frost penetration. The waveforms of the frozen materials resulted in a significantly lower calculated moisture content. This result was not anticipated prior to instrumentation but served as additional data to verify the depth of frost penetration. A similar effect was shown in the Ohio test site data (Heydinger, 2003).

Frost Penetration

The resistivity gage readings showed that thawing occurred from the top down and bottom up. The gage readings supported the observations of other researchers: as ice lenses thaw, unfrozen water is trapped in the subbase layer due to ice in the subgrade prohibiting infiltration.

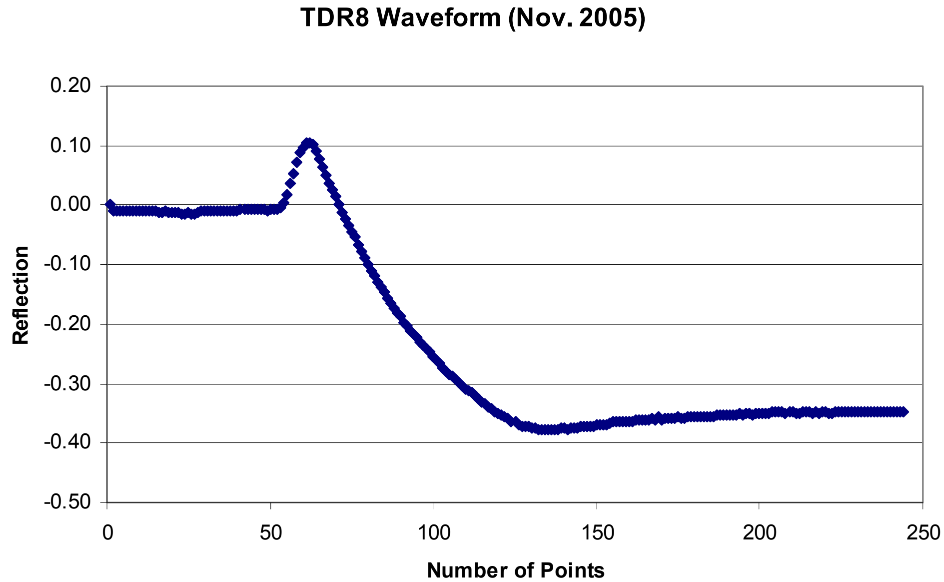

Figure 49. Flat lower reflection peak

Table 12. Frost penetration based on TDR probe waveforms

TDR probe	Dates showing frost penetration
1 & 2	Dec. 2, 2005 to Jan. 4, 2006 Feb. 6, 2006 to Feb. 28, 2006 Dec. 3, 2006 to Dec. 10, 2006 Jan. 13, 2007 to March 2007
3	Dec. 6, 2005 to Dec. 13, 2005 Dec. 18, 2005 to Dec. 26, 2005 Feb. 18, 2006 to March 4, 2006 Jan. 17, 2007 to March 2007
4	Dec. 18, 2005 to Dec. 26, 2005 Feb. 18, 2006 to March 4, 2006 Jan. 17, 2007 to March 2007
5 & 6	Jan. 31, 2007 to March 2007
7	Feb. 7, 2007 to March 2007

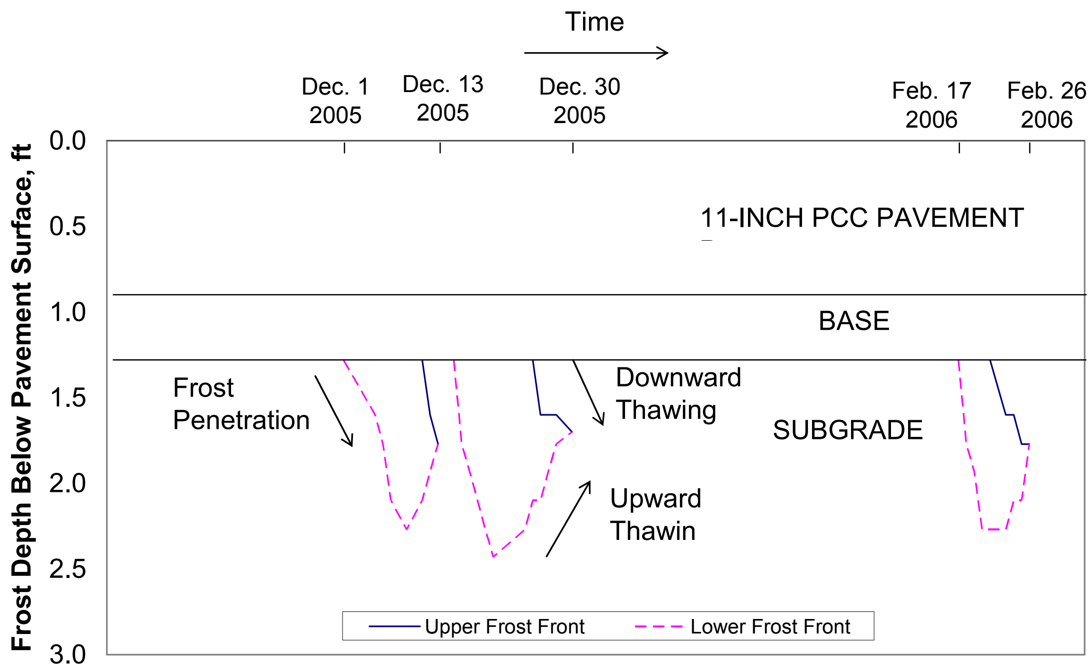

Figure 50. Frost penetration below the pavement surface

The top of the resistivity probe was approximately 1.3 feet below the pavement surface. The resistivity probe was installed below the surface of the subgrade to limit damage during paving operations. Because of this, no frost data exists for the subbase layer material. The dates shown in Table 12 agree well with Figure 49 for frozen/unfrozen conditions within the subbase and subgrade layers. In Figure 50, moving from the left to the right, the penetration of the frost layer was first detected by the resistivity probe on December 1st, 2005. It then reached a maximum penetration on December 9th and completely thawed on December 13th, 2005. A couple days later, another frost lens formed and completely thawed on December 30th, 2005. Of note was that thawing of the ice lens occurred from the top down and bottom up.

Pavement, Subbase and Subgrade Temperature Profiles

The temperature sensors (iButtons) placed farthest below the pavement surface (#10) ceased to operate shortly after operation, likely due to installation damage. About five months after installation, during the winter of 2005, three sensors stopped responding. After that, one sensor ceased operation about every other month. During the last measurement period, only sensor 6 and 8 were operational.

The seasonal trend shown in the temperature data collected from the pavement, subbase layer, and subgrade layers mirrored the air temperature data reported earlier. From the short span of temperature data collected, a sinusoidal pattern can be seen similar in Figure 38. The following figures show the seasonal data for the temperature sensor locations in the pavement, subbase layer, and subgrade layer respectively.

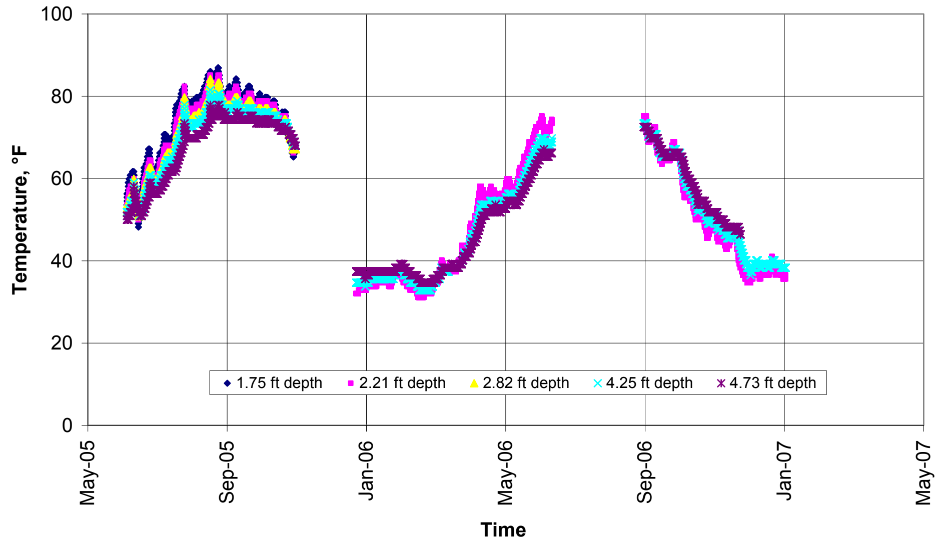

Figure 51. Seasonal trends of the subgrade layer

Figure 51, and more clearly Figure 52, show that the temperature of the pavement changed at a higher rate than the subbase and subgrade layers. In addition, a temperature rise or fall in the pavement layer preceded the subsequent rise or fall in the subbase and subgrade layers. These results agreed with the expected temperature profile below a pavement section. The following figures show the temperature extremes experienced at each temperature sensor location (Note: The maximum temperature at one elevation did not necessarily occur at the exact time as other elevations).

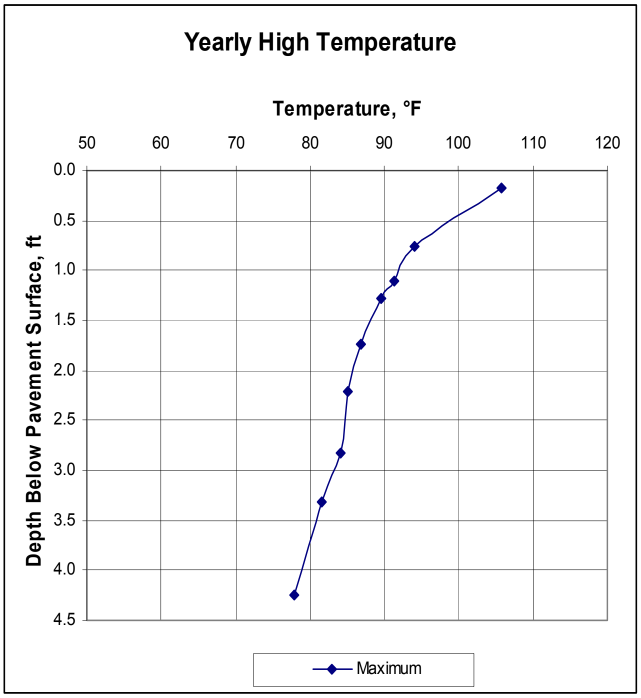

Figure 52. Yearly high profile

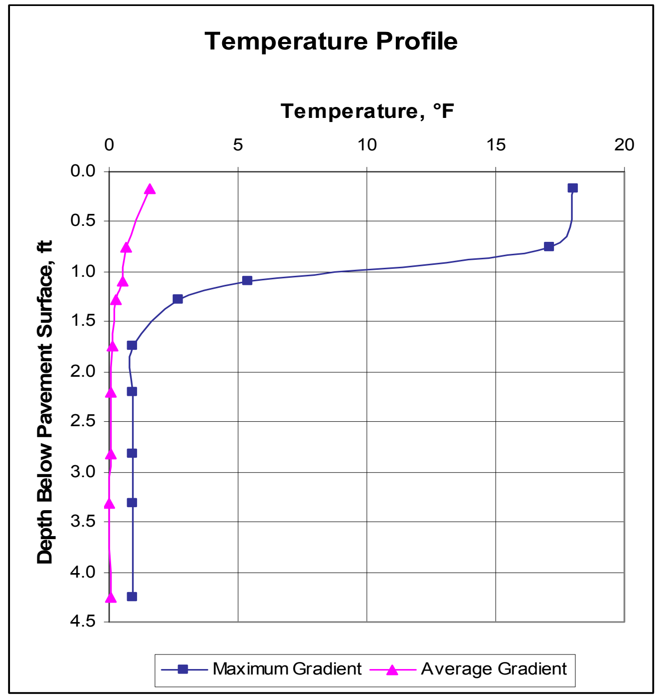

Figure 53. Temperature gradient of roadway

Due to the high failure rate of the temperature sensors, a representative graph of the yearly low temperatures is not shown. Several of the sensors ceased operation prior to the winter months. The maximum gradient of the subgrade soils below a depth of approximately 1½ feet was about one degree Fahrenheit, which corresponds with the sensitivity of the sensors.

Effects of Seasonal Variation on Soil Stiffness

In this study, DCP tests were conducted during construction, the freeze-thaw period, and approximately two years after construction. The penetration index (DPI) was used to compare the stiffness of the subgrade and subbase layers of each period.

During the construction period, a test grid was developed that extended beyond the planned sensor installation location by 48 feet in each direction along pavement. The test locations were spaced six feet apart in the east-west and north-south directions. Subsequent to the initial testing, DCP tests were also conducted to analyze the effects of freeze/thaw on the performance of the subgrade layer. Two locations of 30 feet spanning the shoulder along the pavement were tested. Station 930+00 was at the middle of these two points. During the freezing period, the subbase and subgrade layers were very stiff (Figure 54). The DCP tests were performed 12 feet from the pavement-shoulder boundary.

Figure 54. DCP tests during freeing period

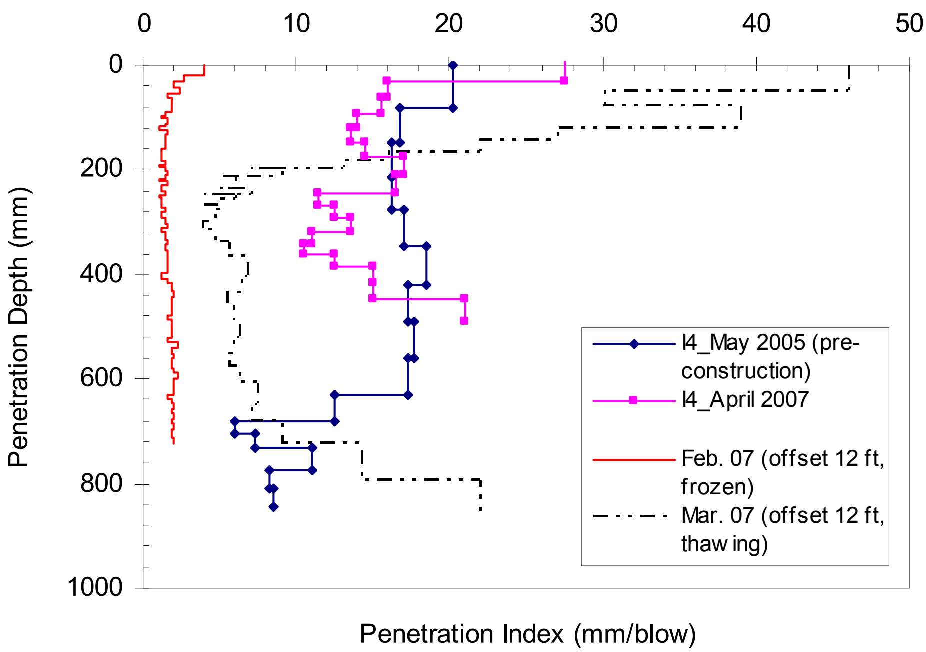

Figure 55. DCP tests during construction, the freeze-thaw period, and two years after construction

Four DCP tests were conducted during the thawing periods. Two DCP tests were performed at the same locations with those in the freezing period. Two other tests were conducted five feet offset from the pavement-shoulder boundary.

The pavement was also cored at five locations on three continuous slabs at station 930+00 to conduct DCP and Clegg Hammer tests two years after construction (April 23, 2007). Shelby tube samples were also collected for resilient modulus testing. This was a normal period of pavement conditions (no freezing and/or thawing). The DCP results representing stiffness of the subbase and subgrade layers were used to compare with those in the freeze/thaw and initial construction periods (Figure 55). Results show that the soil was stiff when it was frozen as expected. The average DPI in this period was approximately 2 mm/blow (CBR = 134). On the contrary, soil was at the weakest state in the thawing period when the average DPI was up to 39 mm/blow (CBR = 5). The DPI diagram can be divided into three parts based on the DPI values with depth. The upper part from the ground surface to a depth of about 200 mm, the DPI value was high and the soil wet/thawed. In this period, the shoulder of the pavement was fully saturated. The DPI values in the second part from 200 mm to 600 mm were lower indicating that soil in that layer was still frozen. The soil layer in the third part was thawing, which resulted in a higher DPI. The DPI diagram of the thawing period showed that the frozen layer was thawing from the top down and bottom up.

Resilient Modulus of Subgrade Soil Layer

The resilient modulus of subgrade materials was previously discussed as an important factor for the design of pavements. It directly affects the performance of pavements. Relevant studies show that the resilient modulus is strongly dependent on the moisture condition of the soil. Approximately two years after highway construction, samples of the subgrade soil layer were taken for grain size distribution and resilient moduli testing in the laboratory. The results of resilient modulus from laboratory tests were used to compare with the resilient modulus obtained during the construction. The resilient modulus tests were conducted following NCHRP 1-28A.

The pavement coring and field tests were conducted on April 23, 2007 at station 930+00. The testing site was on the westbound right lane (Figure 56). As discussed above Clegg Hammer tests were conducted on the subbase layer. The DCP tests were performed through the subbase layer in the subgrade at different locations. Table 13 summarizes the activity of the test section in the field.

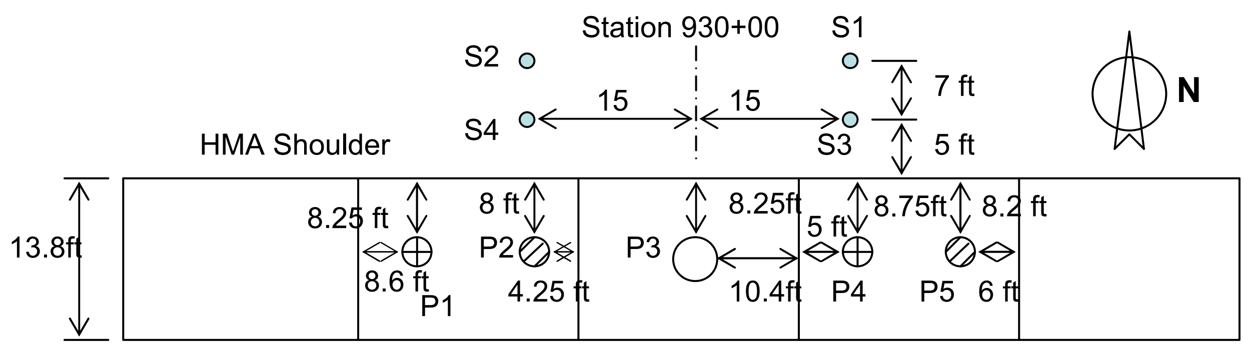

Figure 56. Plan view of test section on April 23, 2007

Table 13. Frost penetration based on TDR probe waveforms

Core/ point	Location	Activity
⊕ (2" core)	P1, P4	DCP
(4" core)	P2, P5	Shelby Tube
○ (10" core)	P3	LWD, Clegg Hammer, DCP, Shelby Tube
●	S1, S2, S3, S4	DCP

Results of the resilient modulus tests are presented in the Figure 57 as a function of deviator stress and confining stress.

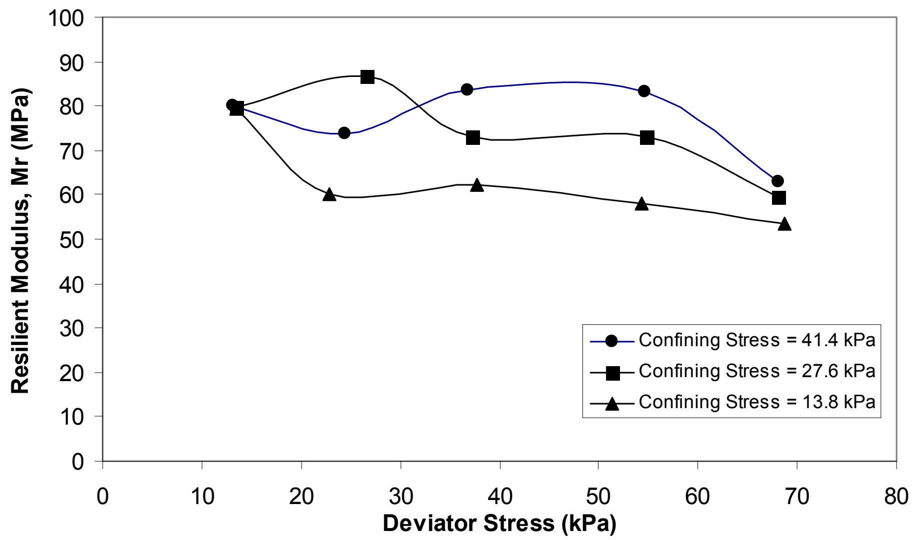

Figure 57. Resilient modulus of the subgrade layer at P2, 18 inches below the pavement surface

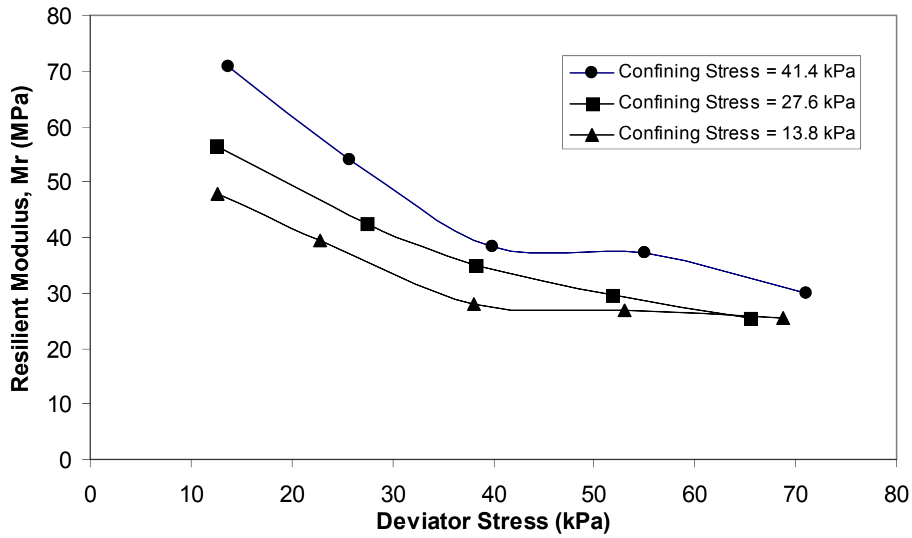

Figure 58. Resilient modulus of the subgrade layer at P3, 24 inches below the pavement surface

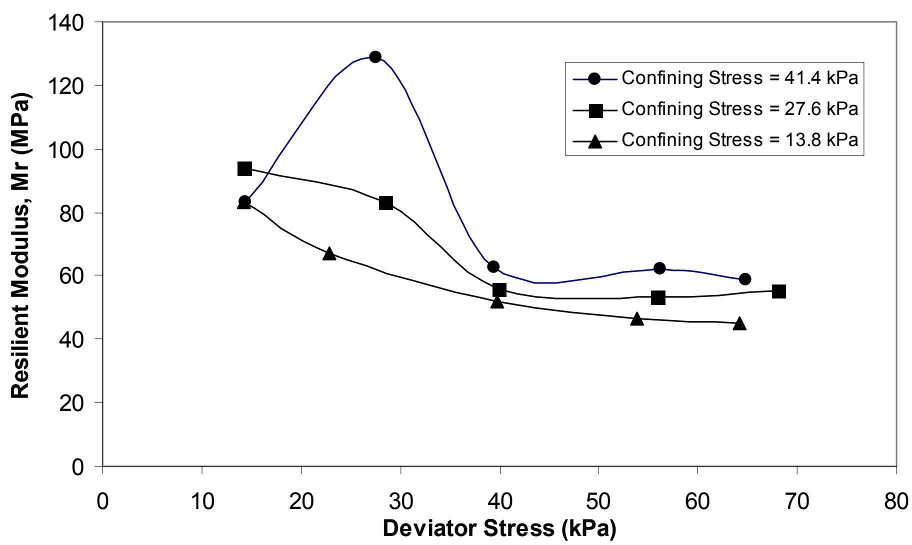

Figure 59. Resilient modulus of the subgrade layer at P3, 30 inches below the pavement surface

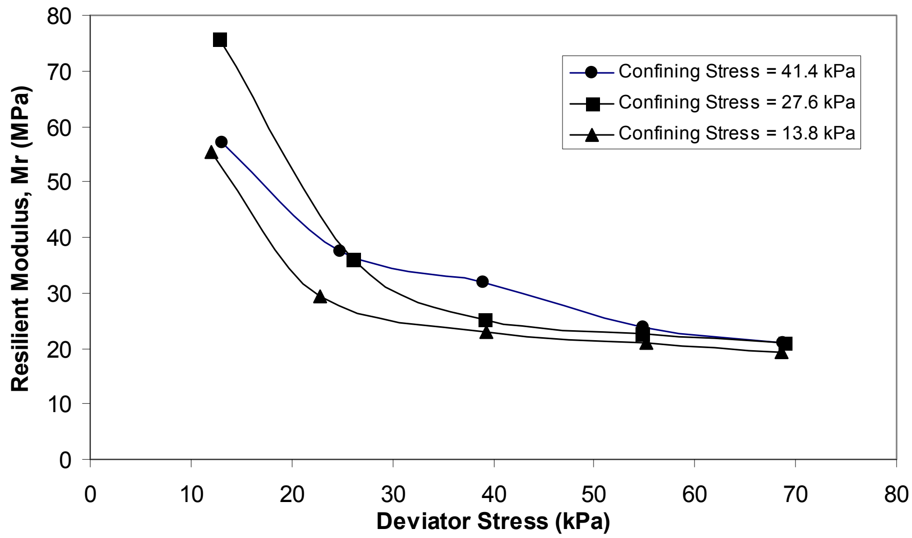

Figure 60. Resilient modulus of the subgrade layer at P5, 18 inches below the pavement surface

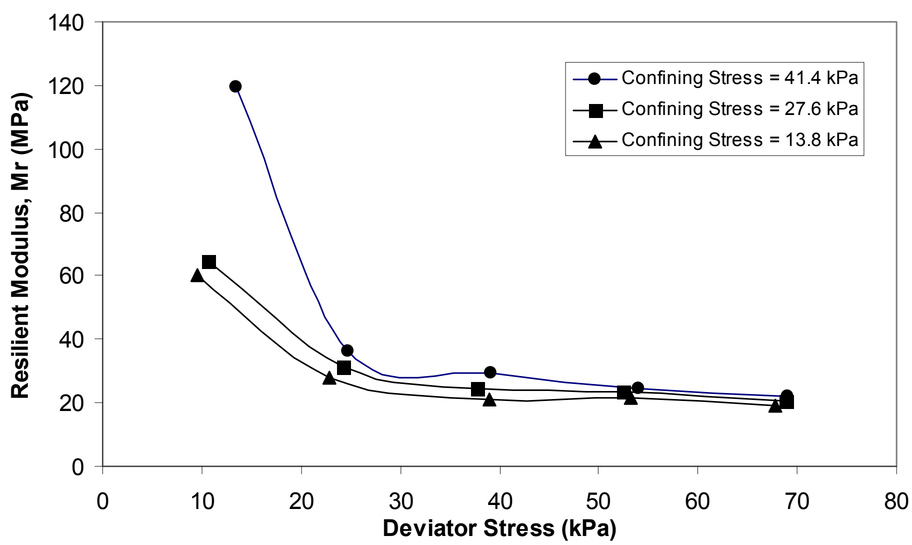

Figure 61. Resilient modulus of the subgrade layer at P5, 24 inches below the pavement surface

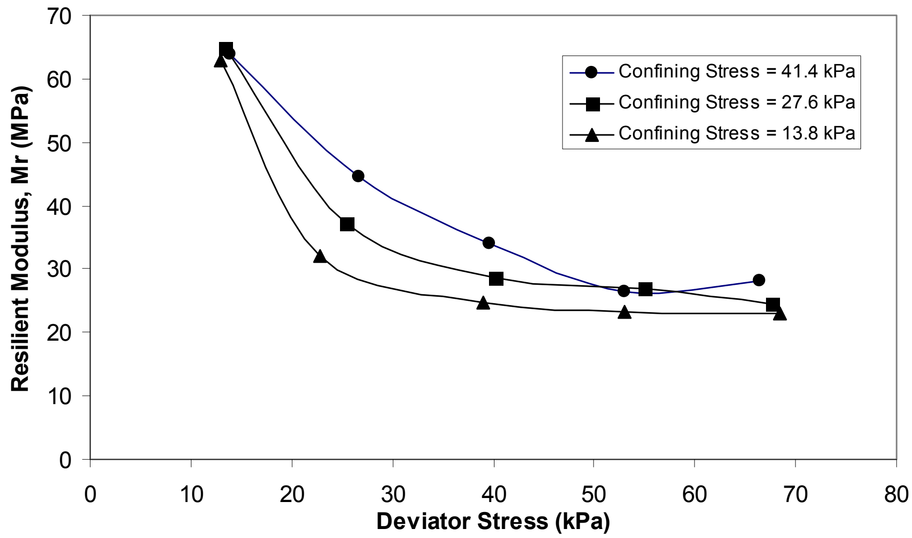

Figure 62. Resilient modulus of the subgrade layer at P5, 30 inches below the pavement surface

Table 14. Moisture content of the Shelby tube samples

Sample No.	**P2-ST1**	**P3-ST2**	**P3-ST3**	**P5-ST1**	**P5-ST2**	**P5-ST3**
Moisture content, %	10.9	11.9	10.6	11.4	11.7	11.0

During the construction period, after each subgrade layer was constructed, a test grid was developed that extended beyond the planned sensor installation location by approximately 50 feet to the east and west. The test locations were spaced six feet apart in the east-west and north-south directions. The test grid consisted of four rows spanning the two lanes of westbound traffic and 16 columns for a total of 64 test locations. The resilient modulus of the locations near points P2, P3, and P5 were calculated for the comparison.

The resilient modulus in terms of MPa could be calculated using the empirical equation (2), as follows:

$$M_r(MPa) = 1500 \times CBR \times 6.894757/1000 \quad (2)$$

Tables 15, 16, and 17 summarize the resilient modulus of subgrade layers at 30 test points from the initial construction testing.

Table 15. Resilient modulus of subgrade layer from 0 to 1ft (MPa)

	Columns from East to West							Directio n
Row	F	G	H	I	J	K	L	
1	114	121	134	152	81	159	145	South
2	119	96	93	117	109	147	154	
3	84	101	113	106	78	94	85	
4	149	127	98	124	98	101	112	North

Table 16. Resilient modulus of subgrade layer from 1 to 2ft (MPa)

	Columns from East to West							Directio n
Row	F	G	H	I	J	K	L	
1	88	80	69	92	144	179	60	South
2	137	117	92	92	108	69	92	
3	113	88	129	119	80	76	111	
4	122	123	115	121	139	98	115	North

Table 17. Resilient modulus of subgrade layer from 2 to 3ft (MPa)

	Columns from East to West							Directio n
Row	F	G	H	I	J	K	L	
1	122	99	98	166	48	118	87	South
2	102	164	106	118	92	84	103	
3	116	154	115	191	154	123	163	
4	111	94	113	250	150	114	123	North

Table 18. Summary of average Mr values from initial construction and after 2 years

Measurements	Initial Construction	2 Years After Construction	% Change
M_r – CBR Clegg (MPa)	222	–	–
M_r – CBR DPI (MPa)			
0 -1 ft	120	121	+1
1-2 ft	109	159	+47
2-3 ft	128	---	–
M_r – Lab (MPa)	–	47	–

Soil samples of subgrade layer at this point were obtained in April 23, 2007 and were conducted resilient modulus tests in the laboratory. The moisture content of the soil sample P3-ST3 was 10.6% (Table 14). This moisture content was within the range of normal moisture content of 10%-11%, which was measured by nuclear gauge during the construction (Figure 25). The moisture content of the subgrade layer did not seem to increase during the thawing time (April 23, 2007). In fact, thawing process had just started two days before the field trip. Figures 44 to 47 suggested that moisture content of the subgrade layers had normally increases from May to its peak in August annually.

The resilient modulus of the subgrade layers at point I4 calculated from CBR using the empirical equation (2) showed that the resilient modulus significantly varied with depth. The values of M_r at this point were from 121 MPa to 250.3 MPa (Tables 15-17). The maximum resilient modulus values of sample P3 at point I4 varied from 80 MPa to 95 MPa (Figure 59). The maximum value of resilient modulus from the samples at points P2 and P5 was approximately 80 MPa. The average resilient moduli estimated from DCP tests after 2 years increase by 1% for the 0-1 ft subgrade layer and 47% for 1-2 ft subgrade layer (Table 18). DCP tests conducted 2 years after the construction was on April 23, 2007, which was in the thawing period. However, the subgrade layer was still frozen.

DISCUSSION AND CONCLUSION

In general, the testing and instrumentation of the tests section on US 20 near Fort Dodge, Iowa was successful. The in-ground instrumentation provided rainfall, moisture content, air temperature, groundwater location and frost depth information during the monitoring period of about 3 years. In-situ testing prior to paving included moisture content, density, Clegg impact hammer, and dynamic cone penetration tests. Tests were performed on a six-by-six-foot test grid. The data provided statistically reliable data for spatial variation analysis and correlations to resilient modulus. The major conclusions derived from this study are as follows:

- From the initial in-situ testing, the average value of Clegg Impact Value was 14. CBR value and M_r – CBR Clegg were 21 and 222 MPa, respectively. The average DPI (mm/blow) for three sub-layers 0-1 ft, 1-2 ft, and 2-3 ft of the subgrade layer were 18, 20, and 18, respectively. CBR values estimated from these DPI indices were 11.6, 10.5, and 12.4, respectively. The resilient moduli, M_r – CBR DPI (MPa), for three sub-layers 0-1 ft, 1-2 ft, and 2-3 ft of the subgrade layer were 120, 109, and 128, respectively. The average moisture content obtained from in-situ testing was 10.2%. The average dry density measure by nuclear gauge was 116.5 pcf.

- The spatial kriging plots showed the variations of soil moisture content, wet density, Clegg impact values, and DPI of the test section. Clegg impact values most clearly showed transverse variation likely a result of the construction process which follows longitudinal paths. The Clegg impact values measure at different locations widely varied. The coefficient of variation of the Clegg impact values was 38%. Meanwhile, moisture content and dry density varied in narrower ranges with coefficient of variations of 9% and 2%, respectively.

- The average values of resilient modulus in the subgrade layer estimated from the DCP after 2 years at depths 0-1 ft and 1-2 ft were 121 MPa and 159 MPa, respectively. These values increased by 1% and 47%, respectively, compared with the corresponding values during the construction period. The average value of resilient modulus obtained from laboratory test was 47 MPa.

- In-ground instrumentation provided mostly reliable measurements with the exception of the temperature sensors. The temperatures sensors in subbase and subgrade layers could not be collected for the full monitoring period due to an unknown error in the sensor.

- The calculated moisture contents from TDR probes in the subbase layer were relatively constant throughout the year except during freezing periods, in which case the moisture content was decrease presumably due to water freezing. The moisture content in the subgrade layer changed with the seasons. Moisture content increased as spring approached and decreased during the fall and early winter. Moisture content in the subgrade soils increased during the spring thaw and peaked in the early summer.

- In the subgrade layer, freezing penetrated downward, but thawing occurred in both downward and upward directions. The temperature in the subgrade layer decreased deeper into the layer when it was above the freezing point but increased deeper into the layer when it was below the freezing point. The PCC pavement experienced greater temperature extremes and it changed at a higher rate than the subbase and subgrade layers. The temperature gradient within one hour at PCC surface was as high as 18^{o}F.

- By comparing the average value of DPI obtained from DCP tests during the construction period and two years later, on April 23, 2007, the subgrade resilient modulus values increased. The initial resilient modulus was derived from an empirical correlation from DCP tests and compared to laboratory resilient tests. The post construction average resilient modulus values for 0-1 ft and 1-2 ft were 1% and 47% higher than the original values obtained from the construction period. However, the slightly frozen subgrade layer on April 23, 2007 might have increased resilient modulus at the depth 1-2 ft.

- In general, the measurement results of air, subbase, and subgrade temperatures; freeze-thaw circles, moisture contents in subbase and subgrade layers; ground water table from the field installation were suitable and within the expectation. The rain gauge did not function correctly for some time periods based on comparison to another weather station in the area. Many temperature sensors ceased to operate shortly after operation. The installation of the instruments in the pavement subbase and subgrade was good.

REFERENCES

American Association of State Highway and Transportation Officials (AASHTO). (1993). *Guide for the Design of Pavement Structures*, Washington D.C.

Dingquing Li, Ernest T. Selig (1993). "Resilient modulus for fine-grained subgrade soils". *Journal of Geotechnical Engineering*, 939-957.

Drumm, C. E., Reeves, S. J., Madgett, R. M., and Trolinger, D. W. (July 1997). "Subgrade resilient modulus correction for saturation effects". *Journal of Geotechnical and Geoenvironmental Engineering*, 663-670.

FHWA, "Seasonal monitoring program guidelines: Version 2.1," FHWA-LTPP staff, April 1994.

Gabr, A. M., Hopkins, K., Coonse, J., and Hearne, T. (November 2000). "DCP criteria for performance evaluation of pavement layers". *Journal of Performance of Constructed Facilities*, 141-148.

Heydinger A.G., "Evaluation of seasonal effects on subgrade soils," *Transportation Research Record 1821*, Paper No. 03-3801, 2003.

Janoo, V., Shepherd, K., "Seasonal variation of moisture and subsurface layer moduli," *Transportation Research Record 1709*, Paper No. 00-0929, 2000.

Kestler, A. M., Hanek, L. G., and Truebe, A. M. (2001). "Evaluating moisture sensors and monitoring seasonal moisture variation in low-volume roads". *Transportation Research Record 1755*, Paper No. 01-0248, 97-107.

NCHRP Synthesis 278: "Measuring in situ mechanical properties of pavement subgrade soils", *Transportation Research Board*, National Research Council, Washington, D.C., 1999.

NCHRP Project 1-28A: "Laboratory Determination of Resilient Modulus for Flexible Pavement Design", *Transportation Research Board*, National Research Council, January 2004.

Rainwater, N. R., Yoder, E. R., Drumm, C. E., and Wilson, V. G. (October 1999). "Comprehensive monitoring systmens for measuring subgrade moisture conditions". *Journal of Transportation Engineering*, 439-448.

Topp, G.C., Davis, J.L., and Annan, A.P., "Electromagnetic determination of soil water content: Measurements in coaxial transmission lines," *Water Resource Research*, 1980.

United Army Corps of Engineers (1992). "Engineering and Design - Bearing Capacity of Soils". *Non-Load Related Design Considerations*, 2-1 to 2-8.

USDA, "Soil survey of Webster County, Iowa," *Natural Resources Conservation Service*, 1975.

Wolfe, W.E., Abdulshafi, O., and Wu T.H. (June 11, 1998). "Seasonal instrumentation of SHRP pavements – The Ohio State University", Final Report, Report No. FHWA/OH-98/014.

Zhou, H., Elkins, G.E. (1994). "Pavement responses to seasonal variations," *4th International Converence, Bearing Capacity of Roads and Airfields*, Minnesota Department of Transportation, 706-719.

http://mesonet.agron.iastate.edu/request/download.phtml?network=IA_ASOS&&station=FOD

APPENDIX A: DYNAMIC CONE PENETRATION PROFILES

DCP profiles for subgrade layer prior to paving – April 29, 2005

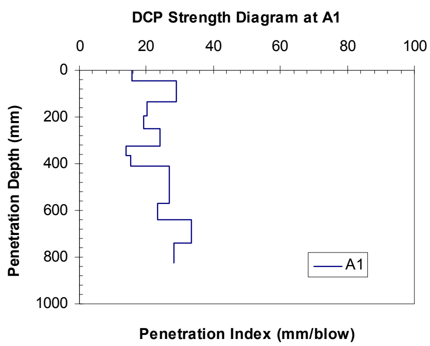

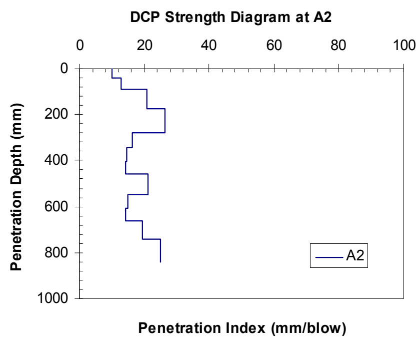

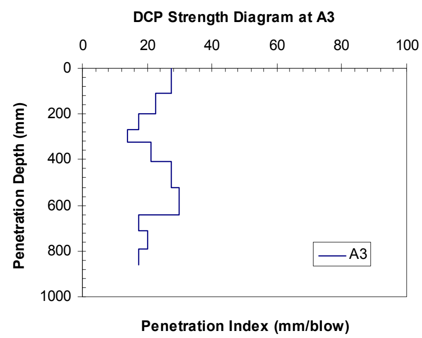

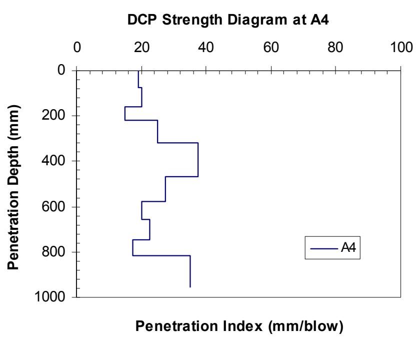

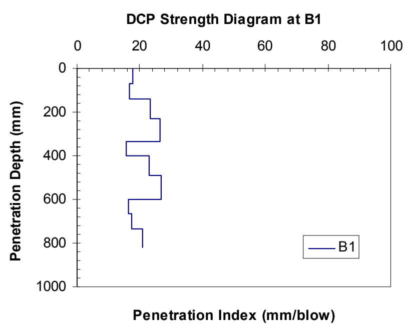

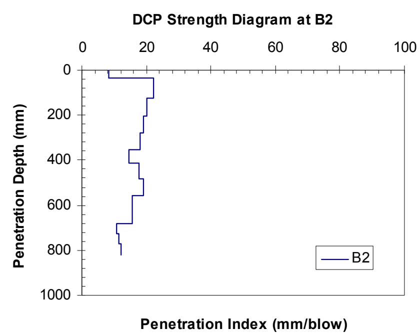

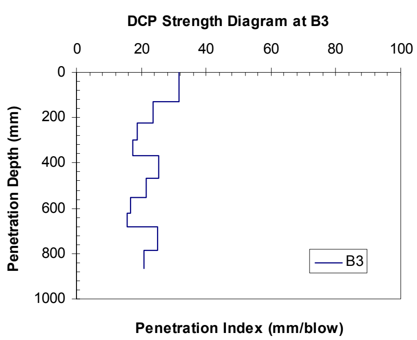

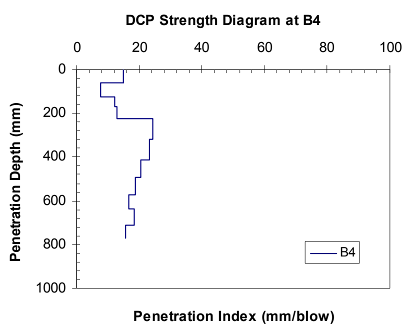

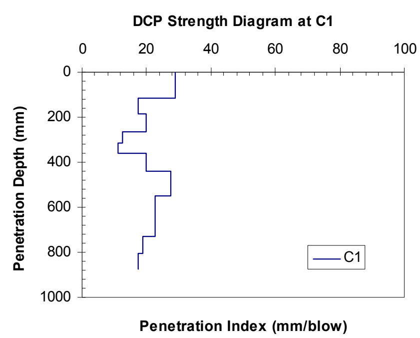

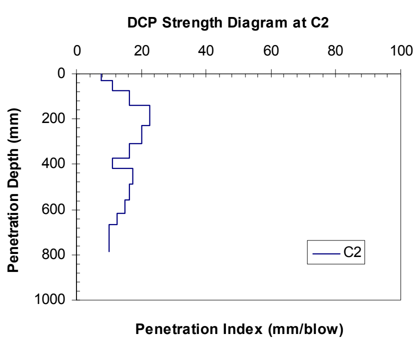

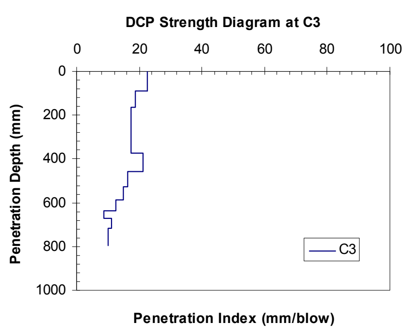

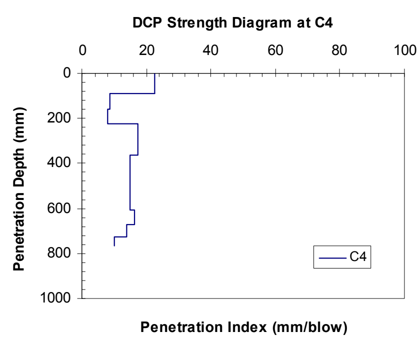

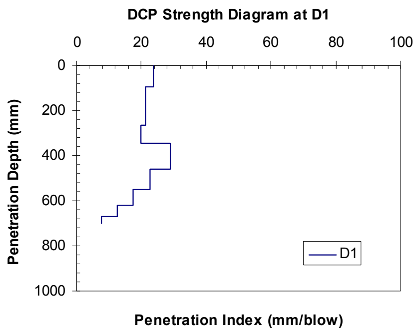
DCP Strength Diagram at D1
0 20 40 60 80 100
0 200 400 600 800 1000
Penetration Depth (mm)
D1
Penetration Index (mm/blow)

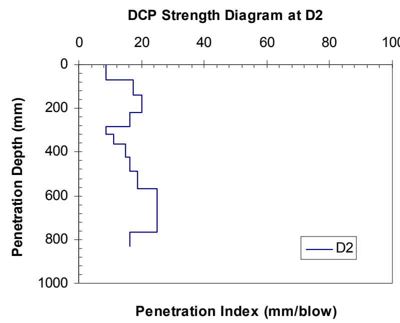
DCP Strength Diagram at D2
0 20 40 60 80 100
0 200 400 600 800 1000
Penetration Depth (mm)
D2
Penetration Index (mm/blow)

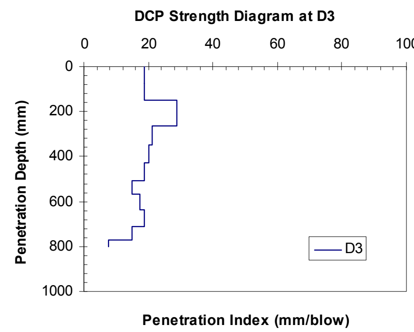
DCP Strength Diagram at D3
0 20 40 60 80 100
0 200 400 600 800 1000
Penetration Depth (mm)
D3
Penetration Index (mm/blow)

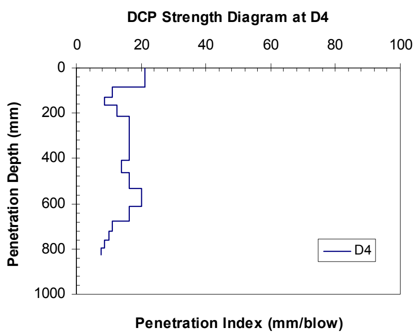
DCP Strength Diagram at D4
0 20 40 60 80 100
0 200 400 600 800 1000
Penetration Depth (mm)
D4
Penetration Index (mm/blow)

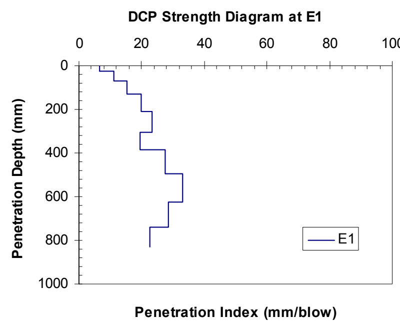
DCP Strength Diagram at E1
0 20 40 60 80 100
0 200 400 600 800 1000
Penetration Depth (mm)
E1
Penetration Index (mm/blow)

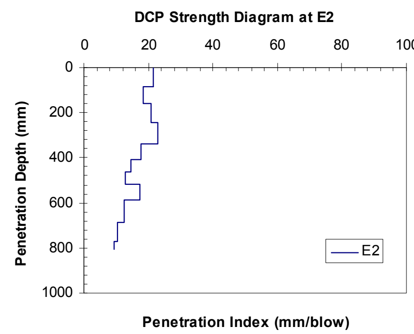
DCP Strength Diagram at E2
0 20 40 60 80 100
0 200 400 600 800 1000
Penetration Depth (mm)
E2
Penetration Index (mm/blow)

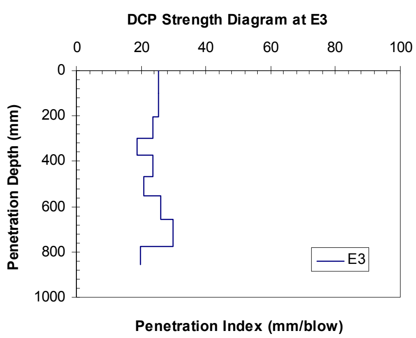
DCP Strength Diagram at E3
0 20 40 60 80 100
0 200 400 600 800 1000
Penetration Depth (mm)
E3
Penetration Index (mm/blow)

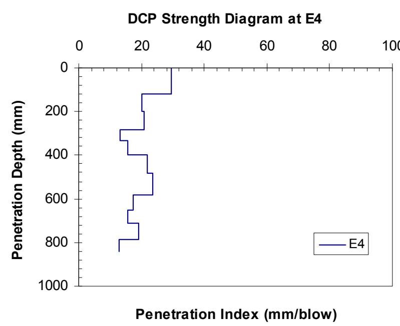
DCP Strength Diagram at E4
0 20 40 60 80 100
0 200 400 600 800 1000
Penetration Depth (mm)
E4
Penetration Index (mm/blow)

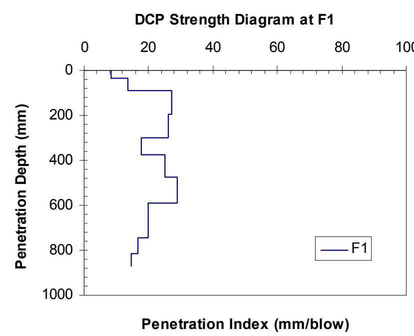
DCP Strength Diagram at F1
0 20 40 60 80 100
0 200 400 600 800 1000
Penetration Depth (mm)
F1
Penetration Index (mm/blow)

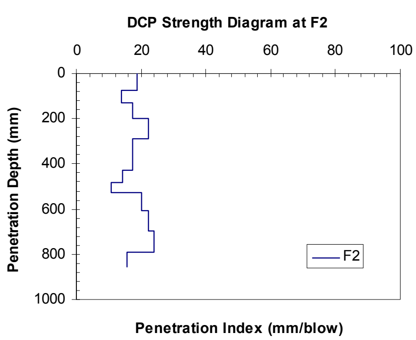
DCP Strength Diagram at F2
0 20 40 60 80 100
0 200 400 600 800 1000
Penetration Depth (mm)
F2
Penetration Index (mm/blow)

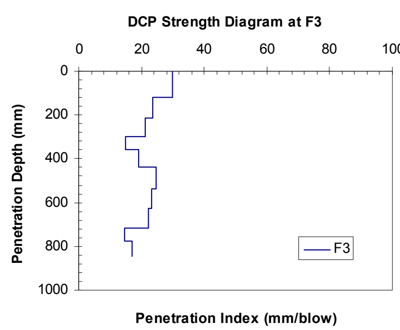
DCP Strength Diagram at F3
0 20 40 60 80 100
0 200 400 600 800 1000
Penetration Depth (mm)
F3
Penetration Index (mm/blow)

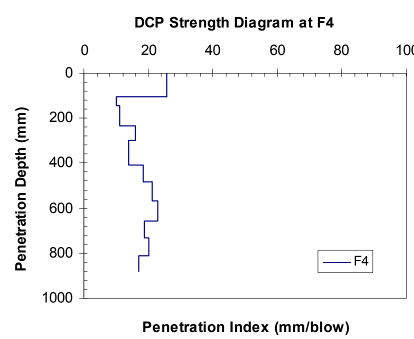
DCP Strength Diagram at F4
0 20 40 60 80 100
0 200 400 600 800 1000
Penetration Depth (mm)
F4
Penetration Index (mm/blow)

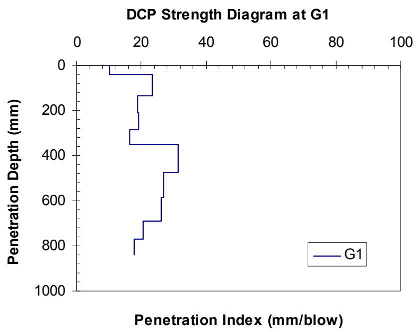
DCP Strength Diagram at G1
0 20 40 60 80 100
0 200 400 600 800 1000
Penetration Depth (mm)
Penetration Index (mm/blow)
G1

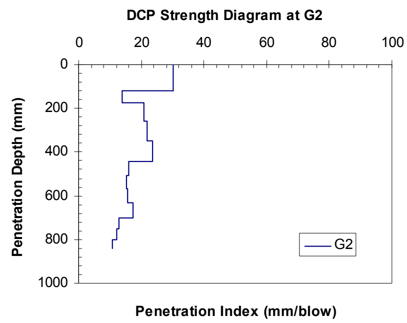
DCP Strength Diagram at G2
0 20 40 60 80 100
0 200 400 600 800 1000
Penetration Depth (mm)
Penetration Index (mm/blow)
G2

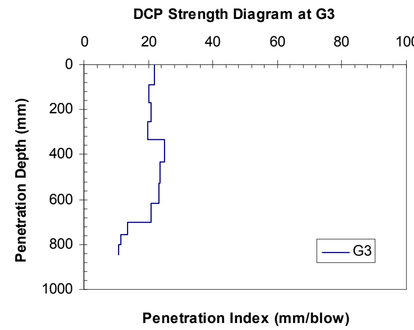
DCP Strength Diagram at G3
0 20 40 60 80 100
0 200 400 600 800 1000
Penetration Depth (mm)
Penetration Index (mm/blow)
G3

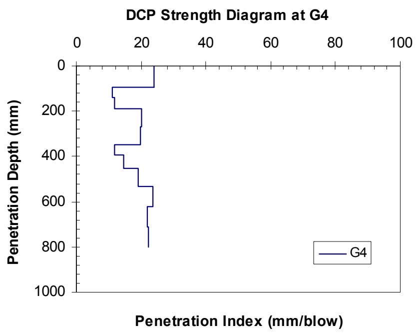
DCP Strength Diagram at G4
0 20 40 60 80 100
0 200 400 600 800 1000
Penetration Depth (mm)
Penetration Index (mm/blow)
G4

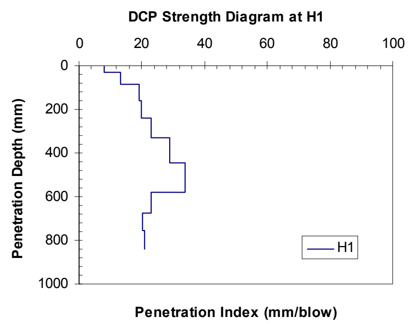
DCP Strength Diagram at H1
0 20 40 60 80 100
0 200 400 600 800 1000
Penetration Depth (mm)
Penetration Index (mm/blow)
H1

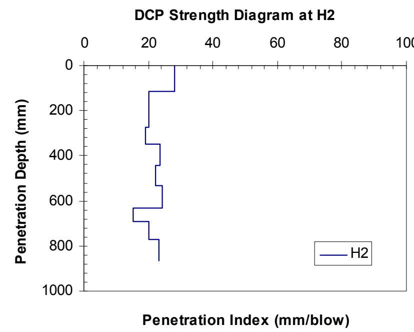
DCP Strength Diagram at H2
0 20 40 60 80 100
0 200 400 600 800 1000
Penetration Depth (mm)
Penetration Index (mm/blow)
H2

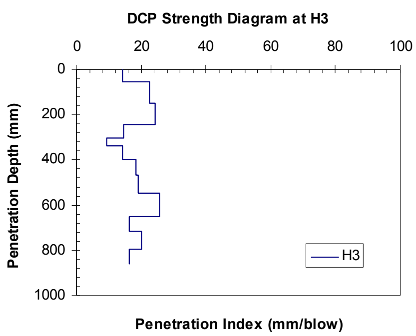
DCP Strength Diagram at H3
0 20 40 60 80 100
0 200 400 600 800 1000
Penetration Depth (mm)
Penetration Index (mm/blow)
H3

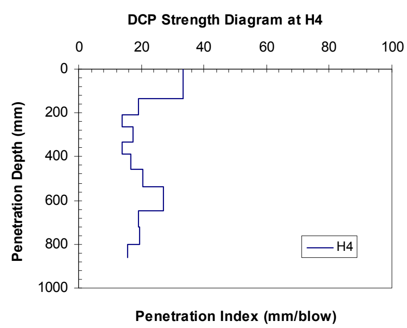
DCP Strength Diagram at H4
0 20 40 60 80 100
0 200 400 600 800 1000
Penetration Depth (mm)
Penetration Index (mm/blow)
H4

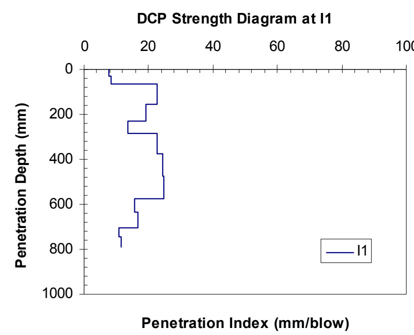
DCP Strength Diagram at I1
0 20 40 60 80 100
0 200 400 600 800 1000
Penetration Depth (mm)
Penetration Index (mm/blow)
I1

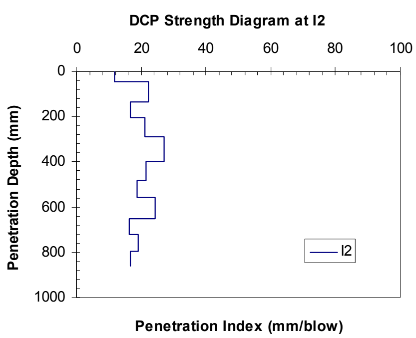
DCP Strength Diagram at I2
0 20 40 60 80 100
0 200 400 600 800 1000
Penetration Depth (mm)
Penetration Index (mm/blow)
I2

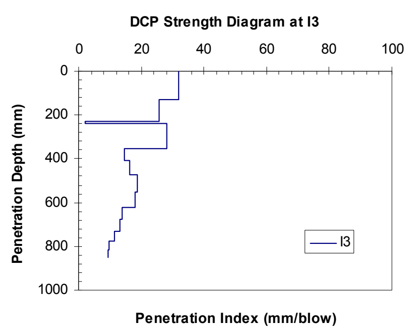
DCP Strength Diagram at I3
0 20 40 60 80 100
0 200 400 600 800 1000
Penetration Depth (mm)
Penetration Index (mm/blow)
I3

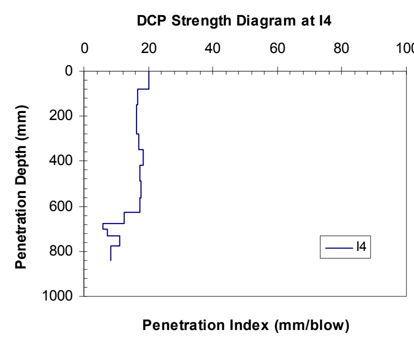
DCP Strength Diagram at I4
0 20 40 60 80 100
0 200 400 600 800 1000
Penetration Depth (mm)
Penetration Index (mm/blow)
I4

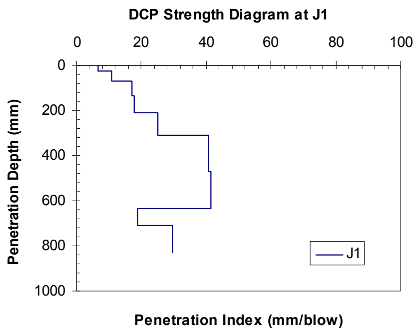
DCP Strength Diagram at J1
Penetration Depth (mm)
Penetration Index (mm/blow)
J1

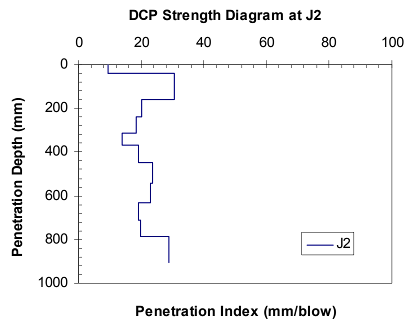
DCP Strength Diagram at J2
Penetration Depth (mm)
Penetration Index (mm/blow)
J2

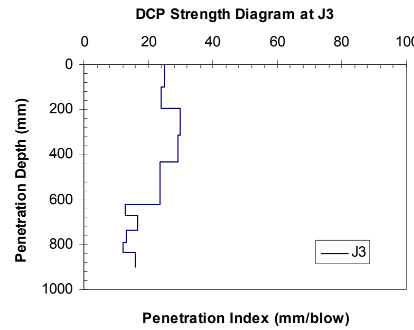
DCP Strength Diagram at J3
Penetration Depth (mm)
Penetration Index (mm/blow)
J3

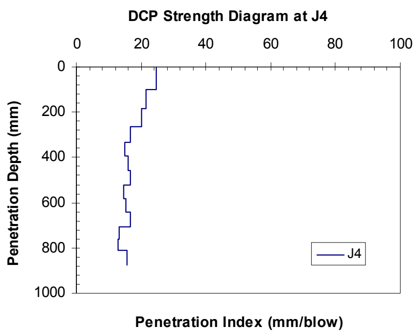
DCP Strength Diagram at J4
Penetration Depth (mm)
Penetration Index (mm/blow)
J4

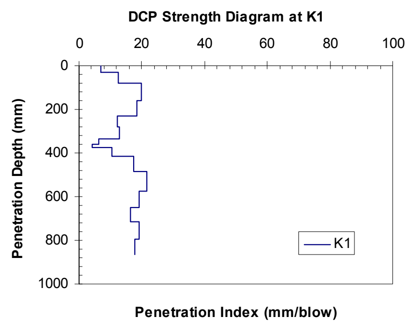
DCP Strength Diagram at K1
Penetration Depth (mm)
Penetration Index (mm/blow)
K1

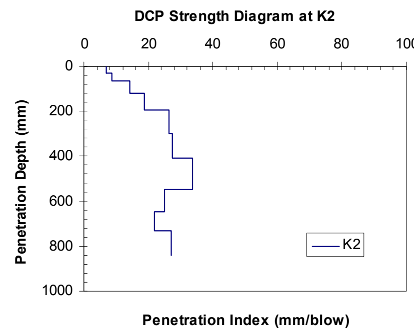
DCP Strength Diagram at K2
Penetration Depth (mm)
Penetration Index (mm/blow)
K2

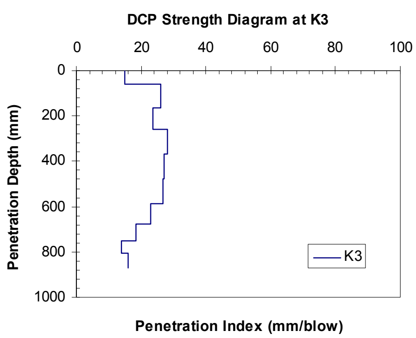
DCP Strength Diagram at K3
Penetration Depth (mm)
Penetration Index (mm/blow)
K3

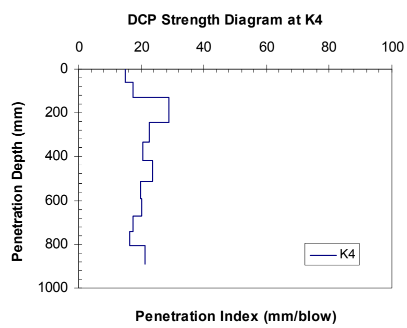
DCP Strength Diagram at K4
Penetration Depth (mm)
Penetration Index (mm/blow)
K4

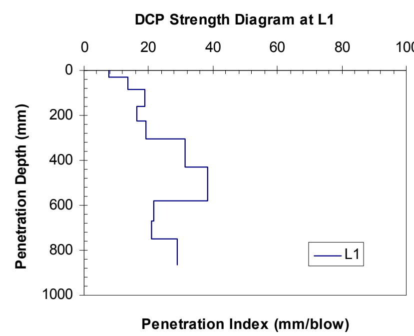
DCP Strength Diagram at L1
Penetration Depth (mm)
Penetration Index (mm/blow)
L1

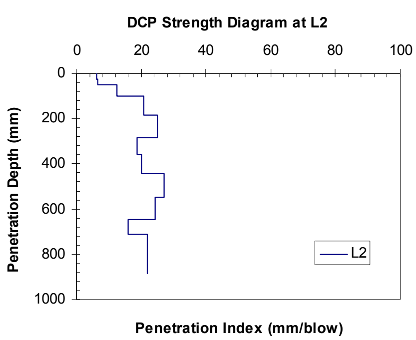
DCP Strength Diagram at L2
Penetration Depth (mm)
Penetration Index (mm/blow)
L2

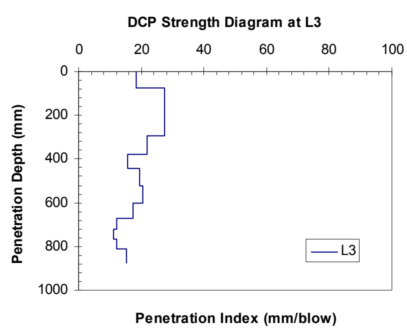
DCP Strength Diagram at L3
Penetration Depth (mm)
Penetration Index (mm/blow)
L3

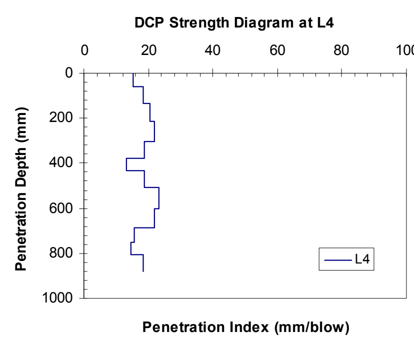
DCP Strength Diagram at L4
Penetration Depth (mm)
Penetration Index (mm/blow)
L4

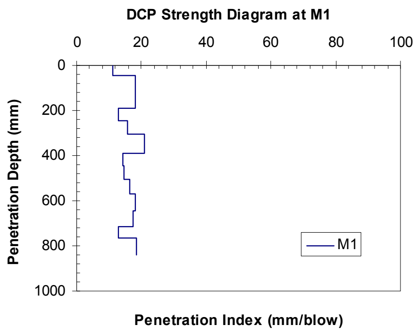
DCP Strength Diagram at M1
0 20 40 60 80 100
0 200 400 600 800 1000
Penetration Depth (mm)
M1
Penetration Index (mm/blow)

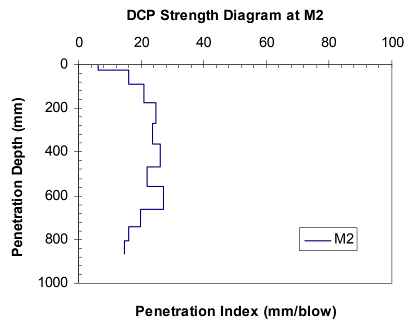
DCP Strength Diagram at M2
0 20 40 60 80 100
0 200 400 600 800 1000
Penetration Depth (mm)
M2
Penetration Index (mm/blow)

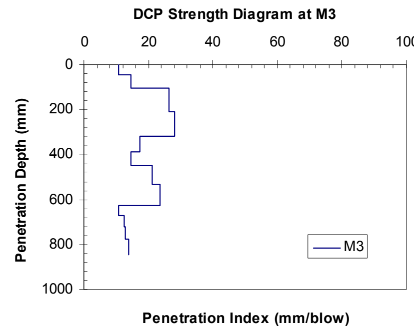
DCP Strength Diagram at M3
0 20 40 60 80 100
0 200 400 600 800 1000
Penetration Depth (mm)
M3
Penetration Index (mm/blow)

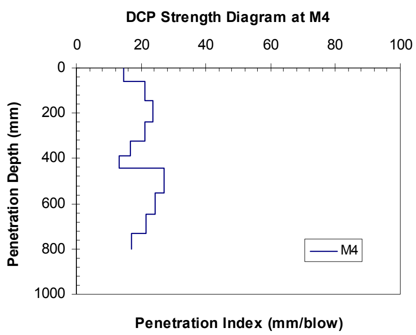
DCP Strength Diagram at M4
0 20 40 60 80 100
0 200 400 600 800 1000
Penetration Depth (mm)
M4
Penetration Index (mm/blow)

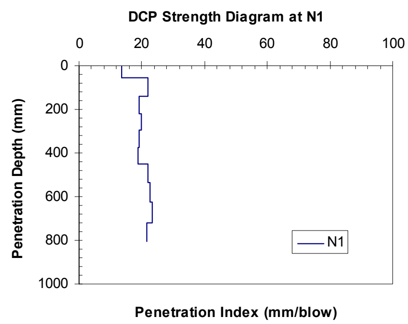
DCP Strength Diagram at N1
0 20 40 60 80 100
0 200 400 600 800 1000
Penetration Depth (mm)
N1
Penetration Index (mm/blow)

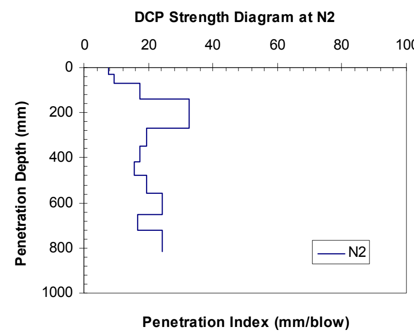
DCP Strength Diagram at N2
0 20 40 60 80 100
0 200 400 600 800 1000
Penetration Depth (mm)
N2
Penetration Index (mm/blow)

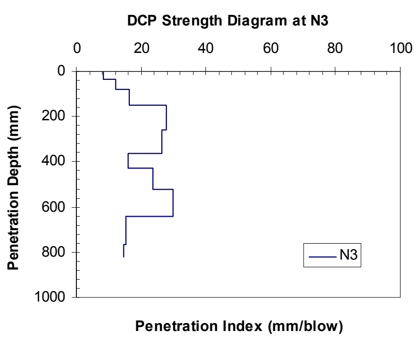
DCP Strength Diagram at N3
0 20 40 60 80 100
0 200 400 600 800 1000
Penetration Depth (mm)
N3
Penetration Index (mm/blow)

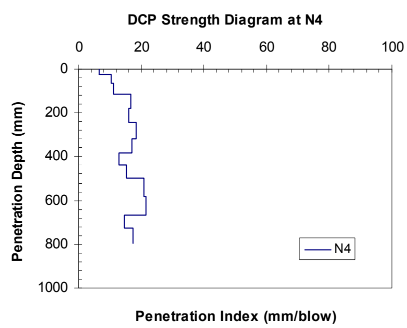
DCP Strength Diagram at N4
0 20 40 60 80 100
0 200 400 600 800 1000
Penetration Depth (mm)
N4
Penetration Index (mm/blow)

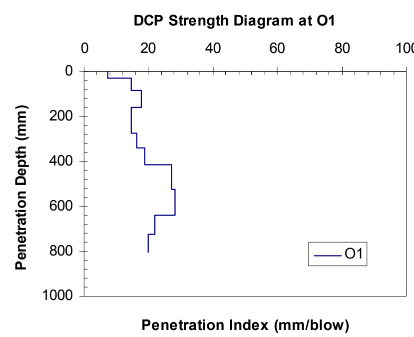
DCP Strength Diagram at O1
0 20 40 60 80 100
0 200 400 600 800 1000
Penetration Depth (mm)
O1
Penetration Index (mm/blow)

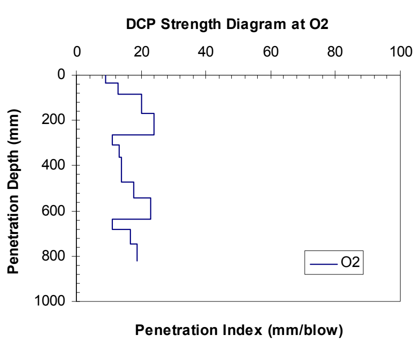
DCP Strength Diagram at O2
0 20 40 60 80 100
0 200 400 600 800 1000
Penetration Depth (mm)
O2
Penetration Index (mm/blow)

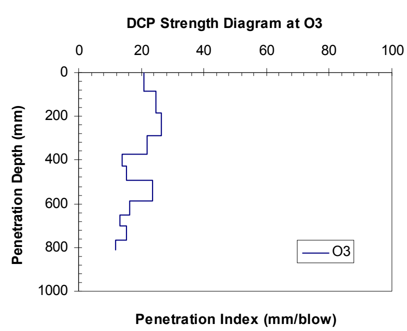
DCP Strength Diagram at O3
0 20 40 60 80 100
0 200 400 600 800 1000
Penetration Depth (mm)
O3
Penetration Index (mm/blow)

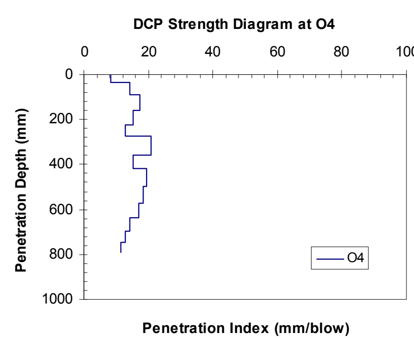
DCP Strength Diagram at O4
0 20 40 60 80 100
0 200 400 600 800 1000
Penetration Depth (mm)
O4
Penetration Index (mm/blow)

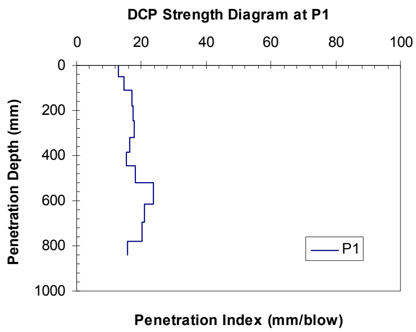
DCP Strength Diagram at P1
Penetration Depth (mm)
Penetration Index (mm/blow)
P1

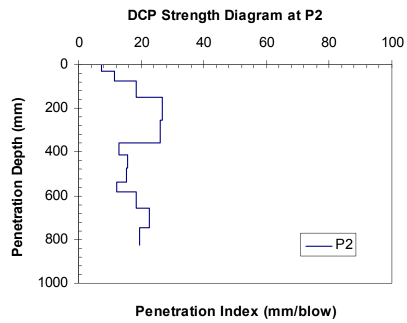
DCP Strength Diagram at P2
Penetration Depth (mm)
Penetration Index (mm/blow)
P2

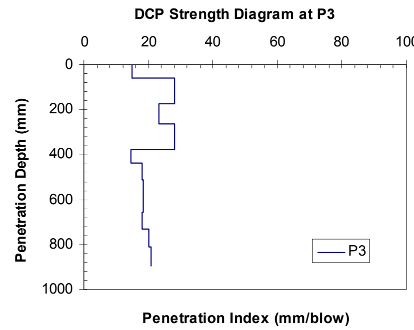
DCP Strength Diagram at P3
Penetration Depth (mm)
Penetration Index (mm/blow)
P3

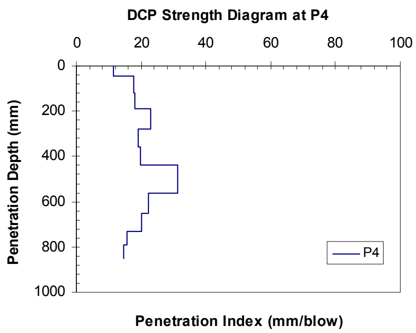
DCP Strength Diagram at P4
Penetration Depth (mm)
Penetration Index (mm/blow)
P4

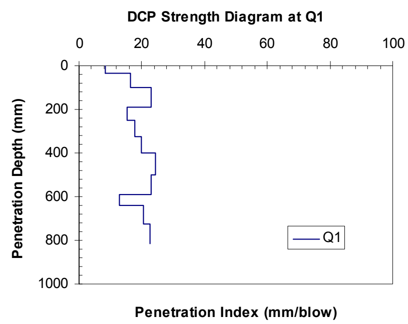
DCP Strength Diagram at Q1
Penetration Depth (mm)
Penetration Index (mm/blow)
Q1

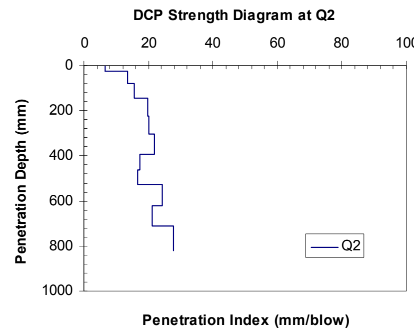
DCP Strength Diagram at Q2
Penetration Depth (mm)
Penetration Index (mm/blow)
Q2

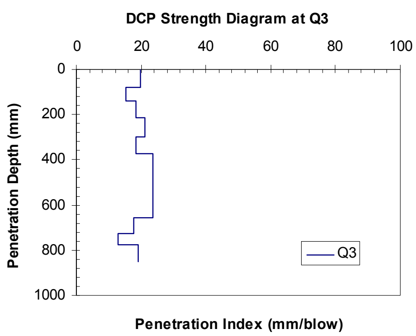
DCP Strength Diagram at Q3
Penetration Depth (mm)
Penetration Index (mm/blow)
Q3

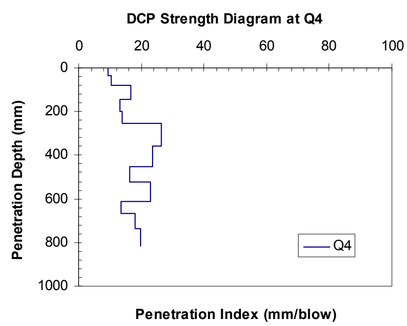
DCP Strength Diagram at Q4
Penetration Depth (mm)
Penetration Index (mm/blow)
Q4

DCP profiles after 2 years at edge of pavement during freezing period – February 18, 2007

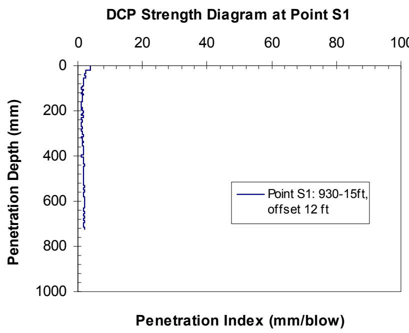

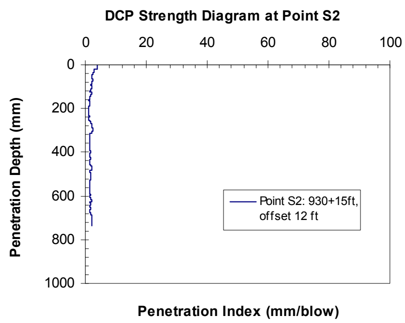

DCP profiles after 2 years for at edge of pavement during thawing period – March 09, 2007

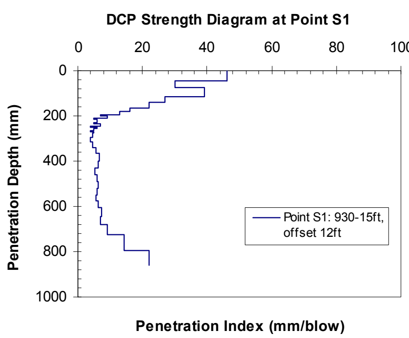

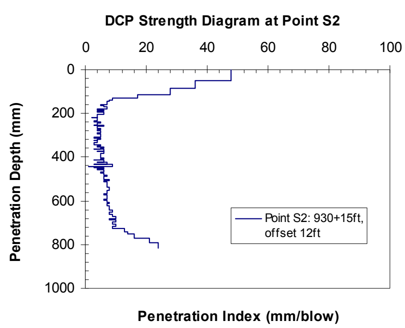

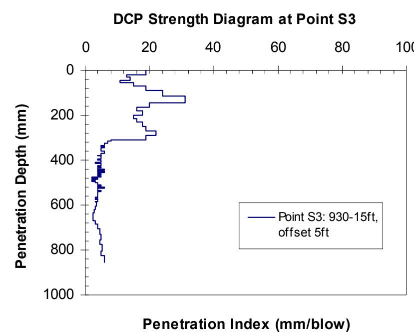

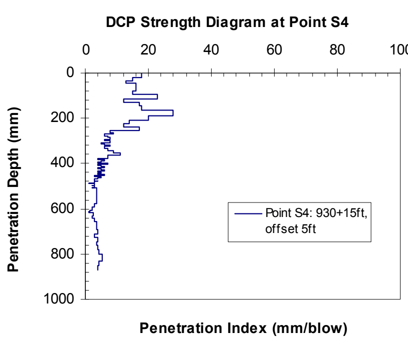

DCP profiles after 2 years at edge of pavement – April 23, 2007

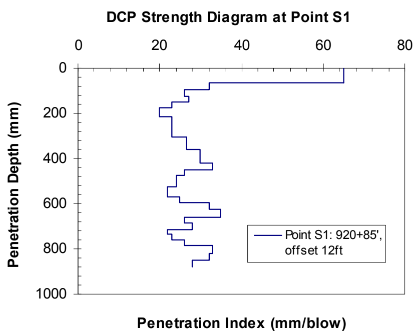

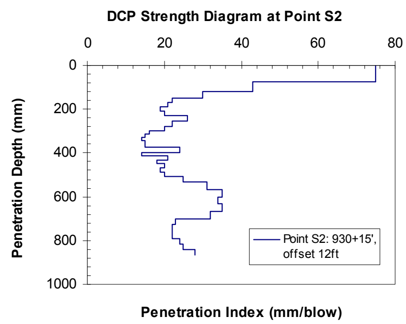

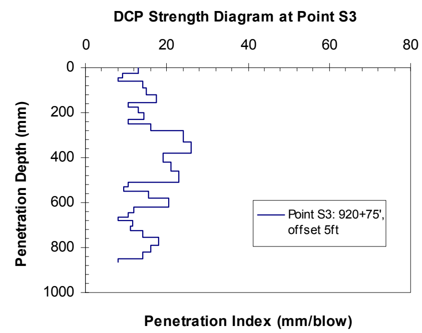

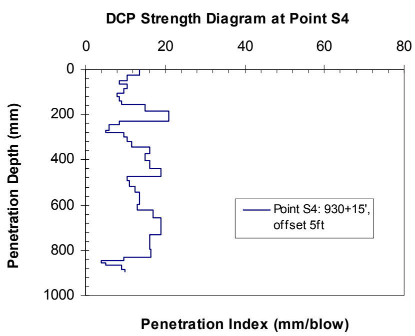

DCP profiles after 2 years in core hole through pavement layer - April 23, 2007

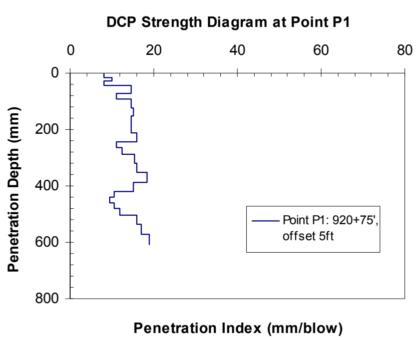

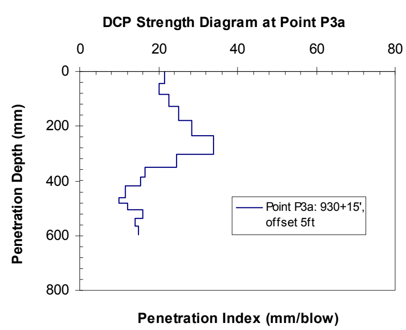

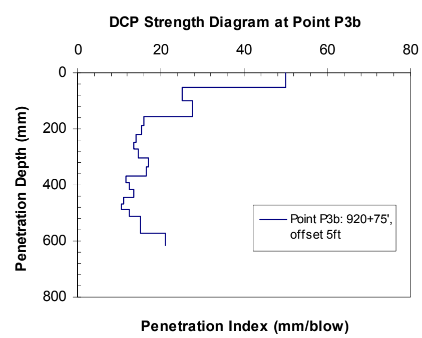

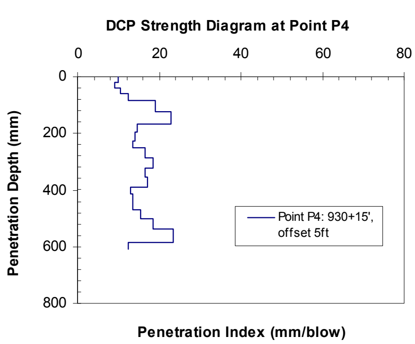

APPENDIX B: IN-GROUND INSTRUMENTATION RESULTS

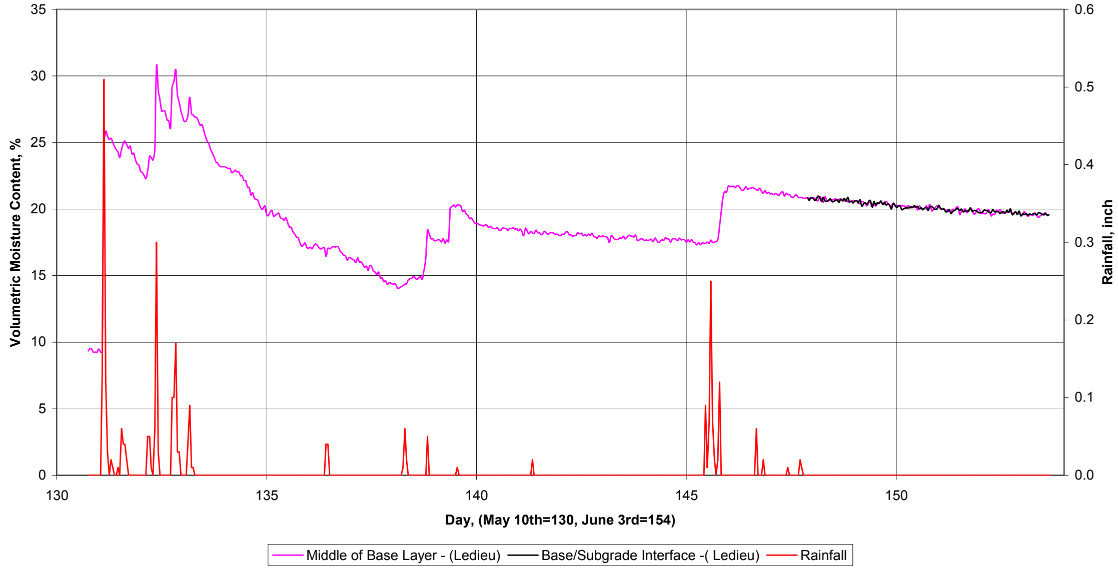

Figure B1. Rainfall and Moisture Content in Subase Layer – May 10 to June 3rd, 2005

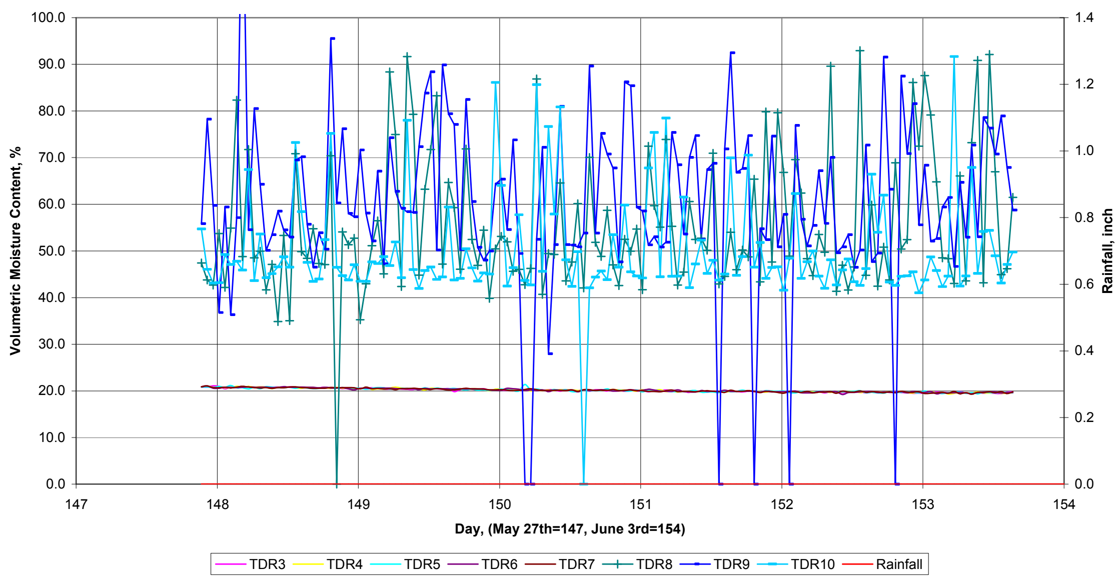

Figure B2. Rainfall and Moisture Content in Subgrade – May 27th to June 3rd, 2005

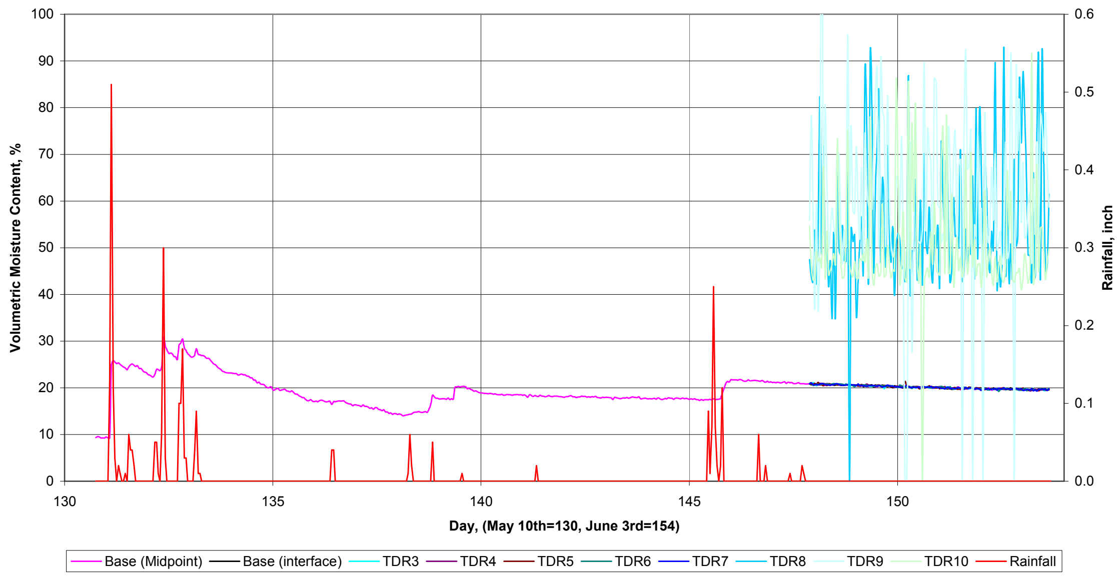

Figure B3. Rainfall and Moisture Content in Base Layer – May 10th to June 3rd, 2005

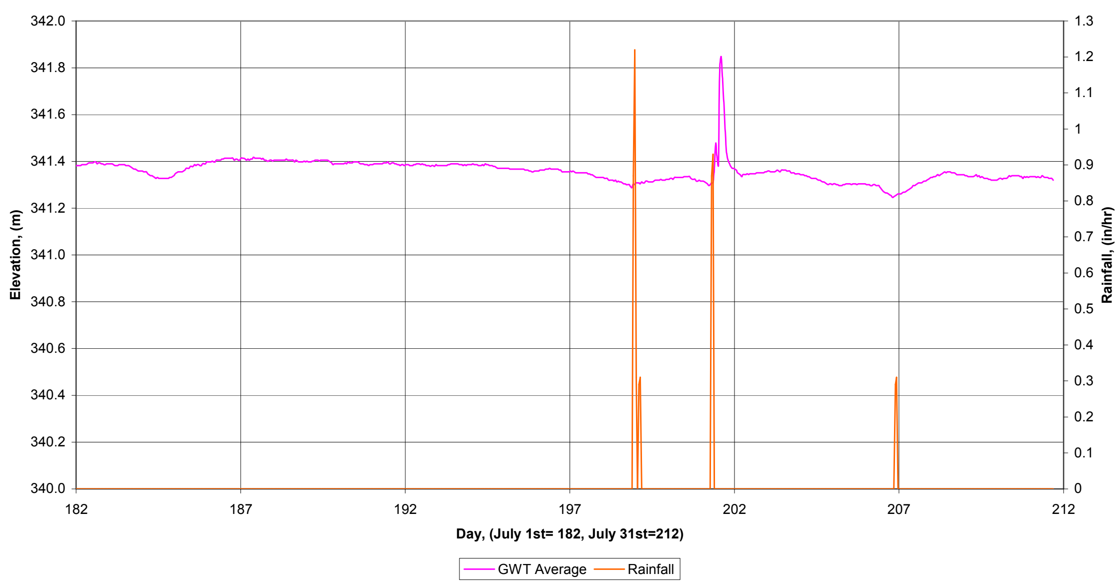

Figure B4. Average Rainfall (in/hr) and Ground Water Table – July 1st to July 31st, 2005

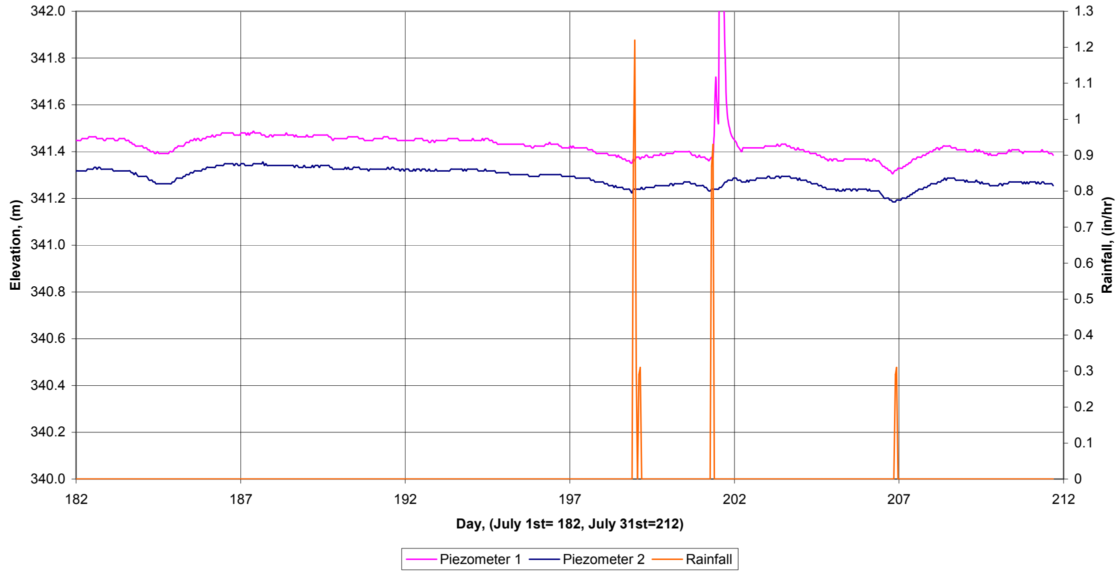

Figure B5. Rainfall (in/hr) and Ground Water Table from Piezometers – July 1st to July 31st, 2005

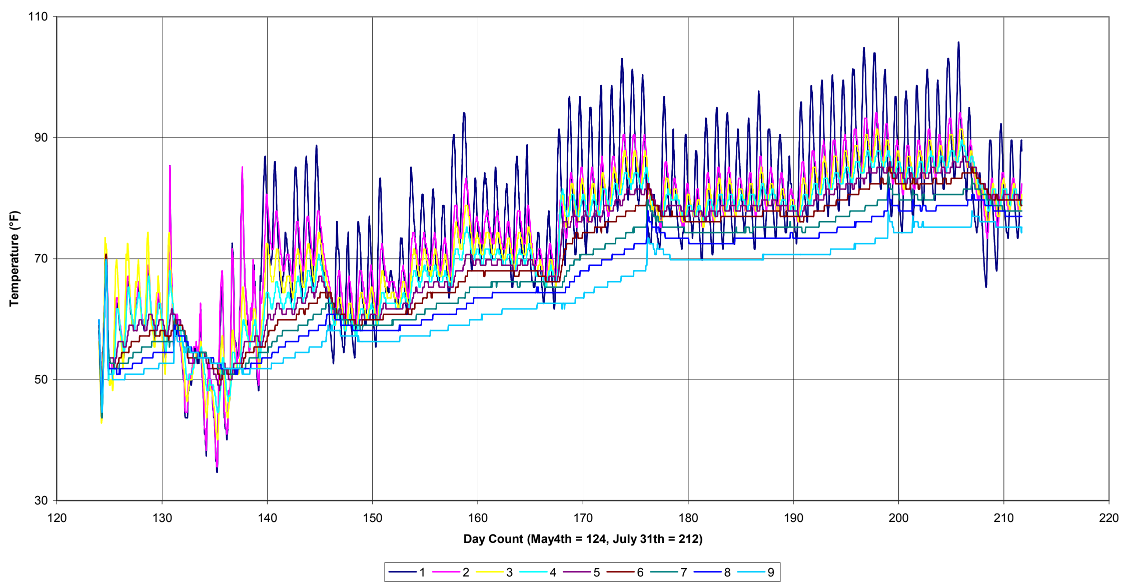

Figure B6. Temperature Readings obtained iBUTTON Readings from May 4th through July 31st, 2005

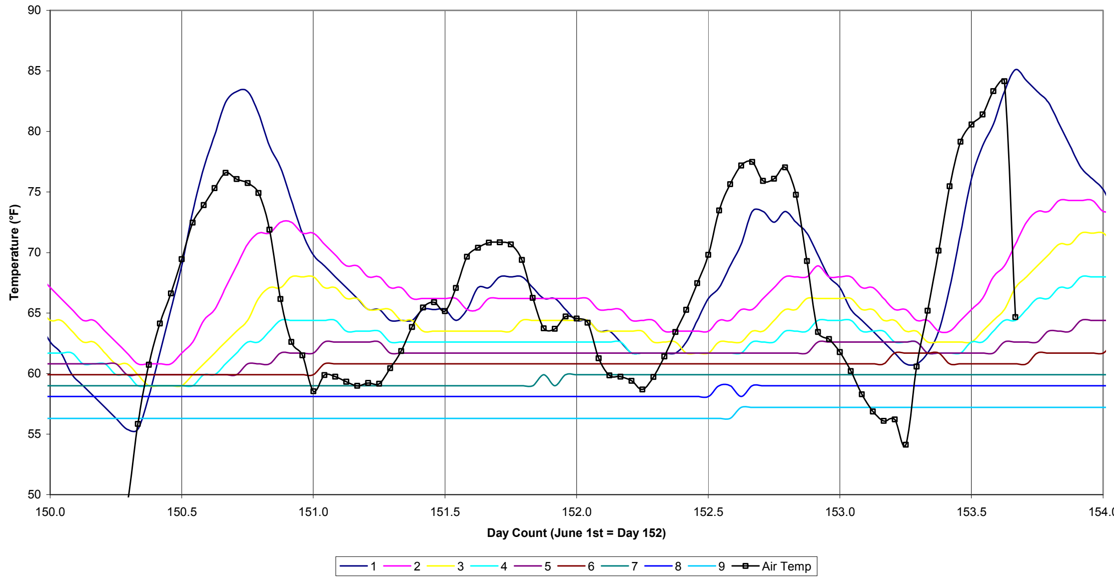

Figure B7. Temperature Readings obtained iBUTTON Readings around June 1st, 2005

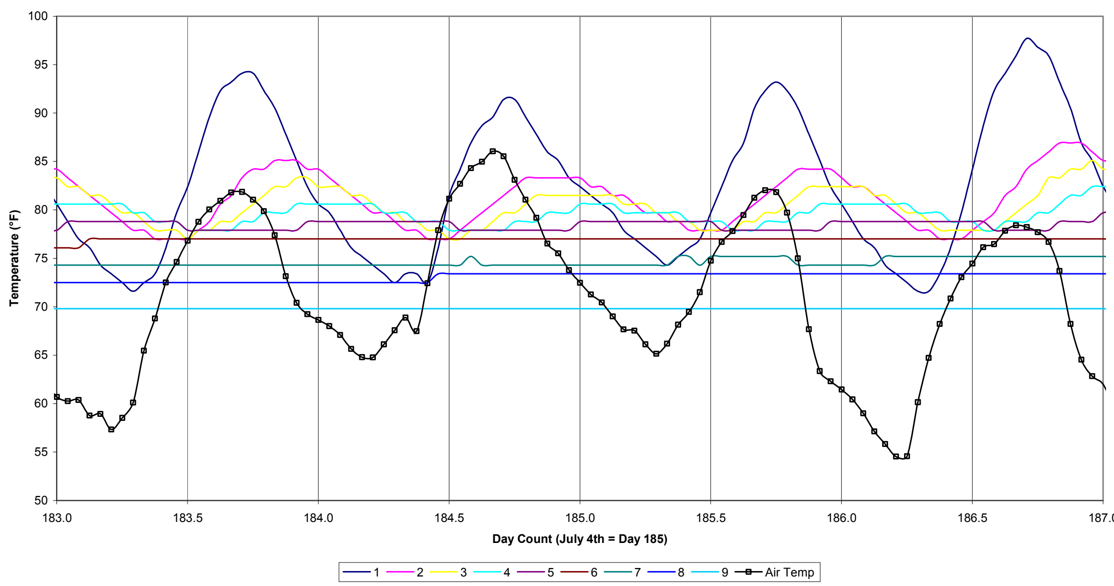

Figure B8. Temperature Readings obtained iBUTTON Readings around July 4th, 2005

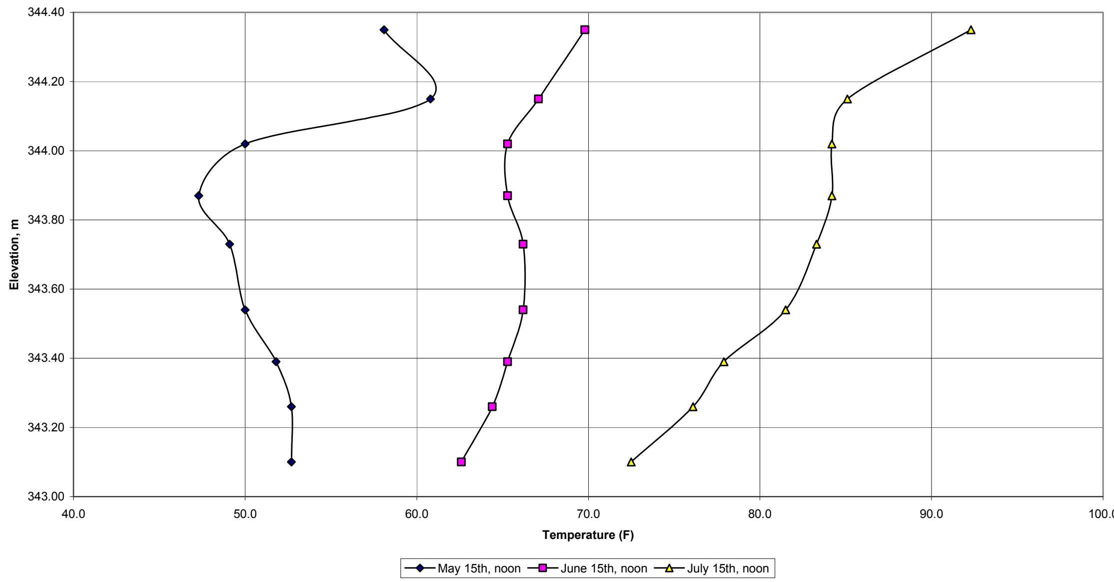

Figure B9. Temperature with Elevation obtained iBUTTON Readings in Mid-Month of May, June, and July, 2005

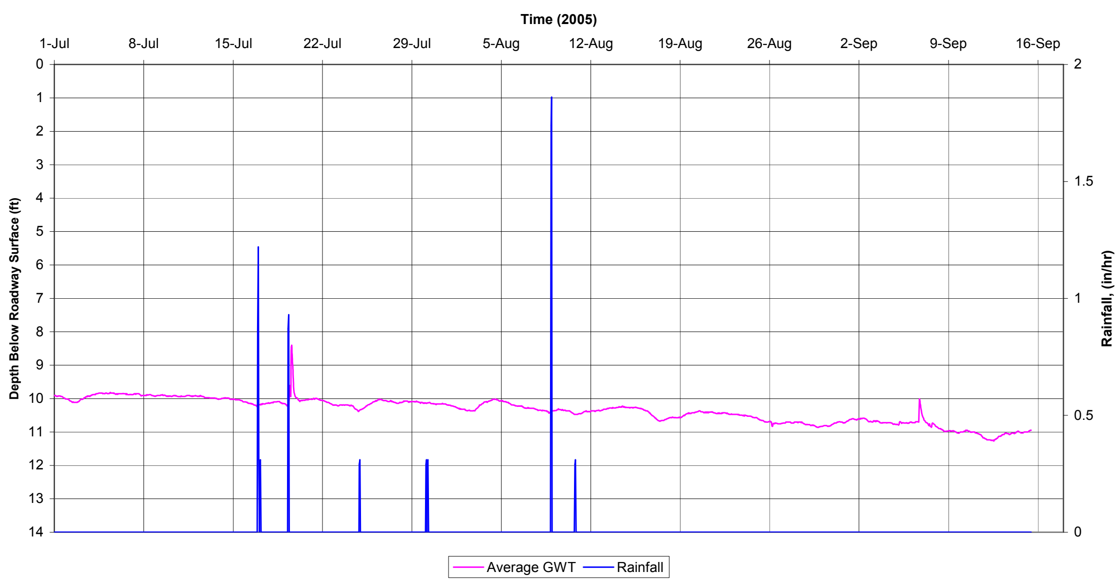

Figure B10. Rainfall (in/hr) and Average Ground Water Table below Roadway Surface

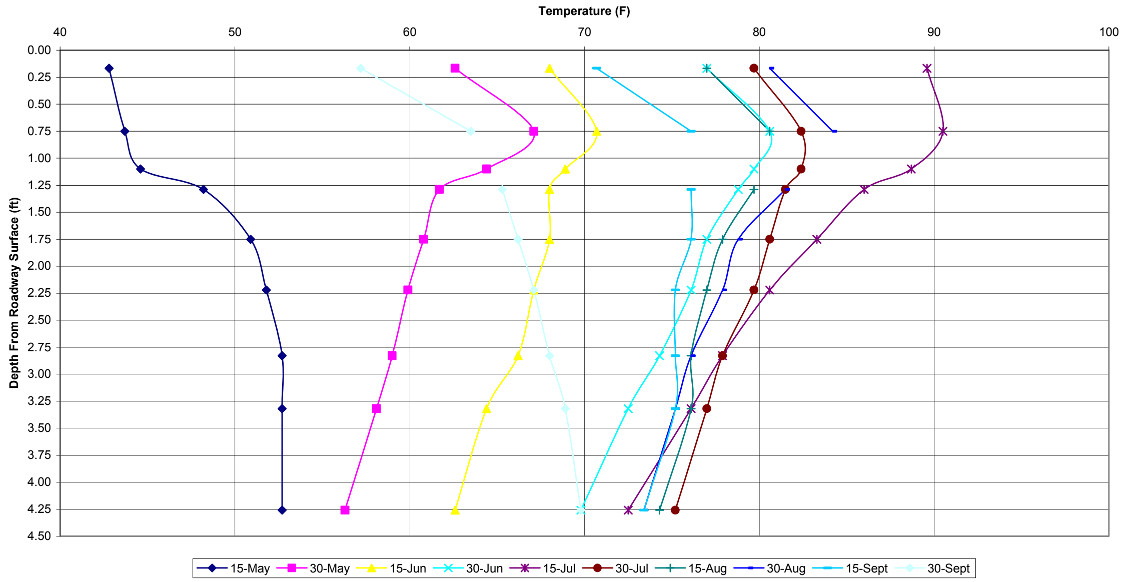

Figure B11. Temperature below Roadway Surface Obtained from iBUTTON Readings on Different Days of the Year 2005

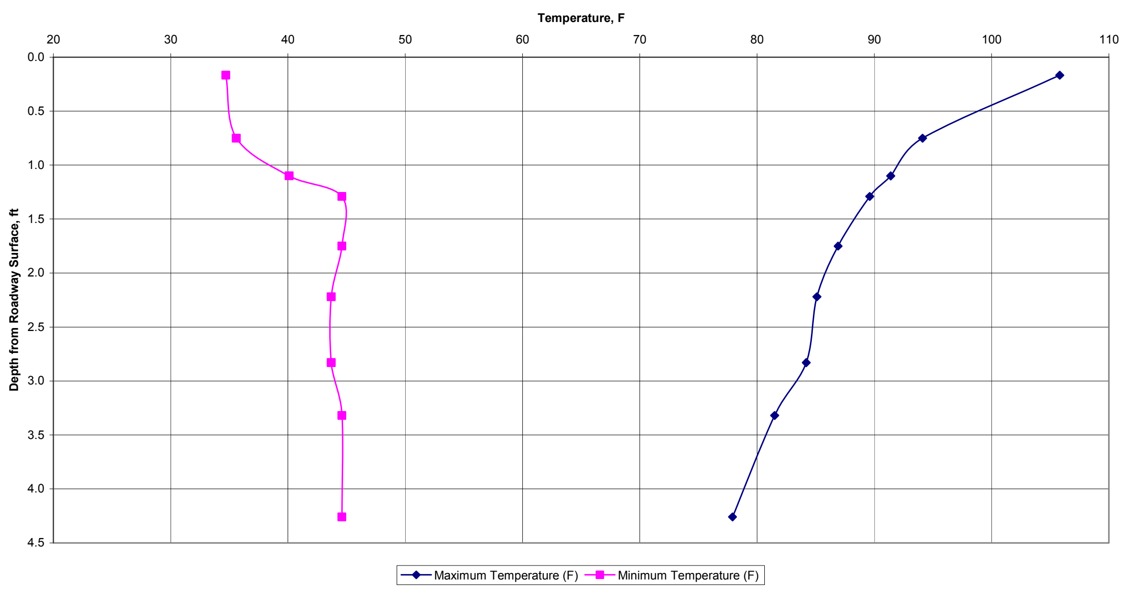

Figure B12. Temperature Extremes below Roadway Surface Obtained from iBUTTON Readings of the Year 2005

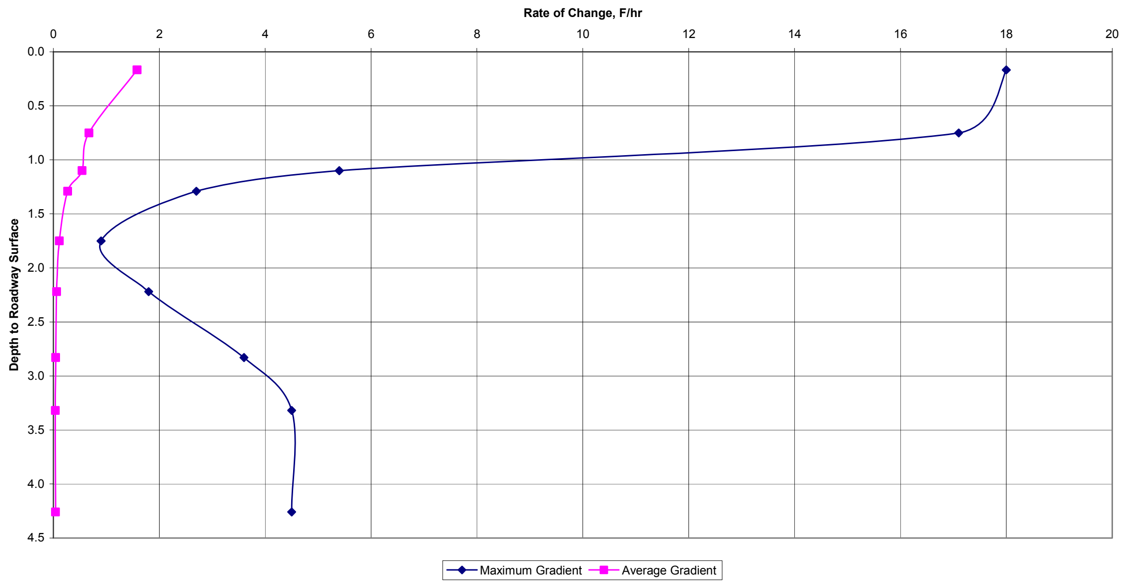

Figure B13. Temperature Changing Rates below Roadway Surface of the Year 2005

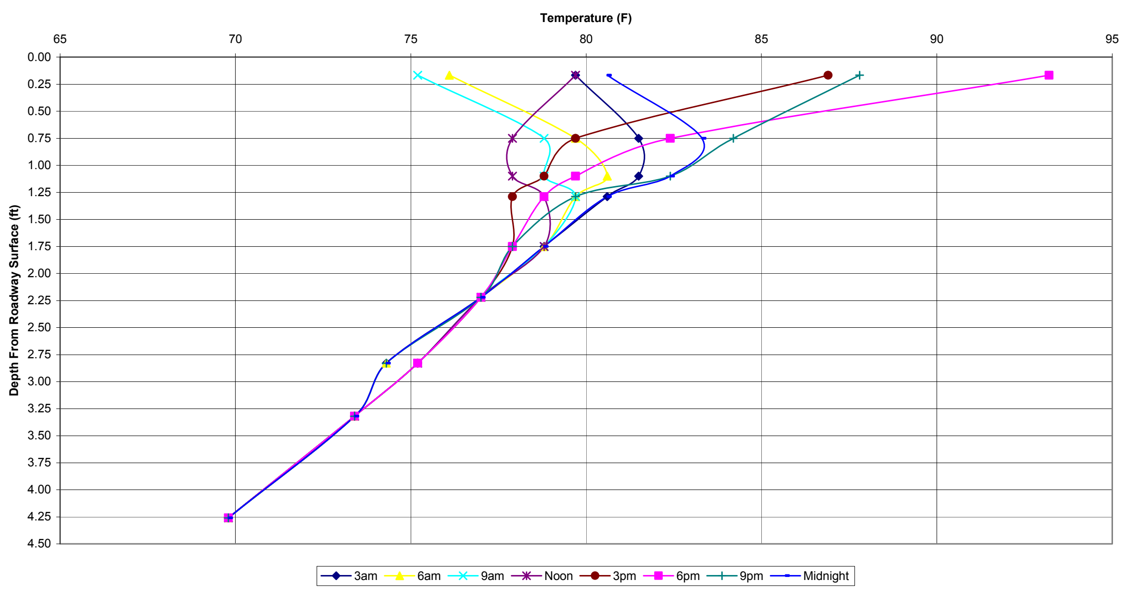

Figure B14. Temperature Changes below Roadway Surface at Different Time in a Day of the Year 2005

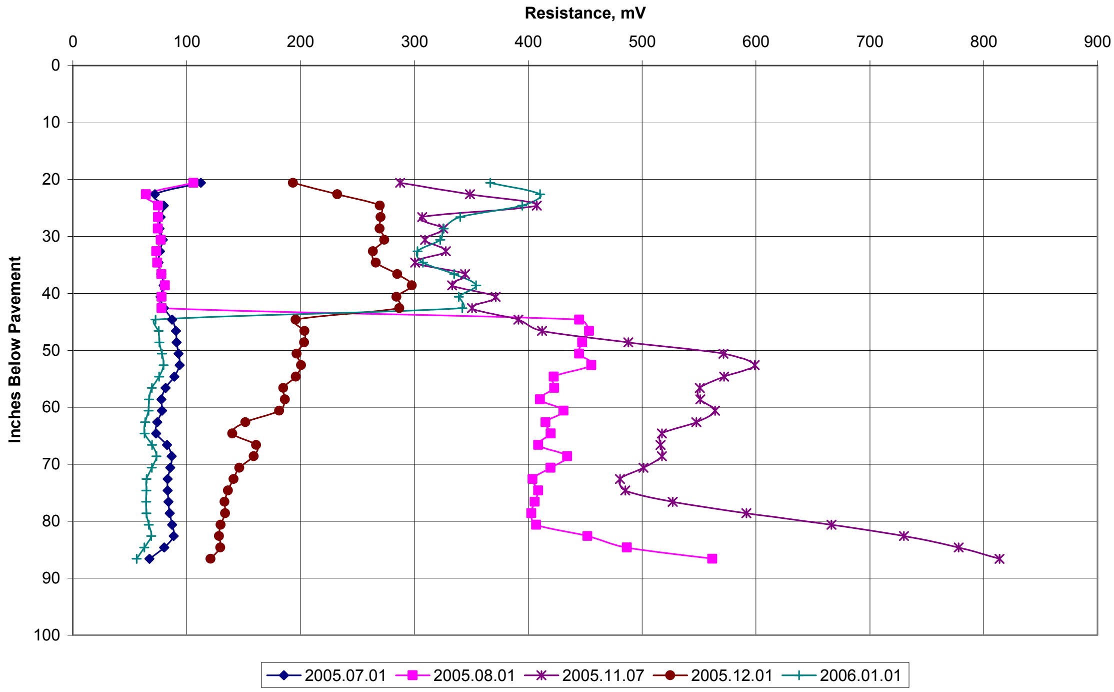

Figure B15. Frost Depth Determination below Pavement – Overview by Months

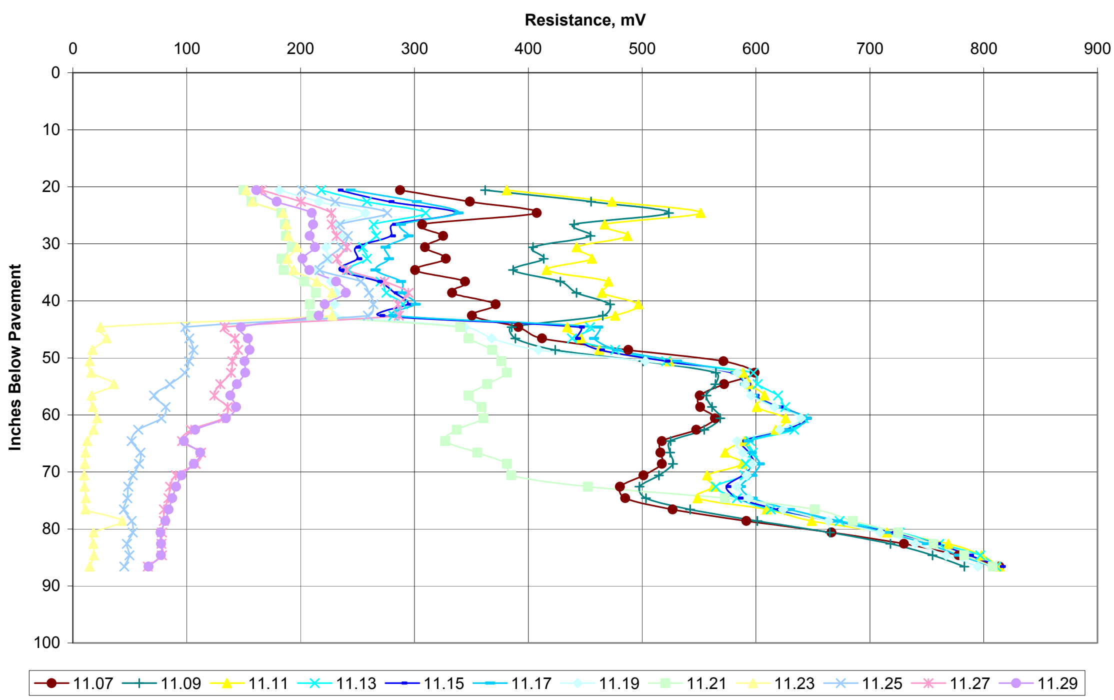

Figure B16. Frost Depth Determination below Pavement – November 2005

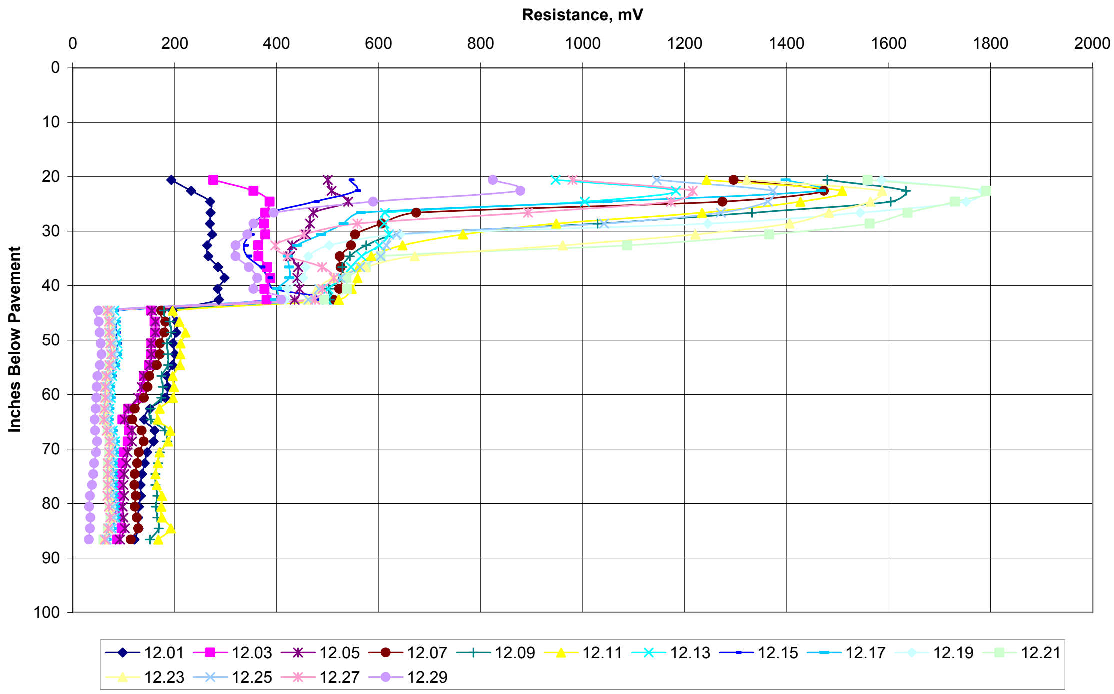

Figure B17. Frost Depth Determination below Pavement – December 2005

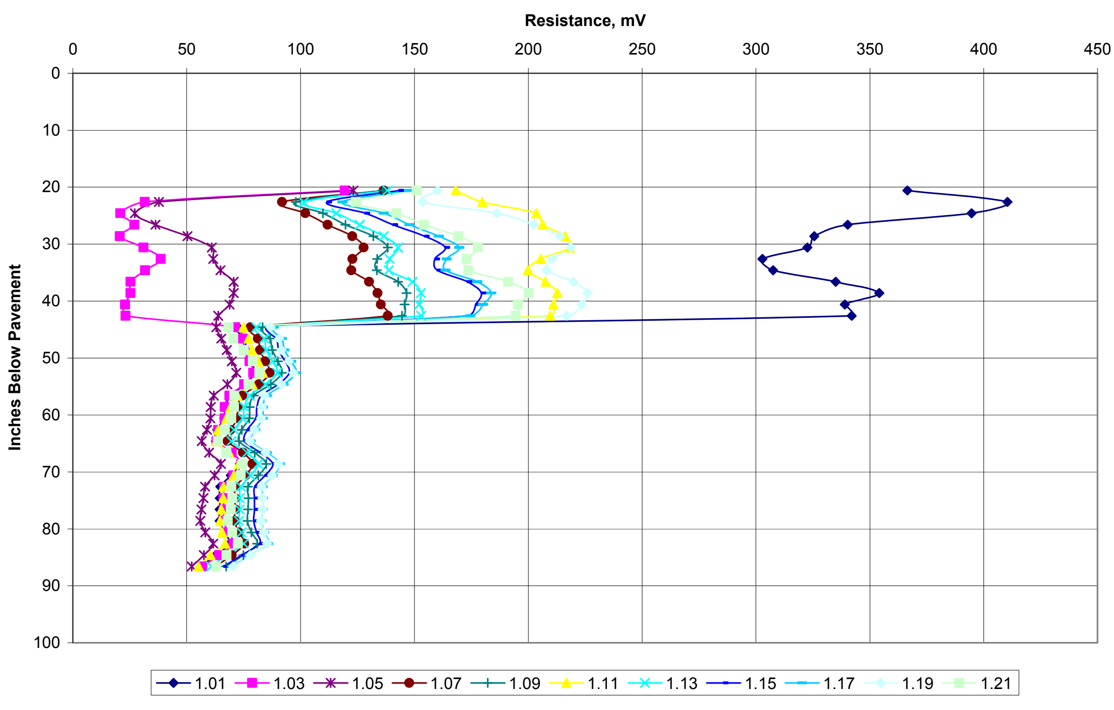

Figure B18. Frost Depth Determination below Pavement – January 2006